Cooperative Communication over Underwater Acoustic Channels

by

Suhail Ibrahim Aldharrab

A thesis
presented to the University of Waterloo
in fulfillment of the
thesis requirement for the degree of
Doctor of Philosophy
in
Electrical and Computer Engineering

Waterloo, Ontario, Canada, 2013

I hereby declare that I am the sole author of this thesis. This is a true copy of the thesis, including any required final revisions, as accepted by my examiners.

I understand that my thesis may be made electronically available to the public.

Abstract

As diverse and data-heavy underwater applications emerge, demanding requirements are further imposed on underwater wireless communication systems. Future underwater wireless communication networks might consist of both mobile and stationary nodes which exchange data such as control, telemetry, speech, and video signals among themselves as well as a central node located at a ship or onshore. The submerged nodes, which can, for example, take the form of an autonomous underwater vehicle/robot or diver, can be equipped with various sensors, sonars, video cameras, or other types of data acquisition instruments. Innovative physical layer solutions are therefore required to develop efficient, reliable, and high-speed transmission solutions tailored for challenging and diverse requirements of underwater applications.

Building on the promising combination of multi-carrier and cooperative communication techniques, this dissertation investigates the fundamental performance bounds of cooperative underwater acoustic (UWA) communication systems taking into account the inherent unique characteristics of the UWA channel. We derive outage probability and capacity expressions for cooperative multi-carrier UWA systems with amplify-and-forward and decode-and-forward relaying. Through the derived expressions, we demonstrate the effect of several system and channel parameters on the performance. Furthermore, we investigate the performance of cooperative UWA systems in the presence of non-uniform Doppler distortion and propose receiver designs to mitigate the degrading Doppler effects.

Acknowledgements

Praises and thankfulness to Allah, the most merciful and most compassionate for the great bounties bestowed upon me and granting me the strength to seek knowledge.

My sincere gratitude and appreciations go to my advisor Prof. Murat Uysal, who has supported and motivated me throughout the PhD program. His insightful suggestions, fruitful discussions, kindness, and patience have inspired me throughout my graduate studies. I would like to thank my co-supervisor Prof. Oussama Damen for his assistance, cooperation, and valuable advices.

It is my pleasure to thank my doctoral thesis committee members, Prof. Jan Huissoon, Prof. Guang Gong, Prof. Amir Khandani, and Prof. Kemal Tepe for their valuable time in reviewing my thesis, and their insightful suggestions. I wish also to thank Prof. Liang-Liang Xie who served on my comprehensive examination committee.

My thanks extend to King Fahd University of Petroleum and Minerals for their financial support during my PhD program. I thank the Ministry of Higher Education and Saudi Cultural Bureau in Canada for their support and assistance during my stay in Canada.

I would like to thank all my friends and colleagues for their valuable help during my PhD study especially, Dr. Osama Amin, Dr. Mohamed Feteiha, Mazen Al-Sabaan, Majid Al-Tamimi, Dr. Salama Ikki, Dr. Walid Abediseid, Mohsen Tehrani, Reza Heidarpour, and Ibrahim Al-Solami.

My heartiest thanks go to my parents, Munira and Ibrahim, and my siblings, Abdulaziz, Nada, Moath, and Mohammed, for their continuous motivation, kindness, and patience. I am indebted to them for their unconditional love and cordial support during my study.

Last, but not least, I express my deepest appreciation to the numerous people who have contributed to my education and my well-being at University of Waterloo and elsewhere.

Table of Contents

List of Tables

List of Figures

List of Abbreviations

AF	Amplify-and-forward
AS	All-subcarriers
AUV	Autonomous underwater vehicle
BER	Bit error rate
BLAST	Bell labs layered space-time
BS	Base station
CDF	Cumulative distribution function
CFO	Carrier frequency offset
CP	Cyclic prefix
CW	Continuous wave
DATS	Digital acoustic telemetry system
DF	Decode-and-forward
DFE	Decision feedback equalizer
DH	Dual-hop
DLST	Diagonal layered space-time
DSP	Digital signal processing
DT	Direct transmission
EXIT	Extrinsic information transfer
FFT	Fast Fourier transform
FG	Francois Garrison
FIR	Finite impulse response
FSK	Frequency-shift keying
HCRB	Hammersley Chapman Robbins bound
ICI	Intercarrier interference

IFFT	Inverse fast Fourier transform
ISI	Inter-symbol interference
LDC	Linear dispersion code
LDPC	Low-density parity-check
LED	Light-emitting diode
LFM	Linearly-frequency-modulated
LMMSE	Linear minimum mean square error
LST	Layered space-time
MF	Matched Filter
MIMO	Multiple-input multiple-output
ML	Maximum likelihood
MMSE	Minimum mean square error
MR	Multiple resampling
MSE	Mean square error
NLOS	Non-line-of-sight
OCP	Orthogonal cooperation protocol
OFDM	Orthogonal frequency division multiplexing
OWC	Optical wireless communication
PDP	Power delay profile
PHY	Physical layer
PLL	Phase locked loop
PS	Per-subcarrier
PSD	Power spectral density
PSK	Phase-shift keying
QAM	Quadrature amplitude modulation
RF	Radio-frequency
RLS	Recursive least squares
SDE	Spatial diversity equalizer
SISO	Single-input single-output
SNR	Signal-to-noise ratio
SPRE	Sparse partial response equalizer

SR	Single resampling
SSB-SC	Single-side band suppressed carrier
STBC	Space-time block code
STC	Space-time coding
STTC	Space-time trellis code
TLST	Threaded layered space-time
TR	Time reversal
UWA	Underwater acoustic
VLSI	Very-large-scale integration
ZF	Zero Forcing
ZP	Zero-padded

Notations

$(.)^T$	Transpose
$(.)^*$	Complex conjugate
$(.)^H$	Hermitian (conjugate transpose)
$E\ [.]$	Statistical expectation
var(.)	Statistical variance
Pr{}	Probability
$\mid . \mid$	Absolute value
$\mid\mid . \mid\mid$	Frobenius norm
$n!$	Factorial of n
$\begin{pmatrix} n \\ k \end{pmatrix}$	Binomial coefficient (n choose k)
$(.)_k$	Pochhammer symbol for $k \geq 0$
$\otimes$	Kronecker product
$\stackrel{d}{=}$	Equality of the finite-dimensional probability distribution
$\stackrel{d}{\sim}$	Approximately equivalent in probability distribution
sup{.}	Supremum
$\lim_{x \to c}(.)$	Limit as x goes to c
$\max(x_1, ..., x_N)$	Maximum of $x_1, ..., x_N$
$\min(x_1, ..., x_N)$	Minimum of $x_1, ..., x_N$
$\arg\max_x f(x)$	Argument of the maximum
$\arg\min_x f(x)$	Argument of the minimum
$\mathbb{R}$	Set of real numbers
$\mathbb{C}$	Set of complex numbers

$\mathbf{A}(i,j)$	$(i,j)^{\text{th}}$ entry of matrix $\mathbf{A}$
$\mathbf{A}^{-1}$	Inverse of matrix $\mathbf{A}$
$\det(\mathbf{A})$	Determinant of matrix $\mathbf{A}$
$\text{Tr}\{\mathbf{A}\}$	Trace of matrix $\mathbf{A}$
$\mathbf{I}_N$	$N \times N$ identity matrix
$\text{diag}(x_1, ..., x_N)$	$N \times N$ diagonal matrix with elements $x_1, ..., x_N$
$f^{(n)}(.)$	n^{th} derivative of function $f(.)$
$\exp(.)$	Exponential function
$\delta(.)$	Dirac delta function
$Q(x)$	Q-function (tail probability of standard normal distribution)
$\text{sinc}(.)$	Normalized sinc function
$\Re\{z\}$	Real part of z ($z \in \mathbb{C}$)
$\Im\{z\}$	Imaginary part of z ($z \in \mathbb{C}$)
$I_0(.)$	Zero-order modified Bessel function of the first kind
$W_{\lambda,\mu}(.)$	Whittaker function
$\Gamma(.)$	Gamma function
$L_k^{(\alpha)}(.)$	k^{th} generalized Leguerre polynomial, $\alpha \in \mathbb{R}$
${}_1F_1(a;b;c)$	Confluent hypergeometric function of the first kind

Chapter 1

Introduction

The abundance of water on Earth distinguishes our "Blue Planet" from others in the solar system. Nearly 71% of the Earth's surface is covered with water, 97% of it being sea water. This vast underwater world is extremely rich in natural resources such as valuable minerals and oilfields waiting to be explored. Underwater exploration activities are mainly hampered by the lack of efficient means of real-time communication below water. Although wire-line systems through deployment of fiber optical links have been used to provide real-time communication in some underwater applications, their high cost and operational disadvantages become restrictive for many cases. Wireless communication is a promising alternative and an ideal transmission solution for a wide range of underwater applications including offshore oil field exploration/monitoring, oceanographic data collection, maritime archaeology, environmental monitoring, disaster prevention, and port security among many others.

The traditional approach for underwater data acquisition is to deploy underwater sensors which record data during the monitoring mission and then recover the information from the storage unit of sensor. Such an approach is not able to deliver real-time information which can be particularly critical in surveillance and seismic monitoring. Furthermore, if hardware or software failures occur before the monitoring devices are recovered, it is not unlikely that all recorded data can be lost. Due to the lack of interaction between submerged sensors and central control system, the amount of data that can be recorded is also limited by the storage capacity of sensors and system reconfiguration is not possible.

As diverse and data-heavy underwater applications emerge, demanding requirements are further imposed on underwater acoustic (UWA) communication systems. Future UWA communication networks might consist of both mobile and stationary nodes which exchange data such as control, telemetry, speech, and video signals among themselves as well as a central node located at a ship or onshore. The submerged nodes (which can, for example, take the form of an autonomous underwater vehicle (AUV)/robot or diver) can be equipped with various sensors, sonars, video cameras, or other types of data acquisition instruments. Innovative physical layer (PHY) solutions are therefore required to develop efficient, reliable, and high-speed transmission solutions tailored for challenging and diverse requirements of underwater applications.

Underwater wireless communication has received much attention over the last few years. This has been triggered by the increasing demand for reliable high-speed wireless links to accommodate a wide range of underwater applications. In this chapter, we will first discuss possible carrier options (i.e., radio, optical versus acoustic waves) for underwater wireless communication and then present a historical overview of UWA communication with major milestones. The rest of the chapter addresses cooperative UWA communication that will be the focus of this thesis.

1.1 Underwater Wireless Communications

Wireless transmission of information under water can be achieved through radio, optical, or sound waves. Due to the high attenuation of radio-frequency (RF) signals in water, long-range RF communication is problematic and requires the use of extra low frequencies which necessitate large antennas and high transmit powers. An experimental study of underwater RF communication with a measurement campaign in the Atlantic Ocean can be found in [1]. Although early military use of underwater RF communications is known, the first commercial underwater RF modem was introduced only back in 2006 [2]. However, their short transmission range (between 1-100 meters) makes this option unappealing for most practical purposes.

Optical waves do not suffer much attenuation, but are affected by absorption, scattering, and high level of ambient light limiting the transmission ranges [3, 4]. In [5], Lanbo et al.

discuss that underwater optical wireless communication (OWC) is limited to very short distances due to the severe water absorption at optical frequency band and substantial back-scatter from suspending particles. In [6], Arnon and Kedar propose a non-line-of-sight (NLOS) underwater OWC system by considering the back-reflection of the optical signal from ocean-air interface and report substantial performance improvements in link reliability. In [7], Baiden et al. test experimentally an underwater OWC system using light-emitting diodes (LEDs) in the green and blue light spectrum. They demonstrate that pure seawater is absorptive except in around 400-500 nm wavelengths (i.e., the blue-green region of the visible light spectrum). From their experimental set-up, they observe that turbidity level, viewing angle and separation distance affects severely the behaviour of blue light in water. In [8], Doniec et al. discuss the hardware and software implementation aspects of testbed AquaOptical underwater communication system. These underwater OWC modems achieve a data rate of 1.2 Mbps at a distance up to 30 m in clear water.

In comparison to RF and optical waves, acoustic transmission is more practical to use in underwater with its support for long-range transmission due to relatively favourable propagation characteristics of sound waves. It is therefore the commonly employed method in practical modems [9]. A historical overview of UWA communication with major milestones is presented in the next section followed by recent advances in this research field.

1.2 Historical Overview of Underwater Acoustic Communication

The earliest traces of underwater acoustics can be traced back to late 14^{th} century when renowned painter, polymath Leonardo Da Vinci is quoted for discovering the possibility of using sound to detect distant ships by listening to the noise they radiate into water. The practical applications of acoustic waves were however delayed until the beginning of the 20^{th} century. Starting in the World War I era, research efforts first focused on the design of sonars to detect obstacles for navigation and targets. The development of UWA communication was later in the era of World War II during which US navy deployed underwater telephones for communication with submarines. This first UWA telephone operated at 8.3 kHz and used single-side band suppressed carrier (SSB-SC) amplitude

modulation [10]. Until 1980's, the research efforts on UWA communication were mainly dominated by military applications. Following the advances of digital signal processing (DSP) and very-large-scale integration (VLSI) technologies, new generations of digital UWA communication systems were introduced targeting a variety of applications for the civilian market.

In the 1980's, it was commonly believed that the time variability and the dispersive multipath propagation characteristics of the ocean would not allow the use of phase-coherent modulation techniques such as phase-shift keying (PSK) and quadrature amplitude modulation (QAM). The prevailing design choice for modulation in acoustic modems at that time was frequency-shift keying (FSK) [11]. It is well known that FSK suffers from bandwidth inefficiency. Encoupled with the limited bandwidth availability of the underwater channel, FSK becomes a bottleneck limiting the operation of UWA communication systems at very low rates, which is unacceptable for many applications.

In the 1990's, with increasing demands for higher data rates, research focus shifted towards design of coherent acoustic modems. One approach towards this purpose was to employ differentially-coherent detection to ease the problematic carrier recovery in UWA channels. However, differential techniques inevitably result in performance degradation with respect to coherent detection. In [11], Stojanovic et al. adopted "purely" phase-coherent detection and designed a receiver built upon adaptive joint carrier synchronization and equalization. The maximum likelihood (ML) algorithm for such a joint estimator suffers from excessive complexity particularly for the underwater channel characterized by long channel impulses. Therefore, as a low-complexity solution, the receiver algorithm in [11] adopts a decision feedback equalizer (DFE) whose taps are adaptively adjusted using a combination of a recursive least squares (RLS) algorithm and a second-order phase locked loop (PLL). Since the seminal work of Stojanovic et al. in [11], there has been a growing interest on phase-coherent UWA communication systems. Much research effort has particularly focused on the design of low-complexity equalization schemes, which is a key issue for underwater channels with large delay spreads. Particularly, sparse channel estimation/equalization and turbo equalization have been investigated by several research groups, e.g., see [12] and the references therein.

1.3 MIMO UWA Communications

Emerging data-heavy underwater applications impose further requirements on UWA communication system design. To address such challenges, recent advances in terrestrial wireless RF systems have been further exploited in the context of UWA communication. One of the research breakthroughs in the last decade is multiple-input multiple-output (MIMO) RF communications. MIMO systems involve the deployment of multiple antennas at the transmitter and/or receiver side and achieve significant improvements in transmission reliability and throughput. Such systems exploit the spatial dimension of the wireless channel to extract diversity advantages and/or multiplexing gains. In a spatial multiplexing scheme, independent encoded streams of data are transmitted from multiple transmit antennas [13] and a multiplexing gain as high as the number of transmit antennas can be obtained. Some well-known spatial multiplexing schemes are Bell labs layered space-time (BLAST), diagonal layered space-time (DLST), threaded layered space-time (TLST) [14, 15], and linear dispersion codes (LDC) [16, 17].

Space-time coding (STC) is a systematic treatment to encode signals at transmitter as an open-loop transmit diversity scheme. Space-time coded systems can be used with multiple receivers antennas leading to a MIMO system. The primary criterion in STC design is to maximize diversity gain, which is the slope of performance curve at high signal-to-noise ratio (SNR). There are several classes of space-time codes. One well-known category of STC is space-time block code (STBC). Alamouti in [18] introduced the first orthogonal STBC design using two transmit antennas. Extension of STBCs to multiple transmit antennas is presented by Tarokh et al. in [19] using the theory of orthogonal designs based on the historical work of Randon and Hurwitz in this branch of mathematics [20]. Space-time trellis codes (STTCs) are able to provide additional coding gains [21] besides the spatial diversity. Initial STTC designs are hand-made, but additional designs can be found in [22–25]. Spatial modulation in MIMO systems avoids inter-channel interference and achieves higher multiplexing gain by spatially mapping the index of each antenna to a block of information bits [26].

MIMO UWA communication has been extensively investigated in the literature. In [27], Song and Ritcey consider a MIMO underwater system with spatial diversity equalizer

(SDE) to increase the effective channel bandwidth and minimize the mean square error (MSE). They apply saddle point integration method to the MIMO channel and compute the probability of error and show that effective bandwidth of MIMO channel increases using joint MIMO equalizers. In [28], Kilfoyle et al. deploy spatial modulation technique to increase the reliable data rate in MIMO UWA communication system. They obtain higher data rate and throughput compared to the temporal modulation techniques. They observe over 5 dB space-time coding gain and near doubling of capacity. In [29], Song et al. present some experimental results of MIMO underwater system with time reversal (TR) communications. They consider different modulation schemes and 1 kHz bandwidth at a range of 8.6 km in 105 m deep water. They show that two-way TR process significantly reduces inter-symbol interference (ISI) inherent in the multipath ocean environment. They observe that an increase in the information rate and spectral efficiency can be further improved by higher-order constellations.

In [30], Roy et al. investigate STC for underwater systems. They use iterative decoding technique at the receiver to obtain high data rates and reliable communication over shallow-water medium-range UWA channel. Particularly, they apply STTCs and layered space-time (LST) codes with adaptive equalizer and obtain high data rate with reliable transmission. They have further confirmed their findings from UWA communication experiments in the Pacific Ocean. In [31], Roy et al. analyze error rate performance for MIMO UWA communication system. They propose a sparse partial response equalizer (SPRE) matching the channel characteristics to mitigate ISI effects and maintain reliable communication. Their proposed SPRE outperforms the conventional DFE proposed under various conditions. In [32], Tao et al. propose a robust detection scheme for MIMO UWA communication systems. They adopt turbo block DFE where the equalizer cancels ISI in the time-domain and multiplexing interference in the space domain successively. They observe that MIMO with block DFE outperforms MIMO systems with linear equalizers and DFE. Furthermore, they confirm their finding using experimental data taken place in the Gulf of Mexico.

1.4 Cooperative UWA Communications

Deployment of multiple antennas at transmitter and/or receiver might not be feasible in some applications due to limitation in size, power, and hardware complexity in end-user devices. Cooperative communications, also known as cooperative diversity or user cooperation has been proposed as a powerful alternative fading-mitigation technique. Cooperative diversity takes advantage of the broadcast nature of wireless transmission where a transmitted signal can be overheard by many unintended nodes. If these unintended nodes (or relays) are willing to share their resources with the source node, they can together create a virtual antenna array to extract the spatial diversity in a distributed fashion. The concept of cooperative communications can be traced back to Van der Meulen's earlier work [33] on relay channels. The recent surge of interest however has followed after the works of Laneman et al. and Sendonaris et al. [34–38].

In [39], Sendonaris et al. propose a cooperative scheme for in-cell mobile users which increase data rate and uplink capacity. This advantage in higher data rate can be sacrificed to reduce power consumption per user or extend cell coverage with the expense of extra complexity at receiver. In [34], Laneman and Wornell develop transmission protocols for amplify-and-forward (AF) and decode-and-forward (DF) relaying assuming single relay. In their cooperation scheme, transmission is carried in two phases: broadcasting and relaying phases. In the broadcasting phase, source node (or user) broadcasts its information to intended destination node (base station (BS) or another user) and other nodes, i.e., relay nodes, located within transmission range of source node. In the relaying phase of AF scheme, relay nodes amplify the received information signal and forward it to the destination node. Hence, destination node receives two faded versions of information, i.e., from broadcasting and relaying phases. In the DF scheme, broadcasting phase is identical to AF scheme; however, in the relaying phase, relay node decodes the received signal and then transmits it to destination node.

For multi-relay deployment, Laneman et al. [35, 36] consider space-time coded and repetition-based cooperative protocols. Repetition-based cooperative protocol provides full spatial diversity at the price of decreasing bandwidth efficiency as the number of cooperating nodes increases. In relaying phase, relay nodes operating under repetition-based

scheme transmit information on orthogonal subchannels. Space-time coded cooperative protocol is an alternative methodology to attain full spatial diversity without sacrificing bandwidth efficiency. In relaying phase, relay nodes use space-time coding among themselves and transmit simultaneously on the same subchannel [35].

After the works in [35–38], a large number of publications have appeared in the area of cooperative communications investigating variety of topics such as information theoretic bounds, cooperation protocols, distributed space-time code design, distributed source coding, optimum power allocation, cross-layer design etc. among others. Detailed surveys of various issues in cooperative communication systems can be found in recent books [40, 41].

Current literature on cooperative communication focuses on terrestrial RF systems. There have been some recent works which apply the principles of cooperative communications in underwater applications. In [42], Vajapeyam et al. adopt TR distributed STBC in an underwater cooperative system. They assume quasi-static Rayleigh fading for channel taps, neglect multipath components beyond few symbols and, based on these assumptions, numerically evaluate bit error rate (BER). Carbonelli and Mitra [43] numerically evaluate the BER of a multi-hop cooperative system using Markov chain analysis over quasi-static Rayleigh fading channel. On the other hand, Yerramalli and Mitra [44] consider a time-varying channel and derive a lower bound on detection error using Hammersley Chapman Robbins Bound (HCRB) for a cooperative multi-carrier system.

In [45], Zhang et al. have investigated a DF type protocol with spatial reuse and periodic transmit/receive schedules for linear multi-hop UWA communication networks. They have considered the frequency dependent signal attenuation, interhop interference, half-duplex constraint, and large propagation delays in their analysis. They have demonstrated an improved performance in multi-hop UWA communication networks. In [46], Cao et al. have investigated channel capacity of relay-assisted UWA communication and discussed time synchronization issues. They have further looked into the effects of source to destination distance, transmit power allocation, and relay location on channel capacity for relay-assisted UWA communication systems. They have observed a capacity increase in relay-assisted UWA communication systems compared to the traditional direct link communication.

1.5 Multi-Carrier UWA Communications

Although cooperative systems successfully exploit the spatial dimension in a distributed manner, their practical implementation over frequency-selective channels (as encountered in underwater channels) is challenging considering the potential high complexity of spatio-temporal equalizers in a single-carrier architecture. A powerful alternative is multi-carrier communication, particularly in the form of orthogonal frequency division multiplexing (OFDM). In an OFDM system, high-rate data stream is spread over a number of orthogonal frequency subcarriers or sub-channels. Then, data sub-streams are modulated using a proper digital modulation scheme at a lower data rate.

The main advantage of OFDM over the conventional single-carrier communication systems is its immunity to time-spread of signals caused by the multipath propagation channels. These channels cause frequency-selective fading that requires complicated equalization filters and techniques. However, with the OFDM technique, sub-streams of low data rate can use a guard interval to overcome the time spreading effects caused by the frequency-selective channel. Consequently, this will eliminate the ISI effects.

The attractive features of OFDM endorse it as a powerful technique for UWA communication; and it has been recently studied in the UWA literature. In [47], Mason et al. propose OFDM technique to facilitate detection, synchronization and Doppler scale estimation in UWA communication systems. They characterize the receiver operating characteristic in terms of false alarm probability and probability of detection. They further evaluate BER for their scheme and show that it outperforms conventional linearly-frequency-modulated (LFM) waveforms preambles. In [48], Huang et al. propose nonbinary low-density parity-check (LDPC) codes for multicarrier OFDM underwater communication. They evaluate the performance in terms of block error rate of regular and irregular LDPC codes and show that they outperform several convolutional codes.

In [49], Kang and Iltis consider several receiver structures to mitigate carrier frequency offset (CFO) in OFDM underwater communication. They evaluate the convergence behavior of their iterative receivers using extrinsic information transfer (EXIT). They further demonstrate the BER performance of OFDM receiver through numerical simulations and experimental data. In [50], Leus and Walree propose multiband OFDM technique for un-

derwater communication at low SNR ratio for covert applications. In their multi-band OFDM approach, the available frequency band is divided into smaller sub-bands where each sub-band is modulated using OFDM. Their proposed receiver reduces the complexity compared to single-band OFDM technique. They demonstrate BER performance through numerical simulation under different underwater conditions.

1.6 Effect of Doppler Distortion in UWA Channels

Motion of transmitter and/or receivers, e.g. in AUVs, cause motion-induced Doppler effects in UWA communication systems. Even drifting by waves, currents, and tides may induce considerable Doppler effects that require compensating at the receiver design [9]. Let the transmitted signal be donoted by $p(t)$ with a duration T and bandwidth B. The Doppler effect distorts the signal in two ways: a time-scale of the signal, which is called *motion-induced Doppler spreading* and a frequency offset known by *Doppler shift*. The time-scale of $p(t)$ is by a factor $(1 + a)$, where a stands for Doppler factor and is given by $a = v/c$. Here, v is the velocity of the transmitter or receiver and c is the speed of sound in water. The received signal therefore has a duration $T/(1 + a)$ and a bandwidth of $B(1 + a)$. The frequency offset affecting $p(t)$ is af_c, where f_c is the carrier frequency.

In single-carrier UWA communication systems, Doppler shift is estimated and Doppler rate a is computed at the receiver. Then, the signal is resampled to perform delay synchronization through decompressing the signal in time [9]. This technique is used adaptively to compensate for the variations in UWA channel conditions. In multicarrier UWA systems, with narrowband assumption, Doppler shift appears almost the same for all the subcarriers. However, in wideband acoustic systems, Doppler effect causes non-uniform frequency shifting. This occurs when the signal bandwidth is much larger than each subcarrier frequency; hence, the subcarriers are attenuated by significantly various Doppler shifts. In RF systems, the motion-induced Doppler spreading effect, i.e. time-scaling of transmitted pulse, is neglected due to the relatively low Doppler factors in highly mobile systems. However, these systems experience Doppler shift (or frequency offset) that results from the mismatch between local oscillators, or transmitter/receiver motion. For wideband RF communication systems, e.g. OFDM-based ultrawideband systems, subcarriers are shifted

by different factors causing non-uniform frequency shifting.

Some authors [47, 51–53] assume Doppler factor is approximately the same for all distinct paths, which is not realistic but considered as a simplification for the analysis and receiver design. In [51], Li et al. consider zero-padded (ZP) OFDM communication over wideband UWA channels with non-uniform Doppler shifts. They propose to compensate for the Doppler effect through resampling first and then perform uniform compensation for the residual Doppler. They assume in their analysis a common Doppler factor on all propagation paths. They have also assumed that path delays, gains, and Doppler scaling factor are constant over the OFDM symbol and guard interval duration. They have observed through experimental results a good performance when transmitter and receiver are moving at relative speeds up to 10 knots in shallow-water environment.

Mason et al. in [47] consider ZP-OFDM for data transmission and two identical OFDM symbols and a cyclic prefix (CP) for synchronization over UWA channel. They propose a synchronization algorithm based on a bank of self-correlators where each one is matched to a different periodicity. They assume that all paths have a similar Doppler scaling factor and that path gains, delays, and Doppler scaling factor are constant over preamble duration. In testing proposed algorithm, they assume both non-dispersive and dispersive channels. For dispersive channels, exponentially decaying channel profile is chosen that loses around 20 dB within 10 ms. Performance of their proposed algorithm is quantified by probability of detection and false alarm. They have also evaluated BER and tested their results based on experimental data of [51].

In [54], Huang et al. study single-input single-output (SISO) ZP-OFDM underwater communication system. They propose a progressive iterative receiver based on the turbo principle to mitigate intercarrier interference (ICI). Their receiver adapts to channel conditions to account for the cases of same Doppler factor (ICI-ignorant) or different Doppler factors (rates) in all paths (ICI-aware).

Yerramalli and Mitra in [55] consider SISO CP-OFDM underwater communication system. They investigate the effect of using single resampling operation with the assumption of single Doppler scale, when the channel paths have different Doppler scaling values. They observe that optimal resampling parameter is close to the Doppler scale of the path with largest signal energy. Further, they notice that when the received signal has comparable

energy on the different paths, optimal resampling results in significant performance gain.

In [56], Wang et al. consider SISO ZP-OFDM with raised-cosine pulse shaping window for underwater communication. They propose frequency-domain oversampling to improve the system performance. They observe that receivers with frequency-domain oversampling outperform conventional time-domain ones considerably. They further observe an increase in the gain as the Doppler spread increases.

There are some works in the literature that analyze the Doppler distortion in MIMO underwater communication systems [30, 57, 58]. In [57], Carrascosa and Stojanovic study adaptive channel estimation exploiting frequency and time correlation for MIMO underwater systems. They also include an algorithm for non-uniform Doppler prediction and tracking. Performance results shown are based on experimental data for several shallow-water environments. Tu et al. in [58] consider a two-user MIMO-OFDM system where two independent source nodes communicate with a destination node with two receiving elements. They propose multiple resampling structure for multipath channel with path-specific Doppler scaling. They observed performance gain over conventional detection techniques with a moderate additional complexity.

There are only sporadic works [42,44,59] on analyzing cooperative UWA systems where the channel models include the non-uniform Doppler effects. In [42], Vajapeyam et al. study cooperative communication with distributed space-time coding over UWA channel. They consider AF relays and time-reversal STBC. Ray-based underwater channel model is deployed as in [60,61] and DFE is used at receiver. They considered Doppler spread effect, i.e. time variations of the underwater channel; however, they ignore Doppler shift, time-scaling, in their system model. Recently, Wang et al. in [59] have investigated physical-layer network coding in a two-way relay underwater network. They consider iterative receivers and assume that the source and destination nodes are either stationary or moving with similar velocities. In their simulation analysis, they assume Rayleigh fading channel with time variation caused by distinct Doppler scaling factors over the paths. They observe through simulation and experimental results a considerable improvement in performance with iterative decoding.

1.7 Contributions

Building on the promising combination of OFDM and cooperative communication, this thesis investigates the fundamental performance bounds of cooperative OFDM UWA communication systems, considering the inherent unique characteristics of the UWA channel and demonstrate the effect of several system and channel parameters on the performance. It also discusses relay selection strategies over UWA channels in the presence of Doppler distortion.

In Chapter 2, we present an overview of characteristics of the UWA channels including large-scale path loss, small-scale fading and ambient noise. Within this chapter, we also propose an approximate statistical model for the non-stationary ambient noise. The proposed model allows mathematical tractability and is a good fit for most operating frequencies in practical UWA communication systems.

In Chapter 3, we derive closed-form expressions for the outage probability of precoded OFDM cooperative system with AF relaying over UWA channel. We assume orthogonal cooperation protocol and consider different assumptions on the availability of colored ambient noise information at the receiver side. If the covariance matrix of ambient noise is unknown to the receiver, we assume that the communication system is designed with the ability to operate in the worst-case scenario and treat the noise as white Gaussian. On the other hand, if noise covariance matrix is known at the receiver, the received signals are first applied to a whitening filter to remove the effects of correlated noise. Using the derived expressions, we investigate the effect of several system and channel parameters such as relay location, underwater temperature, carrier frequency, and noise correlation on the performance [62–64]. In Chapter 4, we return our attention on DF relaying and derive closed-form expressions for the outage probability of cooperative OFDM systems over UWA channel under the assumptions of both known and unknown covariance of ambient noise.

In Chapter 5, we consider three cooperation protocols that vary in degrees of broadcasting and collision. Under the assumption of DF relaying, we derive the maximum achievable sum-rate expressions and common/individual outage capacity regions for these three protocols. We further demonstrate the effect of several system and environmental parameters

on the outage capacity regions [63–65].

In Chapter 6, we investigate a multi-relay cooperative system over UWA channels with non-uniform Doppler distortion. We propose different receiver structures and demonstrate their performances through extensive Monte Carlo simulation results [66].

Chapter 2

Channel Model

In this chapter, we present an overview of characteristics of the underwater acoustical channels including large-scale path loss, small-scale fading and ambient noise. We further propose an approximate statistical model for the non-stationary ambient noise. The proposed model allows mathematical tractability and is a good fit for most operating frequencies in practical UWA communication systems.

2.1 Large-Scale Path Loss in UWA Channels

In this section, we discuss the inherent characteristics of the UWA channel emphasizing the main differences and similarities with the well-known RF channel models. The path loss in an UWA channel results from spreading and absorption losses. When an acoustic signal propagates away from its source, the wavefront occupies an increasingly larger surface area. Therefore, with the increasing propagation distance, the wave energy per unit surface decreases which is known as spreading loss. Absorption loss, on the other hand, results from the signal energy being converted to heat in the water. Let s and $a(f)$ denote the spreading factor and absorption coefficient, respectively. The overall path loss[1] in dB is

[1]If the performance estimate in a specific geographical location is required, Bellhop software can be used assuming that one has access to some detailed information such as boundary conditions, general bathymetry, refracting sound speed profile, grazing angle, weather conditions, source angle, receiver angle, etc.

given by

$$L_U = 10\, s\, \log_{10} d_{\mathrm{SD}} + 10\, d_{\mathrm{SD}} \log_{10} a(f) \tag{2.1}$$

where d_{SD} is the distance between the transmitter and receiver. The spreading factor depends on the geometry of propagation and a spreading factor of 1.5 is often taken as representative of practical spreading based on a partially bounded sphere. The absorption coefficient $a(f)$ is a function of frequency as well as pressure, temperature, salinity and acidity. Moreover, viscosity of pure water, relaxation of magnesium sulphate ($MgSO_4$), and relaxation of boric acid ($B(OH)_3$) mainly contribute to sound attenuation at frequencies 100 Hz-100 kHz. Several empirical formulas have been developed over the years for the characterization of the absorption coefficient including Schulkin-Marsh [67], Thorp [68], Mellen-Browning [69], Fisher-Simmons [70], and Francois-Garrison [71, 72]. A comparison of different models can be found in Table 2.1.

Table 2.1: Formulas for the calculation of sound absorption coefficient.

	Frequency-range	**Related parameters**	**Field measurement locations**	**Laboratory measurements**
Schulkin-Marsh (1962)	2 kHz - 25 kHz	Frequency, temperature, salinity, and pressure	North Atlantic Ocean	Yes
Thorp (1965)	100 Hz - 10 kHz	Frequency	Bahamas (500 miles between Bermuda and Eleuthera Island)	No
Mellen-Browning (1976)	$\leq$ 10 kHz	Frequency	North and South Pacific Ocean	No
Fisher-Simmons (1977)	10 kHz - 400 kHz	Frequency, temperature, and pressure	N/A	Yes
Francois-Garrison (1982)	200 Hz - 1 MHz	Frequency, temperature, salinity, depth, and acidity	Arctic, Northeast Pacific Ocean, Atlantic Ocean, Mediterranean, Red Sea, and Gulf of Aden	Yes

Thorp's formula is widely used in the literature mainly due to its simplicity. However, this formula is merely a function of frequency and ignores other parameters of the acoustic channel. The most comprehensive formula for the absorption coefficient is that of Francois-Garrison's (FG) [71] and applies for the frequency range of 200 Hz-1 MHz. In their initial work [71], Francois and Garrison consider the effect of pure water and magnesium sulphate for high-frequency region. They later extend their work in [72] to include the effect of boric acid on sound absorption in low-frequency region, i.e. 200 Hz-10 kHz. They verify their empirical formula with measurements from various oceans and compare further with Schulkin-Marsh [67] and Fisher-Simmons [70] at different frequencies. They observe that above 10 kHz their expression is in agreement with Fisher-Simmons equation more than

Schulkin-Marsh equation with maximum difference of 20%. It has better agreement with Schulkin-Marsh equation in below 1 kHz in warm waters. They also observe that the proposed formula is accurate in absorption prediction over most ocean conditions and over frequencies of interest.

Francois and Garrison formula for absorption coefficient, $\alpha(f)$ in dB/km, is given by [72]

$$\alpha\left(f\right) = \frac{A_1 P_1 f_1}{f^2 + f_1^2} f^2 + \frac{A_2 P_2 f_2}{f^2 + f_2^2} f^2 + A_3 P_3 f^2 \tag{2.2}$$

where boric acid $\mathrm{B(OH)_3}$ contribution is quantified by

$$A_1 = \frac{8.86}{c} 10^{(0.78 \text{ pH } -5)}, \tag{2.3}$$

$$P_1 = 1, \tag{2.4}$$

$$f_1 = 2.8\sqrt{\frac{S}{35}} 10^{(4-1245/(273+T_\mathrm{u}))}. \tag{2.5}$$

In the above, c is the speed of sound in m/s under the water, which is approximately

$$c = 1412 + 3.21 T_\mathrm{u} + 1.19 S + 0.0167 D, \tag{2.6}$$

and T_u is the temperature in Celcius (°C), pH is the acidity, S is the salintiy (‰), D is the depth in meters. The contribution of magnesium sulphate $\mathrm{MgSO_4}$ is quantified by

$$A_2 = 21.44 \frac{S}{c} \left(1 + 0.025 T_\mathrm{u}\right), \tag{2.7}$$

$$P_2 = 1 - 1.37 \times 10^{-4} D + 6.2 \times 10^{-9} D^2, \tag{2.8}$$

$$f_2 = \frac{8.17 \times 10^{(8-1990/(273+T_\mathrm{u}))}}{1 + 0.0018(S - 35)}. \tag{2.9}$$

Pure water contribution for temperature $T_\mathrm{u} \leq 20$ °C is

$$A_3 = 4.937 \times 10^{-4} - 2.59 \times 10^{-5} T_\mathrm{u} + 9.11 \times 10^{-7} T_\mathrm{u}^2 - 1.5 \times 10^{-8} T_\mathrm{u}^3. \tag{2.10}$$

On the other hand, for temperatures $T_\mathrm{u} > 20$ °C, the contribution is

$$A_3 = 1 - 3.83 \times 10^{-5} D + 4.9 \times 10^{-10} D^2. \tag{2.11}$$

In Figure 2.1, we evaluate the sound absorption coefficient for seawater and pure water for temperatures 0, 10 and 20 °C, depth of 0 m, salinity 35 ‰, and acidity of 8.0 pH according to the FG model. We observe that the sound absorption for sea water is larger than that in pure water. Furthermore, as we increase the temperature from 0 °C to 20 °C,

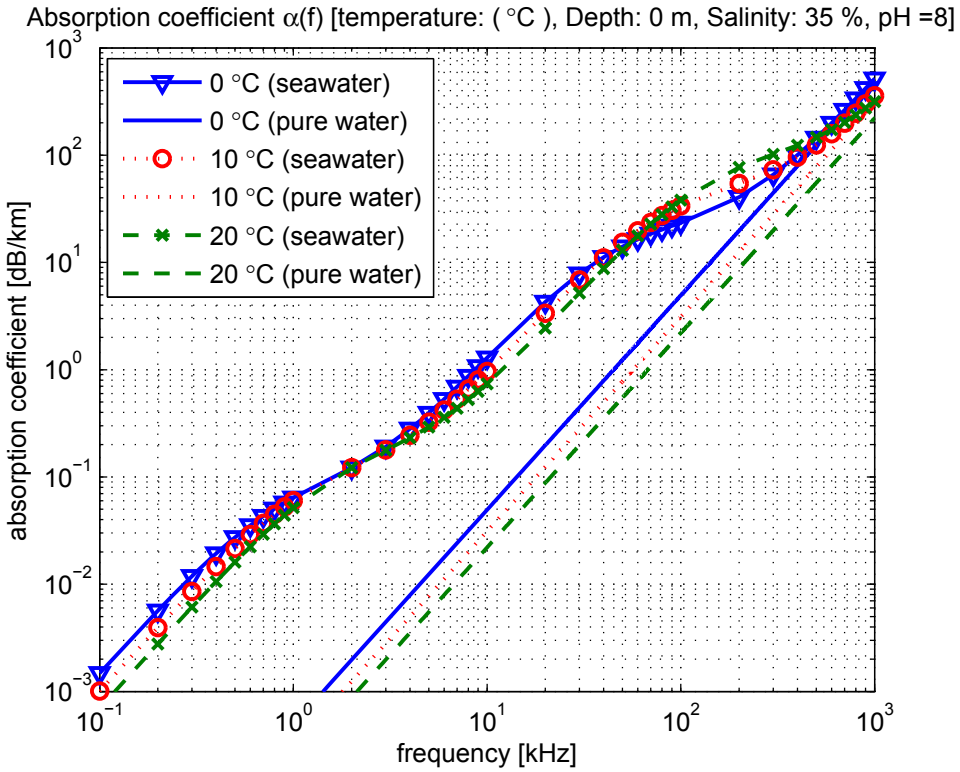

Figure 2.1: Absorption coefficient for pure and sea water assuming different temperatures.

the sound absorption will decrease for pure water. However, for sea water, decrease will be observed only for some frequency ranges, i.e. frequencies less than 40 kHz.

In Figure 2.2, we demonstrate the effect of practical parameters on the underwater path loss using (2.1). The absorption coefficient is calculated using (2.2) based on Francois-Garrison model. The distance between the transmitter and receiver is set to be 2 km. In the figure on the left, we consider UWA channel at depth of 50 m, acidity of 8 pH, salinity of 35 ‰ (or 35 parts per thousand (p.p.t.)), and practical spreading factor of 1.5. We observe that total acoustic path loss has a significant variation as we increase the carrier frequency in the practical range, i.e. 10-60 kHz. Furthermore, we investigate the path loss as temperature changes from -4 °C to 35 °C and observe significant variation at higher carrier frequencies.

For the figure on the right, we investigate the total underwater path loss in dB as function of salinity (p.p.t.) and acidity (pH). We consider a fixed carrier frequency of 15 kHz, temperature of 15 °C, depth of 50 m, practical spreading factor of 1.5, and a distance

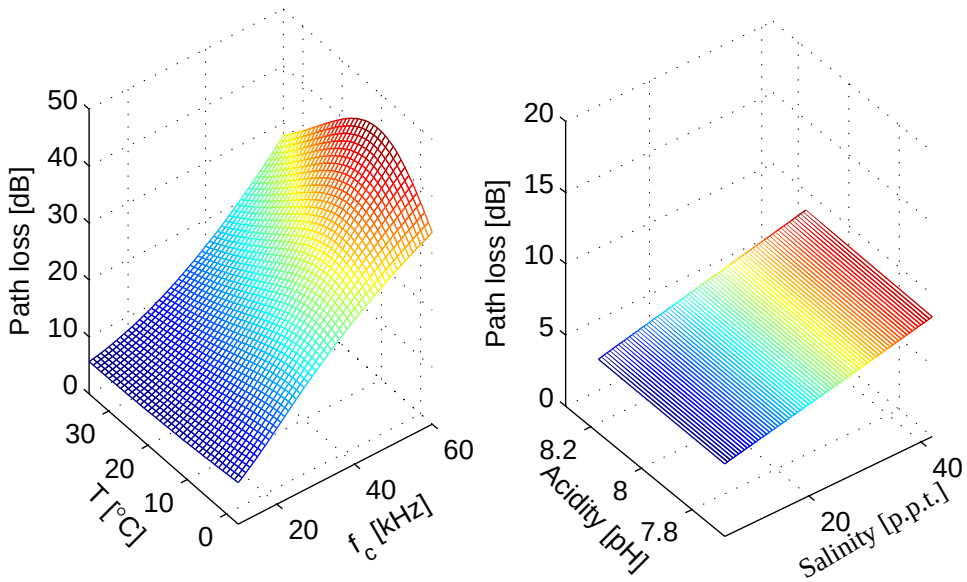

Figure 2.2: Effect of carrier frequency f_c in kHz, temperature in °C, salinity in p.p.t., and acidity in pH for a distance of 2 km.

separation of 2 km. We notice the variation in acoustic path loss as we increase the salinity from 5‰ to 42‰ and acidity from 7.67 pH to 8.3 pH. Normal salinity values could range from 33‰ to 37‰ in various oceans and seas and there is an insignificant change in the overall path loss. Similarly, we notice that variation in acidity is insignificant over the range of possible values.

2.2 Small-Scale Fading in UWA Channels

The average received power is determined by the path loss, but instantaneous level of the received power fluctuates as a result of small-scale fading effects due to multipath propagation in underwater environments. In shallow water, multipath occurs due to signal reflections from the surface, bottom, and any objects in the water. In deep water, it is primarily due to a phenomenon known as ray bending, i.e., the tendency of acoustic waves to travel along the axis of lowest sound speed. Regardless of its origin, multipath propagation causes multiple echoes of the transmitted signal to arrive at the receiver with different delays overlapping each other. This leads to a frequency-selective channel model where

distinct frequency components of the transmitted signal undergo different attenuations. The velocity of sound in underwater is around 1500 m/s. This relatively slow speed results in typical delay spreads of 10-100 milliseconds. These are four orders of magnitude higher than those typically experienced in RF channels. The UWA channel also exhibits sparse channel characteristics, therefore, the impulse response consists of a large number of zero taps since the channel energy is mainly localized around several small ranges of delays.

The resulting UWA channel is commonly modeled as a tapped-delay line model with tap gains modeled as stochastic processes with certain distributions and power spectral densities. Although there is not a general consensus within the research community about the theoretical distribution for statistical characterization of tap gains in underwater channels, the small-scale effects are often modeled as Rayleigh or Rician fading [73–77] while some studies suggest K-distribution [78] or chi-square distribution [79].

In [74], Catipovic et al. justify the use of Rayleigh fading model based on the measurements collected in Woods Hole Harbor. They measure the fading characteristic of group of continuous wave (CW) tones using Digital Acoustic Telemetry System (DATS) over short ranges. With the assumption of stationary time series, they observe that the fading has an envelope following Rayleigh distribution. In [73], Chitre provides a statistical model in medium and very shallow water in high frequency. He considers the eigenray amplitude as Rayleigh random process with the median based on ray theory [73]. Chitre considers 15 m water depth and a transmission range up to 1 km; moreover, single path and 2-path cases are compared with observation fading results. In 100 m range, he observes five distinguishable arrivals corresponding to direct, surface-reflected, and multiple surface-bottom interaction. Proposed statistical model is further justified with experimental measurements in [80]. In addition, Catipovic in [81], and Galvin and Coates in [82] support the choice of Rayleigh to model small-scale effects in UWA channels.

Several researchers further consider Rician fading model for UWA channel [75–77, 83–90]. In [83], Urick proposes Rician model to describe amplitude fluctuations for received signals in oceans and conducts model verification by fitting experimental field data. He validates the proposed Rician model by showing that distribution of data sample groups obeys Rician distribution reasonably well. In [77], Jourdain uses the Rician model and characterizes underwater channels by time-bandwidth product and fading rate. He fur-

ther verifies the accuracy of the proposed model with experimental measurements using Kolmogorov-Smirnov test. In [76], Geng and Zielinski model acoustic channel with distinct eigenpath signals that are characterized by signal-to-multipath ratios with envelopes following Rician fading model. In [84], Bjerrum-Niese et al. propose a turbulent shallow-water channel model based on the Rician fading model. They use $\Phi - \Lambda$ method to characterize the fluctuations of the acoustic medium which can be found in [91], then use Pearson's skew-kurtosis chart along with numerical tests to deduce the validity of Rician distribution model.

Considering the availability of recent experimental works supporting the validity of Rician model and further noting that Rician model includes Rayleigh as a special case, we will consider Rician distribution in our work to model the small-scale UWA fading effect. Specifically, we represent a frequency-selective sparse channel by an L^{th}-order finite impulse response (FIR) filter as $\mathbf{h} = [h(v_0)\ 0\ ...\ 0\ h(v_i)\ 0\ ...\ h(v_{L_s})]^T_{(L+1)\times 1}$ where $\mathbf{v} = [v_0\ ...\ v_i\ ...\ v_{L_s}]$ corresponds to location of significant channel delay taps with $L \gg L_s$. Each channel delay tap is assumed to be a complex Gaussian random variable with independent real and imaginary parts with mean $\mu_m/\sqrt{2}$ and variance σ_m^2, $m \in \mathbf{v}$ leading to a Rician fading model. Let $\Omega_m = E\left[|h(m)|^2\right] = \mu_m^2 + 2\sigma_m^2$ denote the power of the m^{th} tap where $\sum_m \Omega_m = 1$, $\forall m \in \mathbf{v}$ and the vector $\mathbf{\Omega}$ denotes the power delay profile (PDP). The Rician factor for the m^{th} tap is the ratio of the power in the mean component to the power in the diffuse component and is given by $k_m = \mu_m^2/2\sigma_m^2$. Therefore, each channel tap can be written as

$$h(m) = \sqrt{\frac{\Omega_m k_m}{k_m + 1}} \left(\frac{1+j}{\sqrt{2}}\right) + \sqrt{\frac{\Omega_m}{k_m + 1}}\, \widetilde{x}(m), \qquad m \in \mathbf{v} \tag{2.12}$$

where $\widetilde{x}(m)$ is a complex Gaussian random variable with zero mean and unit variance.

2.3 Ambient Noise Model

In UWA channels, there are many sources for ambient noise such as seismic events, shipping, thermal agitation, rainfall, sound waves by marine animals among others. According to the widely used Wenz model [92], there are four main noise sources each of which becomes dominant in different frequency ranges. In the frequency range below 10 Hz, turbulence in

the ocean and atmosphere is the primary noise source. In the frequency range between 10-100 Hz, noise caused by distant ship traffic dominates and is modeled by shipping activity factor sa, which takes values between 0 and 1 for low and high activity, respectively. Surface agitation caused by wind-driven waves becomes the major noise source in the frequency range of 100 Hz-100 kHz that spans the major operating frequencies in UWA communication systems. The wind speed w is the main determining parameter for this type of noise. At frequencies above 100 kHz, thermal noise as a result of the molecular motion in the sea becomes the dominating factor.

Ambient noise power spectral density (PSD) for UWA channel in dB re 1μPa per Hz is given in [92] is given by

$$10\log_{10} N_t(f) = 17 - 30\log_{10} f, \tag{2.13}$$

$$10\log_{10} N_s(f) = 40 + 20\,(sa - 0.5) + 26\log_{10} f - 60\log_{10}(f + 0.03), \tag{2.14}$$

$$10\log_{10} N_w(f) = 50 + 7.5w^{1/2} + 20\log_{10} f - 40\log(f + 0.4), \tag{2.15}$$

$$10\log_{10} N_{th}(f) = -15 + 20\log_{10} f \tag{2.16}$$

where $N_t(f)$, $N_s(f)$, $N_w(f)$, and $N_{th}(f)$ respectively denote turbulence noise PSD, shipping noise PSD, waves noise PSD, and thermal noise PSD with f in kHz. Total ambient noise PSD, $N(f)$, for underwater channel is the sum of different spectral densities and expressed as

$$N(f) = N_t(f) + N_s(f) + N_w(f) + N_{th}(f) \tag{2.17}$$

In Figure 2.3, we present $N(f)$ considering different shipping activities factors $0 \leq sa \leq 1$ and various wind speeds. Although a white Gaussian noise assumption is dominantly used in the literature (mainly for simplification purposes), it is apparent from Figure 2.3 that PSD significantly changes over the considered frequency range and exhibits a non-white nature. Even, in the frequency range of 10-100 kHz where most current practical UWA communication systems operate, non-white nature of the noise is obvious and should be considered for a realistic performance analysis and system design/optimization.

For a tractable and practical noise model, we can approximate the overall noise PSD by considering only the PSD of the waves noise. However, resulting noise PSD represents a special class of random processes, namely, $1/f$ fractal random processes, where it is char-

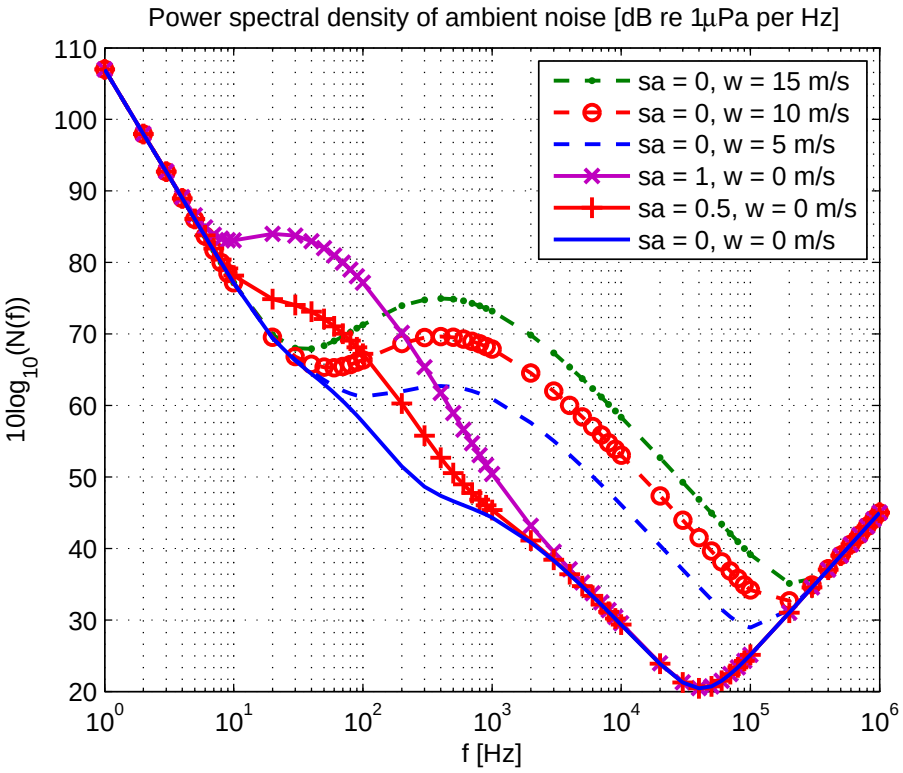

Figure 2.3: PSD of ambient noise for different shipping activity factors and wind speeds.

acterized by fractional-power-law, self-similarity or fractal behavior [93, 94]. An example of such processes is $1/f$ noise [95] (pink noise) which is widely used to model the noise in many physical systems [96–98]. This type of noise has randomness between the white uncorrelated noise and Brownian motion noise where the increments are uncorrelated [97].

We propose to approximate the non-stationary random process of underwater ambient noise by a stationary process (see Appendix A). Following a similar approach as in [95], we assume the existence of a lowest frequency $\overline{f}_0$ below which the shape of the spectrum changes such that the integral of PSD would converge [95]. In the literature, ambient noise in underwater channels is assumed to be stationary due to small variations of sources of ambient noise over short period of times [99]. Hence, we can obtain the approximate continuous PSD of complex-valued equivalent baseband ambient noise as

$$N(f) \approx \frac{\overline{f}_0 \sigma_n^2}{\pi \left(f^2 + \overline{f}_0^2 \right)} \tag{2.18}$$

where f is the frequency in kHz, $\sigma_n^2 = E\left[n(t)n^*(t)\right]$ is the variance of the zero-mean complex

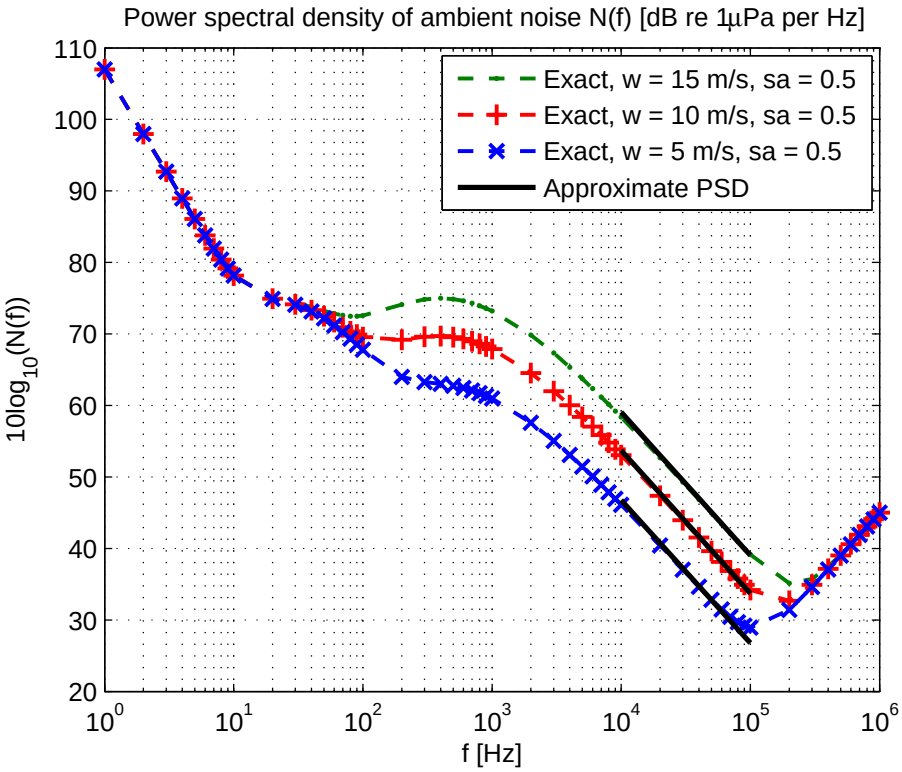

Figure 2.4: Exact and approximate ambient noise PSDs for various wind speeds.

Gaussian random process (depending on the wind speed) and $\overline{f}_0$ is the lowest frequency at which the shape of the spectrum changes to yield finite integral of approximate PSD. The autocorrelation function using Wiener-Khintchine theorem is given by

$$R_n(\tau) = \sigma_n^2 \exp\left(-2\pi \overline{f}_0 |\tau|\right), \qquad \forall \tau \in \mathbb{R}. \tag{2.19}$$

In Figure 2.4, we illustrate this approximate PSD and confirm a close match between the approximate and exact PSDs in the region of 10-100 kHz for various wind speeds.

Chapter 3

Outage Performance of Cooperative Multicarrier UWA Communication with AF Relaying

In this chapter, we investigate the outage performance of AF cooperative OFDM system over UWA channels based on the availability of the statistics of ambient noise. We derive closed-form expressions for the outage probability and outage capacity of the cooperative OFDM UWA system. Through numerical results, we demonstrate a close match between derived expressions and the exact outage performance. We observe that AF cooperative UWA system brings improvements and outperforms the direct transmission at high SNR values. Moreover, we study the effect of relay location, operating frequency, availability of ambient noise statistics, and underwater temperature on the outage performance.

3.1 System Model

We consider a cooperative precoded OFDM communication system in a single-relay scenario. Figure 3.1 illustrates this three-node model where S, D, and R respectively denote source, destination and relay nodes.

Following the discussions in Section 2.2, we adopt an aggregate channel model that takes into account both large-scale path loss and small-scale fading effects. We assume frequency-

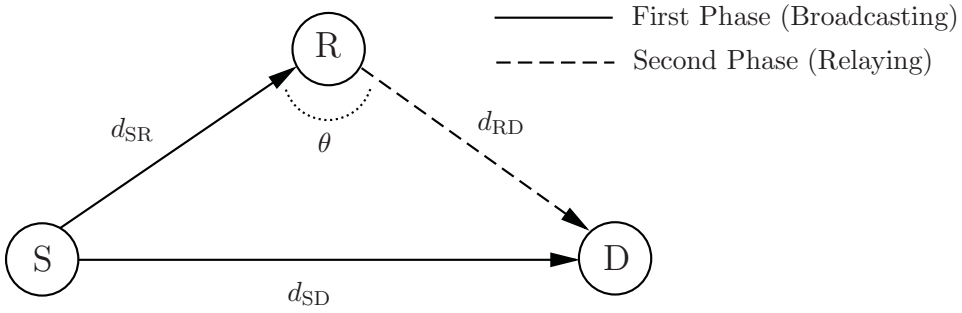

Figure 3.1: Three-node underwater system model.

selective sparse channels for source-to-destination (S $\rightarrow$ D), source-to-relay (S $\rightarrow$ R), and relay-to-destination (R $\rightarrow$ D) underwater links with intra-distances given by d_{SD}, d_{SR}, and d_{RD}. These channels are modeled by FIR filters with orders of $\tilde{L}_{\mathrm{SD}}$, $\tilde{L}_{\mathrm{SR}}$, and $\tilde{L}_{\mathrm{RD}}$ respectively. Let $\mathbf{h}_{\mathrm{AB}} = [h_{\mathrm{AB}}(v_{\mathrm{AB}}^0)\ 0 \ldots h_{\mathrm{AB}}(v_{\mathrm{AB}}^1) \ldots h_{\mathrm{AB}}(v_{\mathrm{AB}}^{L_{\mathrm{AB}}})]^T_{\left(\tilde{L}_{\mathrm{AB}}+1\right)\times 1}$. Further define $\mathbf{v}_{\mathrm{AB}} = [v_{\mathrm{AB}}^0\ v_{\mathrm{AB}}^1\ \ldots\ v_{\mathrm{AB}}^{L_{\mathrm{AB}}}]$ which denotes the locations of non-zero channel delay taps.

Each non-zero channel delay tap is modeled by a complex Gaussian random variable for a channel link A $\rightarrow$ B with independent real and imaginary parts having $\mu_{\mathrm{AB},n}/\sqrt{2}$ and $\sigma^2_{\mathrm{AB},n}$, $\forall n \in \{0, 1, \ldots, L_{\mathrm{AB}}\}$ as mean and variance, respectively. The power of the $(n+1)^{\text{th}}$ non-zero channel delay tap is denoted by $\Omega_{\mathrm{AB},n} = E\left[|h_{\mathrm{AB}}(v_{\mathrm{AB}}^n)|^2\right] = \mu^2_{\mathrm{AB},n} + 2\sigma^2_{\mathrm{AB},n}$ where $\sum_n \Omega_{\mathrm{AB},n} = 1$, $\forall n \in \{0, 1, \ldots, L_{\mathrm{AB}}\}$ and the PDP for channel link A $\rightarrow$ B is $\mathbf{\Omega}_{\mathrm{AB}}$. The ratio of the power in direct line-of-sight component to the power in scattered component is called the Rician factor and $k_{\mathrm{AB},n} = \mu^2_{\mathrm{AB},n}/2\sigma^2_{\mathrm{AB},n}$ represents the $(n+1)^{\text{th}}$ non-zero tap Rician factor. Hence, each non-zero channel delay tap is given by

$$h_{\mathrm{AB}}(v_{\mathrm{AB}}^n) = \sqrt{\frac{\Omega_{\mathrm{AB},n} k_{\mathrm{AB},n}}{k_{\mathrm{AB},n}+1}}\left(\frac{1+j}{\sqrt{2}}\right) + \sqrt{\frac{\Omega_{\mathrm{AB},n}}{k_{\mathrm{AB},n}+1}}\,\widetilde{\omega}_{\mathrm{AB}}(n), \quad n \in \{0, 1, \ldots, L_{\mathrm{AB}}\} \tag{3.1}$$

where $\widetilde{\omega}_{\mathrm{AB}}(n)$ is modeled by a zero mean and unit variance complex Gaussian random variable. Due to sparseness of typical underwater channels, we have $\tilde{L}_{\mathrm{SD}} \gg L_{\mathrm{SD}}$, $\tilde{L}_{\mathrm{SR}} \gg L_{\mathrm{SR}}$, and $\tilde{L}_{\mathrm{RD}} \gg L_{\mathrm{RD}}$.

We further define the geometrical gains for our cooperative underwater system using the law of cosines as a function of S $\rightarrow$ D link distance d_{SD} (in km), the ratio $\beta = d_{\mathrm{RD}}/d_{\mathrm{SR}}$ (in dB), and the angle θ (in radians) formed by S $\rightarrow$ R and R $\rightarrow$ D links. These geometrical

gains are given by

$$G_{\mathrm{SD}}(f) = d_{\mathrm{SD}}^{-s} a(f)^{-d_{\mathrm{SD}}}, \tag{3.2}$$

$$G_{\mathrm{SR}}(f) = \left((1+\beta^2-2\beta\cos\theta)/d_{\mathrm{SD}}^2\right)^{s/2} a(f)^{-\alpha_R}, \tag{3.3}$$

$$G_{\mathrm{RD}}(f) = \left((1+\beta^{-2}-2\beta^{-1}\cos\theta)/d_{\mathrm{SD}}^2\right)^{s/2} a(f)^{-\alpha_D} \tag{3.4}$$

where $\alpha_R = d_{\mathrm{SD}} \Big/ \sqrt{1+\beta^2-2\beta\cos\theta}$ and $\alpha_D = d_{\mathrm{SD}} \Big/ \sqrt{1+\beta^{-2}-2\beta^{-1}\cos\theta}$.

Our cooperative system builds upon the orthogonal cooperation protocol of [100] with AF relaying. The nodes operate in half-duplex mode due to the large difference between transmitted and received signal levels. In the first phase (i.e., broadcasting phase) of this cooperation protocol, the source broadcasts to the destination and the relay nodes. In the second phase (i.e., relaying phase), the relay node forwards the received signal to the destination. The destination node uses the received signals over two phases to make the decision on the transmitted signal.

The main processing steps in our system can be summarized as follows: At the source node (see Figure 3.2), the input signal vector $\mathbf{x}$ is first applied to a linear constellation precoder $\mathbf{\Phi}$ satisfying $\mathrm{Tr}\{\mathbf{\Phi}\mathbf{\Phi}^H\} = N$ where N denotes the number of subcarriers. The resulting OFDM symbol $\mathbf{\Phi x}$ is applied to a serial-to-parallel converter followed by an inverse fast Fourier transform (IFFT) block. The parallel stream is converted back into a serial stream and CP of length $L_c = \max\left(\tilde{L}_{\mathrm{SD}}, \tilde{L}_{\mathrm{SR}}, \tilde{L}_{\mathrm{RD}}\right)$ is added to prevent interblock interference.

During the broadcasting phase, the source node transmits this signal which is received by the destination node D and relay R in the presence of fading and noise. At the relay node, it performs an appropriate power scaling on the received signal and forwards it to the destination node. The destination node (see Figure 3.3) makes the decision using the received OFDM blocks over broadcasting and relaying phases. After CP removal and fast Fourier transform (FFT) processing, the resulting signals are applied to a whitening filter (to remove the effects of correlated ambient noise) under the assumptions of the availability of noise covariance at the receiver side and finally applied to a maximum likelihood detector.

At the relay node, the received OFDM symbol corrupted by small-scale fading and

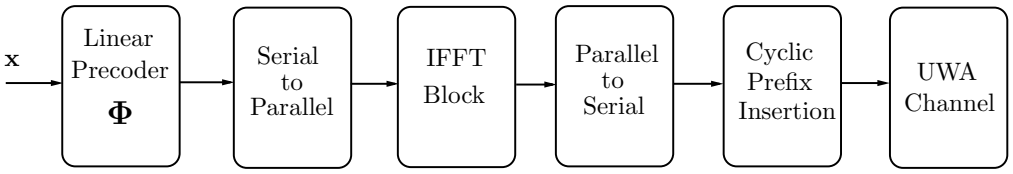

Figure 3.2: OFDM block diagram at source node.

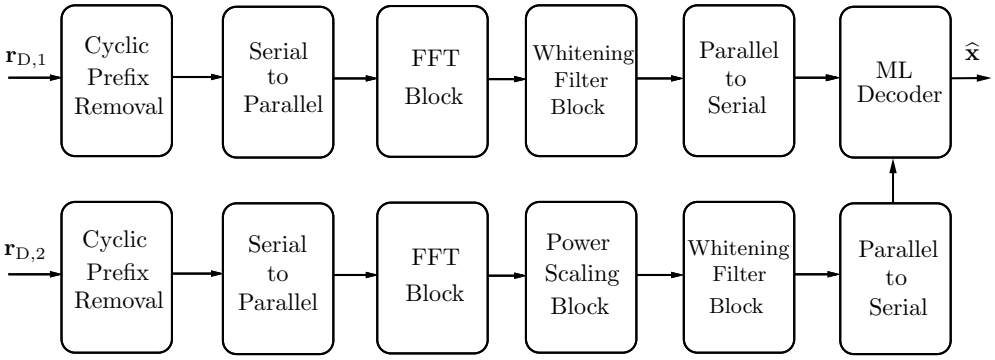

Figure 3.3: OFDM block diagram at destination node in AF relaying.

ambient noise (after CP removal) is given by

$$\mathbf{r}_{\mathrm{R}} = \sqrt{G_{\mathrm{SR}}(f)E_s}\mathbf{H}_{\mathrm{SR}}\mathbf{F}^H\mathbf{\Phi}\mathbf{x} + \mathbf{n}_{\mathrm{R}} \tag{3.5}$$

where $\mathbf{H}_{\mathrm{AB}}$ is an $N \times N$ circulant channel matrix for link with entries $\mathbf{H}_{\mathrm{AB}}(m,n) = h_{\mathrm{AB}}((m-n) \bmod N)$, $\forall m,n \in \{1,\ldots,N\}$, $\mathbf{F}$ is the FFT matrix with entries $\mathbf{F}(m,n) = (1/\sqrt{N})\exp(-j2\pi(m-1)(n-1)/N)$, E_s is the average energy per symbol, and $\mathbf{n}_{\mathrm{R}}$ is complex additive non-white Gaussian noise at relay with zero mean and covariance matrix $N_0\mathbf{\Sigma}_n$. Here, $\mathbf{\Sigma}_n$ is the normalized noise covariance matrix and $E[n_{\mathrm{R}}(i)\, n^*_{\mathrm{R}}(i)] = N_0$, $\forall i \in \{0,1,...,N-1\}$. The destination node makes the decision using the received OFDM blocks over broadcasting and relaying phases. After CP removal and FFT processing, these signals can be written as

$$\mathbf{r}^{\mathrm{AF}}_{\mathrm{D},1} = \sqrt{G_{\mathrm{SD}}(f)E_s}\mathbf{D}_{\mathrm{SD}}\mathbf{\Phi}\mathbf{x} + \mathbf{n}_1, \tag{3.6}$$

$$\mathbf{r}^{\mathrm{AF}}_{\mathrm{D},2} = \sqrt{\frac{G_{\mathrm{SR}}(f)G_{\mathrm{RD}}(f)E_s^2}{G_{\mathrm{SR}}(f)E_s + N_0}}\mathbf{D}_{\mathrm{RD}}\mathbf{D}_{\mathrm{SR}}\mathbf{\Phi}\mathbf{x} + \sqrt{\frac{G_{\mathrm{RD}}(f)E_s}{G_{\mathrm{SR}}(f)E_s + N_0}}\mathbf{D}_{\mathrm{RD}}\mathbf{n}_{\mathrm{R}} + \mathbf{n}_2 \tag{3.7}$$

where $\mathbf{D}_{\mathrm{AB}}$ is a diagonal matrix defined as $\mathbf{D}_{\mathrm{AB}} = \mathbf{F}\mathbf{H}_{\mathrm{AB}}\mathbf{F}^H$ whose diagonal elements correspond to the frequency response of a FIR channel evaluated at FFT grid points for A $\rightarrow$ B link, $\mathbf{n}_1$ and $\mathbf{n}_2$ are complex additive non-white Gaussian noise random vectors at the destination with zero mean and covariance matrix $\mathbf{F}(N_0\mathbf{\Sigma}_n)\mathbf{F}^H$. The structure of receiver depends on the availability of covariance matrix knowledge. In the following, we present the possible two cases.

3.2 Outage Analysis with Unknown Noise Covariance

If the covariance matrix of ambient noise is unknown to the receiver, we need to design the communication system with the ability to operate in the worst-case scenario. As discussed in [101], the *diagonal* covariance matrix of white noise is a special case of the generic set of noise covariance matrices and white noise can be considered as the worst-case scenario. Under this worst-case assumption, the noise terms $\mathbf{n}_{\mathrm{R}}$, $\mathbf{n}_1$, and $\mathbf{n}_2$ in (3.5), (3.6), and (3.7) are treated as white Gaussian with zero mean and $N_0\mathbf{I}_N$ covariance matrix. After proper normalization of the received signal in (3.7), received signals in (3.6) and (3.7) can be written in compact matrix notation as

$$\underbrace{\begin{bmatrix} \mathbf{r}_{\mathrm{D},1}^{\mathrm{AF}} \\ \widetilde{\mathbf{r}}_{\mathrm{D},2}^{\mathrm{AF}} \end{bmatrix}}_{\mathbf{r}_{\mathrm{u}}^{\mathrm{AF}}} = \underbrace{\begin{bmatrix} \sqrt{G_{\mathrm{SD}}(f)E_s}\mathbf{D}_{\mathrm{SD}}\mathbf{\Phi} \\ \sqrt{G_{\mathrm{SR}}(f)G_{\mathrm{RD}}(f)E_s^2}\mathbf{\Lambda}^{-1/2}\mathbf{D}_{\mathrm{RD}}\mathbf{D}_{\mathrm{SR}}\mathbf{\Phi} \end{bmatrix}}_{\mathbf{H}_{\mathrm{u}}^{\mathrm{AF}}} \mathbf{x} + \underbrace{\begin{bmatrix} \mathbf{n}_1 \\ \widetilde{\mathbf{n}}_2 \end{bmatrix}}_{\mathbf{n}_{\mathrm{u}}^{\mathrm{AF}}} \tag{3.8}$$

where $\mathbf{\Lambda} = E_s G_{\mathrm{RD}}(f)\,\mathbf{\Gamma}_{\mathrm{RD}} + (G_{\mathrm{SR}}(f)E_s + N_0)\,\mathbf{I}_N$, $\mathbf{\Gamma}_{\mathrm{AB}} = \mathbf{F}\mathbf{H}_{\mathrm{AB}}\mathbf{H}_{\mathrm{AB}}^H\mathbf{F}^H$ for the channel link A $\rightarrow$ B, and the subscript u is used to denote the assumption of unknown noise covariance. The signal $\mathbf{r}_{\mathrm{u}}^{\mathrm{AF}}$ is then fed to an ML detector.

The outage probability under average power constraint at a rate R is the probability that the instantaneous mutual information is less than R [102]. Therefore, the outage probability for the cooperative system under consideration can be expressed as

$$P_{\mathrm{out,u}}^{\mathrm{AF}} = \Pr\left\{ I\left(\mathbf{r}_{\mathrm{u}}^{\mathrm{AF}}; \mathbf{x} | \mathbf{H}_{\mathrm{u}}^{\mathrm{AF}}\right) \leq R \right\} \tag{3.9}$$

where $I\left(\mathbf{r}_{\mathrm{u}}^{\mathrm{AF}}; \mathbf{x} | \mathbf{H}_{\mathrm{u}}^{\mathrm{AF}}\right)$ is the mutual information between $\mathbf{r}_{\mathrm{u}}^{\mathrm{AF}}$ and $\mathbf{x}$ conditioned on $\mathbf{H}_{\mathrm{u}}^{\mathrm{AF}}$.

The exact outage capacity for the cooperative underwater system is

$$C_{\text{out}}(\gamma) = \sup\left\{R : \Pr\left[I\left(\mathbf{r}_{\text{u}}^{\text{AF}}; \mathbf{x}|\mathbf{H}_{\text{u}}^{\text{AF}}\right) \leq R\right] \leq P_{\text{out,u}}^{\text{AF}}\right\} \tag{3.10}$$

where $\gamma = E_s/N_0$ and sup{.} is the supremum over all achievable rates R. The instantaneous mutual information conditioned on $\mathbf{H}_{\text{u}}^{\text{AF}}$ in (3.8) can be expressed as

$$I\left(\mathbf{r}_{\text{u}}^{\text{AF}}\ ;\ \mathbf{x}|\mathbf{H}_{\text{u}}^{\text{AF}}\right) = \frac{1}{2(N+L_c)}\log_2 \det\left(\mathbf{I}_{2N} + N_0^{-1}\mathbf{H}_{\text{u}}^{\text{AF}}\left(\mathbf{H}_{\text{u}}^{\text{AF}}\right)^H\right)$$

$$= \tfrac{1}{2(N+L_c)} \times \log_2 \det\left(\begin{bmatrix} \gamma\, G_{\text{SD}}(f)\mathbf{\Gamma}_{\text{SD}} + \mathbf{I}_N & \gamma\widetilde{G}(f)\mathbf{D}_{\text{SD}}\mathbf{D}_{\text{SR}}^H\mathbf{D}_{\text{RD}}^H\mathbf{A}^{-1/2} \\ \gamma\widetilde{G}(f)\mathbf{A}^{-1/2}\mathbf{D}_{\text{RD}}\mathbf{D}_{\text{SR}}\mathbf{D}_{\text{SD}}^H & \gamma^2 G_{\text{SD}}(f)G_{\text{SR}}(f)G_{\text{RD}}(f)\mathbf{A}^{-1}\mathbf{\Gamma}_{\text{SR}}\mathbf{\Gamma}_{\text{RD}} + \mathbf{I}_N \end{bmatrix}\right) \tag{3.11}$$

where $\widetilde{G}(f) = \sqrt{E_s G_{\text{SD}}(f)G_{\text{SR}}(f)G_{\text{RD}}(f)}$, $\mathbf{A} = \gamma\, G_{\text{RD}}(f)\,\mathbf{\Gamma}_{\text{RD}} + (\gamma\ G_{\text{SR}}(f) + 1)\,\mathbf{I}_N$, and the pre-log scaling by half accounts for the spectral loss due to half-duplex mode. After some mathematical manipulations, (3.11) can be expressed as

$$I\left(\mathbf{r}_{\text{u}}^{\text{AF}}; \mathbf{x}\ |\mathbf{H}_{\text{u}}^{\text{AF}}\right) = \frac{1}{2\,(N+L_c)} \times \sum_{k=0}^{N-1} \log_2\left(1 + \gamma G_{\text{SD}}(f)\mathbf{\Gamma}_{\text{SD}}(k) + \frac{\gamma^2 G_{\text{SR}}(f)G_{\text{RD}}(f)\mathbf{\Gamma}_{\text{SR}}(k)\mathbf{\Gamma}_{\text{RD}}(k)}{\gamma\, G_{\text{RD}}(f)\,\mathbf{\Gamma}_{\text{RD}}(k) + \gamma\ G_{\text{SR}}(f) + 1}\right). \tag{3.12}$$

Eq. (3.12) can be upper bounded using Jensen's inequality to obtain

$$I_U = \underbrace{\frac{N}{2\,(N+L_c)}}_{T_p} \log_2\left(1 + \underbrace{\frac{1}{N}\sum_{k=0}^{N-1}\left[\gamma G_{\text{SD}}(f)\mathbf{\Gamma}_{\text{SD}}(k) + \frac{\gamma^2 G_{\text{SR}}(f)G_{\text{RD}}(f)\mathbf{\Gamma}_{\text{SR}}(k)\mathbf{\Gamma}_{\text{RD}}(k)}{\gamma\, G_{\text{RD}}\,(f)\mathbf{\Gamma}_{\text{RD}}(k) + \gamma\ G_{\text{SR}}(f) + 1}\right]}_{T_l}\right) \tag{3.13}$$

where $\mathbf{\Gamma}_{\text{AB}}(k)$ denotes the $\mathbf{\Gamma}_{\text{AB}}(k)$ diagonal element of the diagonal matrix $\mathbf{\Gamma}_{\text{AB}}$ for A $\rightarrow$ B link. Using Taylor's expansion of $I_U = f(T_l)$ around $\mu_{T_l} = E[T_l]$, we have

$$I_U = f(T_l) = \sum_{n=0}^{\infty} \frac{f^{(n)}(\mu_{T_l})}{n!}(T_l - \mu_{T_l})^n \tag{3.14}$$

where $f^{(n)}(\mu_{T_l})$ is the n^{th} derivative of the function f evaluated at μ_{T_l}. Based on central limit theorem, I_U in (3.13) is approximately Gaussian distributed and we obtain the

cumulative distribution function (CDF) as

$$F_{I_U}(x) \approx 1 - Q\left(\frac{x - E[I_U]}{\sqrt{\text{var}(I_U)}}\right) \tag{3.15}$$

where $Q(.)$ is the Gaussian Q-function, and var(.) is the statistical variance. Due to the upper bound deployed in (3.13) on mutual information, this expression results in a lower bound on outage probability; hence we have

$$\begin{aligned} P_{\text{out,u}}^{\text{AF}} &\geq F_{I_U}(R) \\ &= 1 - Q\left(\frac{R - E[I_U]}{\sqrt{\text{var}(I_U)}}\right). \end{aligned} \tag{3.16}$$

The upper bound on the outage capacity can be further expressed as

$$C_{\text{out}}(\gamma) \leq E[I_U] + \sqrt{\text{var}(I_U)} Q^{-1}\left(1 - P_{\text{out,u}}^{\text{AF}}\right), \quad P_{\text{out,u}}^{\text{AF}} \in [0, 1]. \tag{3.17}$$

Using the second-order approximation of Taylor's expansion of I_U, the mean and variance of I_U in (3.16) and (3.17) can be found as

$$E[I_U] = E[f(T_l)] \approx T_p \log_2\left(1 + \mu_{T_l}\right) - \frac{T_p \sigma_{T_l}^2 \log_2 e}{2\left(1 + \mu_{T_l}\right)^2}, \tag{3.18}$$

$$\text{var}(I_U) = \text{var}(f(T_l)) \approx T_p^2 (\log_2 e)^2 \left[\frac{\sigma_{T_l}^2}{\left(1 + \mu_{T_l}\right)^2} - \frac{\sigma_{T_l}^4}{4\left(1 + \mu_{T_l}\right)^4}\right] \tag{3.19}$$

where μ_{T_l} and $\sigma_{T_l}^2$ in (3.18) are calculated and presented in Appendix B.

3.3 Outage Analysis with Known Noise Covariance

Under the assumption that noise covariance matrix is known at the receiver, the received signals in (3.6) and (3.7) are first applied to a whitening filter to remove the effects of correlated noise. The whitened signals can be written in a compact matrix form as [64]

$$\underbrace{\begin{bmatrix} \widehat{\mathbf{r}}_{\text{D},1}^{\text{AF}} \\ \widehat{\mathbf{r}}_{\text{D},2}^{\text{AF}} \end{bmatrix}}_{\mathbf{r}_{\text{k}}^{\text{AF}}} = \underbrace{\begin{bmatrix} \sqrt{G_{\text{SD}}(f) E_s} (\mathbf{W}_1)^{-1/2} \mathbf{D}_{\text{SD}} \mathbf{\Phi} \\ \sqrt{\frac{G_{\text{SR}}(f) G_{\text{RD}}(f) E_s^2}{G_{\text{SR}}(f) E_s + N_0}} (\mathbf{W}_2)^{-1/2} \mathbf{D}_{\text{RD}} \mathbf{D}_{\text{SR}} \mathbf{\Phi} \end{bmatrix}}_{\mathbf{H}_{\text{k}}^{\text{AF}}} \mathbf{x} + \underbrace{\begin{bmatrix} \widehat{\mathbf{n}}_1 \\ \widehat{\mathbf{n}}_2 \end{bmatrix}}_{\mathbf{n}_{\text{k}}^{\text{AF}}} \tag{3.20}$$

where the subscript k is used to denote the assumption of known noise covariance. The signal $\mathbf{r}_{\text{k}}^{\text{AF}}$ is then fed to an ML detector. In (3.20), $\mathbf{W}_1$ is defined by $\mathbf{W}_1 = \mathbf{U}\mathbf{\Lambda}_1\mathbf{U}^H$ with $\mathbf{\Lambda}_1$ and $\mathbf{U}$, respectively, denoting the diagonal matrix of the eigenvalues and cor-

responding eigenvectors for $\mathbf{F}\boldsymbol{\Sigma}_n\mathbf{F}^H$. Similarly, we have $\mathbf{W}_2 = \mathbf{V}\boldsymbol{\Lambda}_2\mathbf{V}^H$ where $\boldsymbol{\Lambda}_2$ and $\mathbf{V}$ are, respectively, the diagonal matrix of the eigenvalues and corresponding eigenvectors for $(G_{\mathrm{RD}}(f)E_s/(G_{\mathrm{SR}}(f)E_s + N_0))\,\mathbf{D}_{\mathrm{RD}}\mathbf{F}\boldsymbol{\Sigma}_n\mathbf{F}^H\mathbf{D}_{\mathrm{RD}}^H + \mathbf{F}\boldsymbol{\Sigma}_n\mathbf{F}^H$. $\widehat{\mathbf{n}}_1$ and $\widehat{\mathbf{n}}_2$ are complex Gaussian noise random vectors with zero mean and $N_0\mathbf{I}_N$ covariance matrix. Finally, the whitened signals are fed to a ML detector.

The outage probability for the system under consideration is given by

$$P_{\mathrm{out,k}}^{\mathrm{AF}} = \Pr\left\{I\left(\mathbf{r}_{\mathrm{k}}^{\mathrm{AF}};\mathbf{x}|\mathbf{H}_{\mathrm{k}}^{\mathrm{AF}}\right) \leq R\right\} \tag{3.21}$$

where $I\left(\mathbf{r}_{\mathrm{k}}^{\mathrm{AF}};\mathbf{x}|\mathbf{H}_{\mathrm{k}}^{\mathrm{AF}}\right)$ is the instantaneous mutual information conditioned on $\mathbf{H}_{\mathrm{k}}^{\mathrm{AF}}$. It is given by

$$I\left(\mathbf{r}_{\mathrm{k}}^{\mathrm{AF}};\mathbf{x}|\mathbf{H}_{\mathrm{k}}^{\mathrm{AF}}\right) = \frac{1}{2\left(N + L_c\right)}\log_2\det\left(\mathbf{I}_{2N} + \mathrm{K}\right) \tag{3.22}$$

where K is $2N \times 2N$ partitioned matrix with four $N \times N$ block matrices, i.e.

$$\mathbf{K} = \begin{bmatrix} \mathbf{K}_{11} & \mathbf{K}_{12} \\ \mathbf{K}_{21} & \mathbf{K}_{22} \end{bmatrix}. \tag{3.23}$$

In (3.23), K_{11}, $\mathbf{K}_{12}$, $\mathbf{K}_{21}$, and $\mathbf{K}_{22}$ are defined as [64]

$$\mathbf{K}_{11} = \gamma\, G_{\mathrm{SD}}(f)\mathbf{U}\boldsymbol{\Lambda}_1^{-1/2}\mathbf{U}^H\boldsymbol{\Gamma}_{\mathrm{SD}}\mathbf{U}\boldsymbol{\Lambda}_1^{-1/2}\mathbf{U}^H, \tag{3.24}$$

$$\mathbf{K}_{12} = \gamma\sqrt{\frac{\gamma G_{\mathrm{SD}}(f)G_{\mathrm{SR}}(f)G_{\mathrm{RD}}(f)}{\gamma G_{\mathrm{SR}}(f) + 1}}\mathbf{U}\boldsymbol{\Lambda}_1^{-1/2}\mathbf{U}^H\mathbf{D}_{\mathrm{SD}}\mathbf{D}_{\mathrm{SR}}^H\mathbf{D}_{\mathrm{RD}}^H\mathbf{V}\boldsymbol{\Lambda}_2^{-1/2}\mathbf{V}^H, \tag{3.25}$$

$$\mathbf{K}_{21} = \gamma\sqrt{\frac{\gamma G_{\mathrm{SD}}(f)G_{\mathrm{SR}}(f)G_{\mathrm{RD}}(f)}{\gamma G_{\mathrm{SR}}(f) + 1}}\mathbf{V}\boldsymbol{\Lambda}_2^{-1/2}\mathbf{V}^H\mathbf{D}_{\mathrm{RD}}\mathbf{D}_{\mathrm{SR}}\mathbf{D}_{\mathrm{SD}}^H\mathbf{U}\boldsymbol{\Lambda}_1^{-1/2}\mathbf{U}^H, \tag{3.26}$$

$$\mathbf{K}_{22} = \frac{\gamma^2 G_{\mathrm{SR}}(f)G_{\mathrm{RD}}(f)}{\gamma G_{\mathrm{SR}}(f) + 1}\mathbf{V}\boldsymbol{\Lambda}_2^{-1/2}\mathbf{V}^H\boldsymbol{\Gamma}_{\mathrm{SR}}\boldsymbol{\Gamma}_{\mathrm{RD}}\mathbf{V}\boldsymbol{\Lambda}_2^{-1/2}\mathbf{V}^H. \tag{3.27}$$

A closed form solution for (3.21) is very difficult, if not infeasible. Therefore, one needs to resort to Monte Carlo simulations to numerically compute (3.21).

3.4 Multi-Hop Performance Analysis

In a similar manner we can obtain the outage probability for the multi-hop underwater communication system. We consider M-hop underwater communication system with $M-1$ relays and denote sparse frequency-selective circulant channel matrix between i^{th} and

$(i+1)^{\text{th}}$ relays by with order of the FIR filter for the channel L_{i+1}. With the application of precoded OFDM, the outage probability for M-hop UWA communication with the assumption of unknown noise covariance matrix is

$$P_{\text{out,u}}^{\text{MH}} = \Pr\left\{ \frac{1}{M\left(N+\overline{L}\right)} \log_2 \det\left(\mathbf{I}_N + \gamma G_M(f) \widetilde{\mathbf{\Lambda}}^{-1} \mathbf{\Gamma}_M \prod_{m=1}^{M-1} G_m(f) \mathbf{\Psi}_m \mathbf{\Gamma}_m \right) \leq R \right\} \tag{3.28}$$

where $\overline{L} = \max\left(L_1, \ldots, L_M\right)$, $G_i(f) = \overline{d}_i^{-s} a(f)^{-\overline{d}_i}$ is frequency-dependant geometrical gain of distance $\overline{d}_i$ in km for i^{th} channel, $\mathbf{\Gamma}_i = \mathbf{F}\mathbf{H}_i\mathbf{H}_i^H\mathbf{F}^H$, and

$$\widetilde{\mathbf{\Lambda}} = \sum_{m=1}^{M-1} \prod_{k=m}^{M-1} G_{k+1}(f) \mathbf{\Psi}_k \mathbf{\Gamma}_{k+1} + \mathbf{I}_N, \tag{3.29}$$

$$\mathbf{\Psi}_i = E_s(E_s G_i(f) \mathbf{\Gamma}_i + N_0 \mathbf{I}_N)^{-1}, \text{ for all } i \in \{1, \ldots, M\}. \tag{3.30}$$

Here, the outage probability for multi-hop UWA systems in (3.28) with the assumption of complex additive white Gaussian noise, and we have extended it to the proposed non-white (correlated) noise model in Section 2.3 with the assumption of known noise covariance matrix.

The whitened received signal at the destination node is

$$\mathbf{r}_{\text{k}}^{\text{MH}} = \sqrt{E_s G_M(f)} \mathbf{W}_{\text{M}}^{-1/2} \mathbf{D}_M \prod_{m=1}^{M-1} \sqrt{G_m(f)} \mathbf{\Psi}_m^{1/2} \mathbf{D}_m \, \mathbf{\Phi} \, \mathbf{x} + \mathbf{n}^{\text{MH}} \tag{3.31}$$

where $\mathbf{D}_i = \mathbf{F}\mathbf{H}_i\mathbf{F}^H \; \forall i \in \{1, \ldots, M\}$, $\mathbf{n}^{\text{MH}}$ is complex Gaussian noise random vectors with zero mean and $N_0\mathbf{I}_N$ covariance matrix, and $\mathbf{W}_{\text{M}}$ is defined by $\mathbf{W}_{\text{M}} = \mathbf{U}_{\text{M}}\mathbf{\Lambda}_{\text{M}}\mathbf{U}_{\text{M}}^H$ where $\mathbf{\Lambda}_{\text{M}}$ and $\mathbf{U}_{\text{M}}$ are, respectively, the diagonal matrix of the eigenvalues and corresponding eigenvectors for

$$\sum_{m=1}^{M-1} \left(\prod_{k_1=m}^{M-1} \sqrt{G_{k_1+1}(f)} \mathbf{\Psi}_{k_1}^{1/2} \mathbf{D}_{k_1+1} \right) \mathbf{F}\mathbf{\Sigma}_n\mathbf{F}^H \left(\prod_{k_2=m}^{M-1} \sqrt{G_{k_2+1}(f)} (\mathbf{\Psi}_{k_2}^{1/2})^H \mathbf{D}_{k_2+1}^H \right) + \mathbf{F}\mathbf{\Sigma}_n\mathbf{F}^H.$$

The outage probability for the system under consideration with the assumption of known noise covariance matrix is given by

$$P_{\text{out,k}}^{\text{MH}} = \Pr\left\{ I\left(\mathbf{r}_{\text{k}}^{\text{MH}}; \mathbf{x} | \mathbf{H}_1, \ldots, \mathbf{H}_M\right) \leq R \right\} \tag{3.32}$$

where $I\left(\mathbf{r}_{\text{k}}^{\text{MH}}; \mathbf{x} |\, \mathbf{H}_1, \ldots, \mathbf{H}_M\right)$ is the instantaneous mutual information conditioned on

$\mathbf{H}_1, \ldots, \mathbf{H}_M$ is given by

$$I\left(\mathbf{r}_{\mathrm{k}}^{\mathrm{MH}}; \mathbf{x} | \mathbf{H}_1, \ldots, \mathbf{H}_M\right) = \frac{1}{M\left(N + \overline{L}\right)}$$

$$\times \log_2 \det \left(\mathbf{I}_N + \gamma G_M(f) \mathbf{U}_{\mathrm{M}} \mathbf{\Lambda}_{\mathrm{M}}^{-1/2} \mathbf{U}_{\mathrm{M}}^H \mathbf{D}_M \Big(\prod_{m=1}^{M-1} G_m(f) \mathbf{\Psi}_m \mathbf{\Gamma}_m \Big) \mathbf{D}_M^H \mathbf{U}_{\mathrm{M}} \mathbf{\Lambda}_{\mathrm{M}}^{-1/2} \mathbf{U}_{\mathrm{M}}^H \right) \tag{3.33}$$

3.5 Numerical Results and Discussions

In this section, we present numerical results on the outage performance of multicarrier UWA OFDM systems based on the derived expressions. We consider a carrier frequency of 15 kHz, $N = 256$ subcarriers, and a transmission distance of $d_{\mathrm{SD}} = 3$ km. We assume that the relay node is located on the straight line connecting the source and the destination node, i.e., $\theta = \pi$. For environmental parameters, we assume temperature of 15 °C, depth of 50 m, acidity of 8 pH, salinity of 35‰ and spreading factor of 1.5. In our system, we have UWA channels with multipath spread (T_m) of 13 ms, system bandwidth of 4 kHz which corresponds, nominally, to symbol duration, T, of 0.25 ms. Number of ISI taps $L = T_m/T = 52$. We assume that all underlying UWA links have the same channel order and the same number of significant channel taps, i.e., $\widetilde{L}_{\mathrm{SD}} = \widetilde{L}_{\mathrm{SR}} = \widetilde{L}_{\mathrm{RD}} = 52$ and $L_{\mathrm{SD}} = L_{\mathrm{SR}} = L_{\mathrm{RD}} = 3$. The location vectors for significant taps are given by $\mathbf{v}_{\mathrm{SD}} = \mathbf{v}_{\mathrm{SR}} = \mathbf{v}_{\mathrm{RD}} = [\ 0 \quad 21 \quad 34 \quad 52\ ]$ with the corresponding PDP of $\mathbf{\Omega} = [\Omega_0 \ \ \Omega_1 \ \ \Omega_2 \ \ \Omega_3] = [0.25 \ \ 0.5 \ \ 0.15 \ \ 0.1]$. The spectral efficiency is 1 bps/Hz, and Rician k-factor for significant taps is 2 [103]. For the calculation of (2.18), we select $\overline{f}_0 = 0.04$ kHz resulting $\overline{f}_0 T = 0.01$.

In Figures 3.4 and 3.5, we present the outage capacity and the outage probability of cooperative OFDM UWA system with AF relaying under the assumption that noise covariance is *not known* at the receiver. We assume that relay is located in the middle.

In Figure 3.4, we compare the exact *outage capacity* in (3.10) and the derived expression given by (3.17) assuming a fixed outage probability of 10%. The exact expression is numerically computed through the generation of fading coefficients via Monte Carlo simulation methods. We observe that the derived expression based on the Gaussian approximation along with the truncation of Taylor expansion to second-order moments results in a close match to the exact one. For benchmarking purposes, we further include the outage capac-

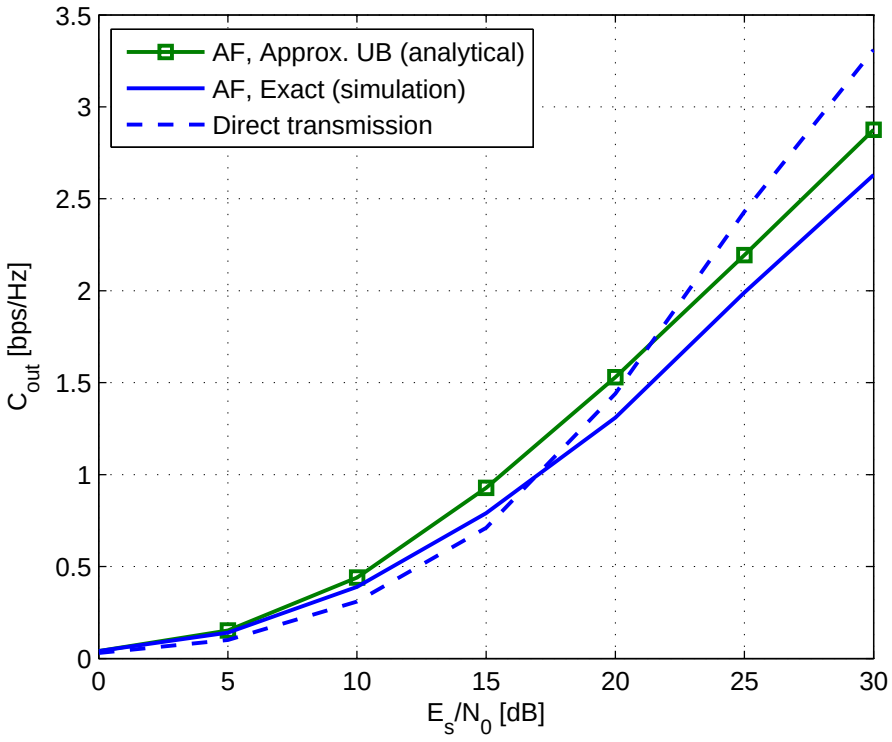

Figure 3.4: Outage capacity for cooperative OFDM UWA system with AF relaying where noise covariance is unknown at the receiver. A fixed outage probability of 10% is assumed.

ity of direct transmission. It is observed that there exists a threshold SNR at around 17 dB, where the direct transmission prevails over the cooperation at the high SNR regime. This is due to rate loss in half-duplex AF cooperation and the significance of degrees of freedom at high SNR. Specifically, at outage capacity of 1.5 bps/Hz, the SNR requirement in direct transmission is less by 1 dB than the cooperative case.

In Figure 3.5, we compare the exact *outage probability* in (3.9) and the derived analytical expression given by (3.16). Similar to Figure 3.4, we observe a close match between exact and derived ones. It is noted from Figure 3.5 that the cooperative system brings improvements over the direct transmission.

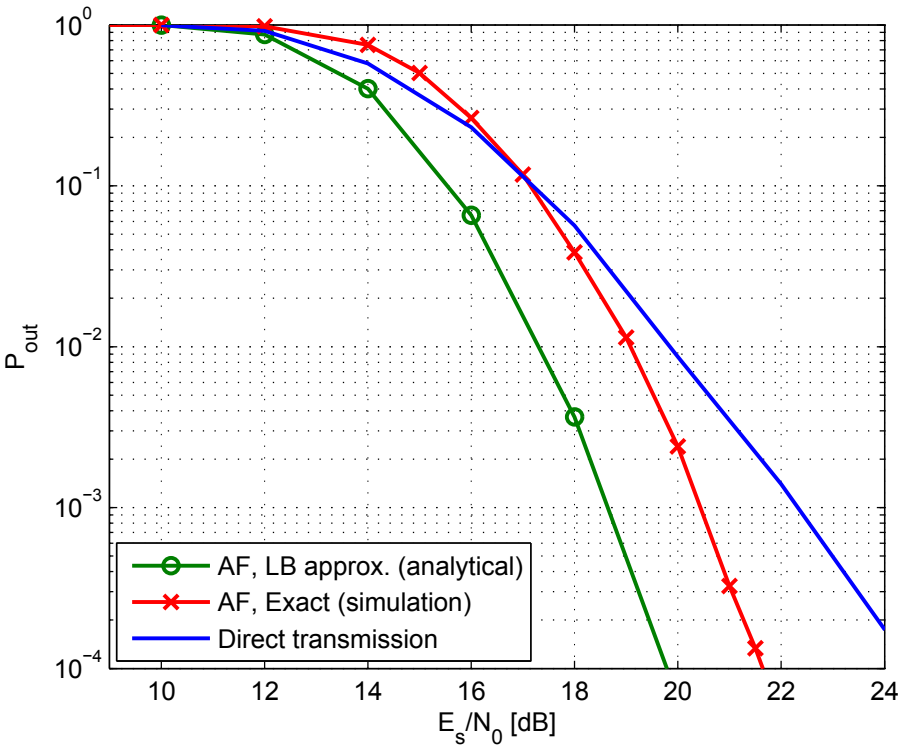

Figure 3.5: Outage probability for cooperative OFDM UWA system with AF relaying where noise covariance is unknown at the receiver.

Specifically, at an outage probability of 10^{-3}, the cooperation brings in an SNR improvement of around 2 dB compared to the direct transmission. Our results clearly demonstrate the superiority of cooperative system within the practical SNR range and we observe that cooperative system outperforms the direct transmission for SNR values larger than 16.5 dB. This is as a result of the extra spatial diversity that cooperative OFDM system is able to extract. At high SNR, diversity orders of $(L_{\mathrm{SD}}+1)+\min\left(L_{\mathrm{SR}}+1, L_{\mathrm{RD}}+1\right)=8$ and $L_{\mathrm{SD}}+1=4$ are respectively achieved for cooperative and direct transmissions.

In Figure 3.6 and Figure 3.7, we analyze the impact of relay location and operating carrier frequency on the outage probability for AF cooperative underwater system assuming noise covariance is unknown at the receiver.

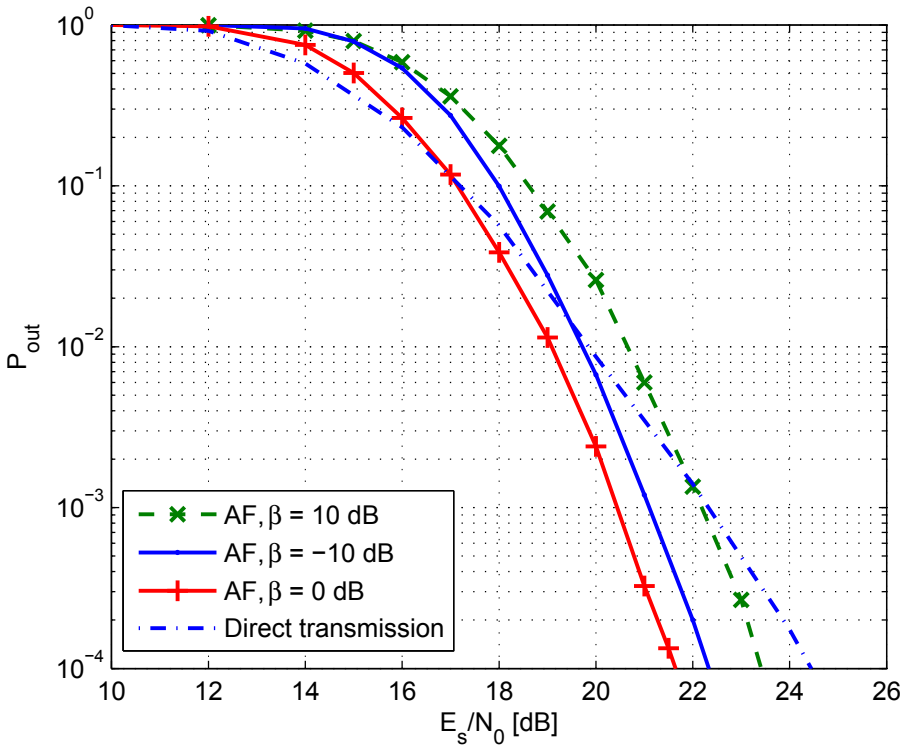

Figure 3.6: Effect of relay location on the outage probability of AF cooperative OFDM UWA system where noise covariance is unknown at the receiver.

Particularly, in Figure 3.6, we consider relay locations β = 0, -10, and 10 dB. We observe that the case of $\beta = 0$ dB in the cooperative system outperforms the other relay locations. We further notice that moving the relay closer to the destination reduces the outage probability compared to the relay placed near the source node. The worst performance occurs at $\beta = 10$ dB, i.e., when the relay is closer to the source. This is due to the deployed orthogonal cooperation protocol [36] in which the performance degrades when the relay is placed near to the source node. The SNR requirement to maintain an outage probability $P_{\text{out,u}}^{\text{AF}} = 10^{-3}$ for the relay placed in the middle is 0.64 dB and 1.75 dB less than the scenarios with $\beta = -10$ dB and $\beta = 10$ dB respectively.

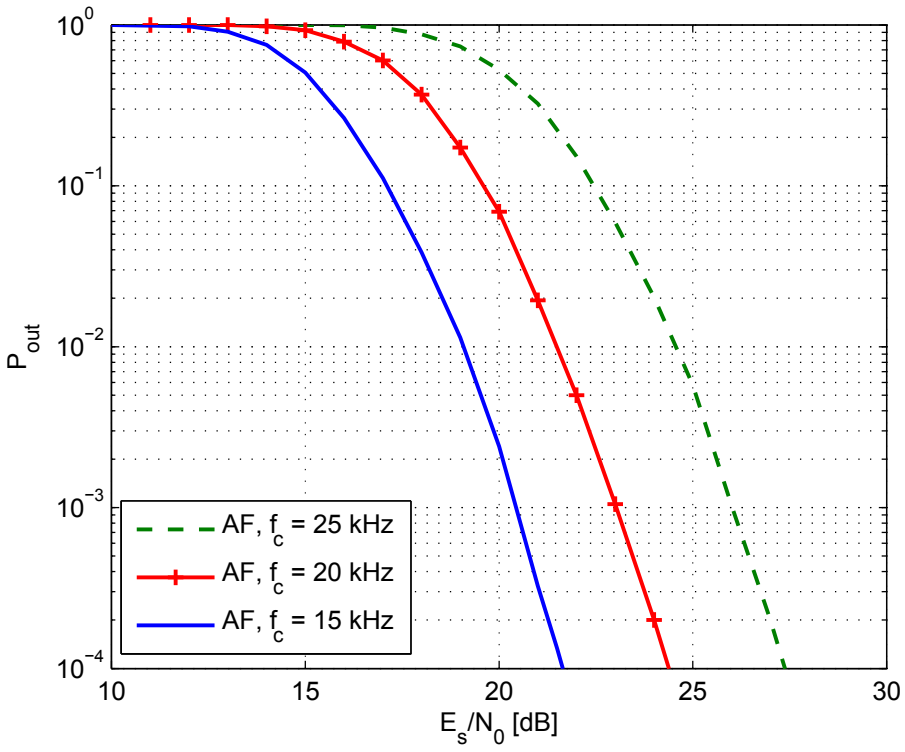

Figure 3.7: Effect of operating carrier frequency (f_c) on the outage performance of AF cooperative OFDM UWA system where noise covariance is unknown at the receiver.

In Figure 3.7, three operating carrier frequencies are considered: 15, 20, and 25 kHz. It is assumed that the relay is placed in the middle. At an outage probability $P_{\text{out,u}}^{\text{AF}} = 10^{-3}$, the SNR requirement for 15-kHz AF system is 2.55 dB and 5.9 dB less than the amount required for 20-kHz and 25-kHz systems respectively. This increase in SNR requirement is due to the dependency of absorption coefficient in underwater path loss on operating carrier frequency.

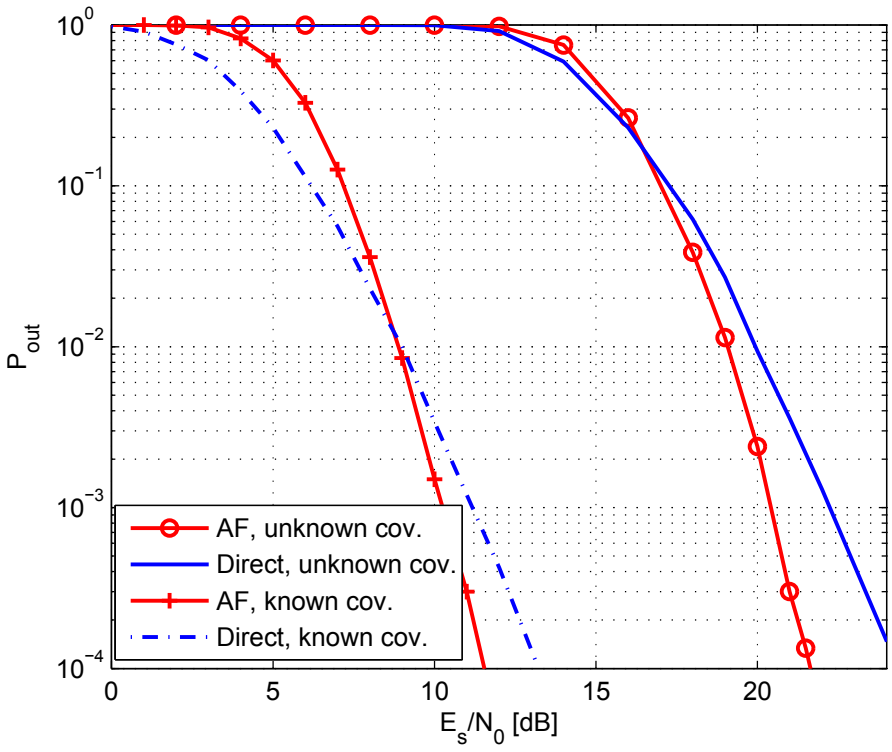

Figure 3.8: Effect of noise covariance information on the outage probability of cooperative OFDM UWA system with AF relaying.

In Figure 3.8, we present the outage probability of cooperative OFDM UWA system with AF relaying under the assumption that noise covariance is *known* at the receiver. As a benchmark, the performance under unknown noise covariance and direct transmission are further included. We observe that the knowledge of noise covariance at the receiver will substantially improve the outage performance of the system. Specifically, we observe at an outage probability of 10^{-3} the SNR requirement for the AF system under known covariance assumption is less by 10.2 dB than the unknown case. Similarly, for the direct transmission and at a target outage probability of 10^{-3}, the SNR requirement for direct transmission under known covariance is less by 11 dB than unknown case.

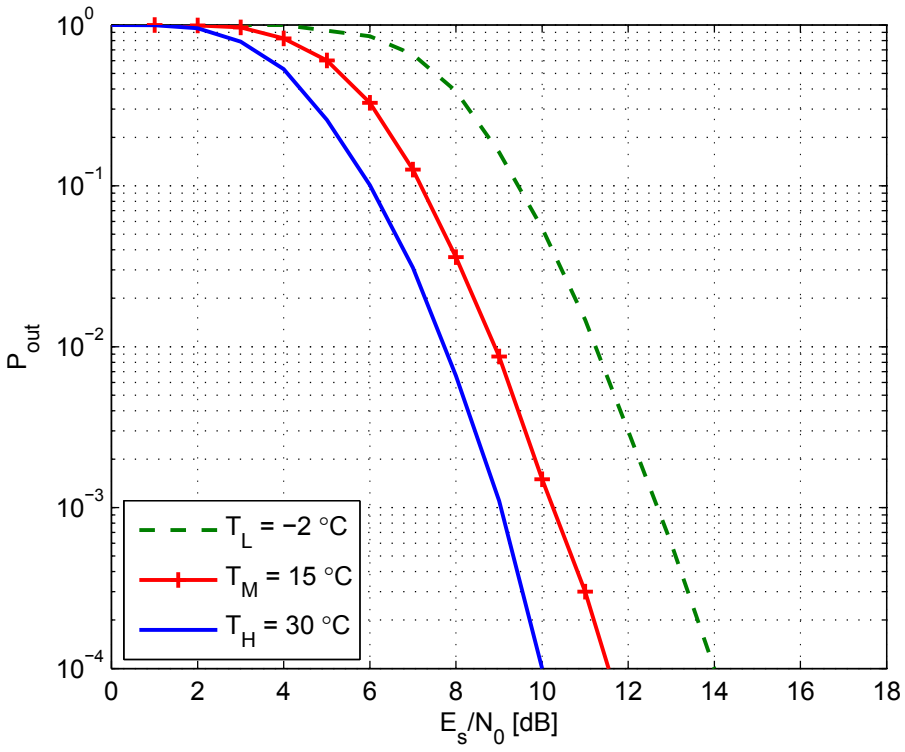

Figure 3.9: Effect of low, moderate and high underwater temperatures on outage probability at depth of 50 m where noise covariance is known at the receiver.

In Figure 3.9, we present the outage probability for cooperative OFDM system for various temperature conditions assuming that noise covariance is known at the receiver. Specifically, we consider three underwater temperatures, -2 °C, 15 °C, and 30 °C at depth of 50 m. We observe that for a targeted outage probability of 10^{-3}, the additional SNR required for a system in low underwater temperature of -2 °C is, respectively, 1.2 dB and 3.6 dB more than that required for systems in moderate and high underwater temperatures of 15 °C and 30 °C respectively. This is as a result of the dependent nature of underwater path loss on temperature.

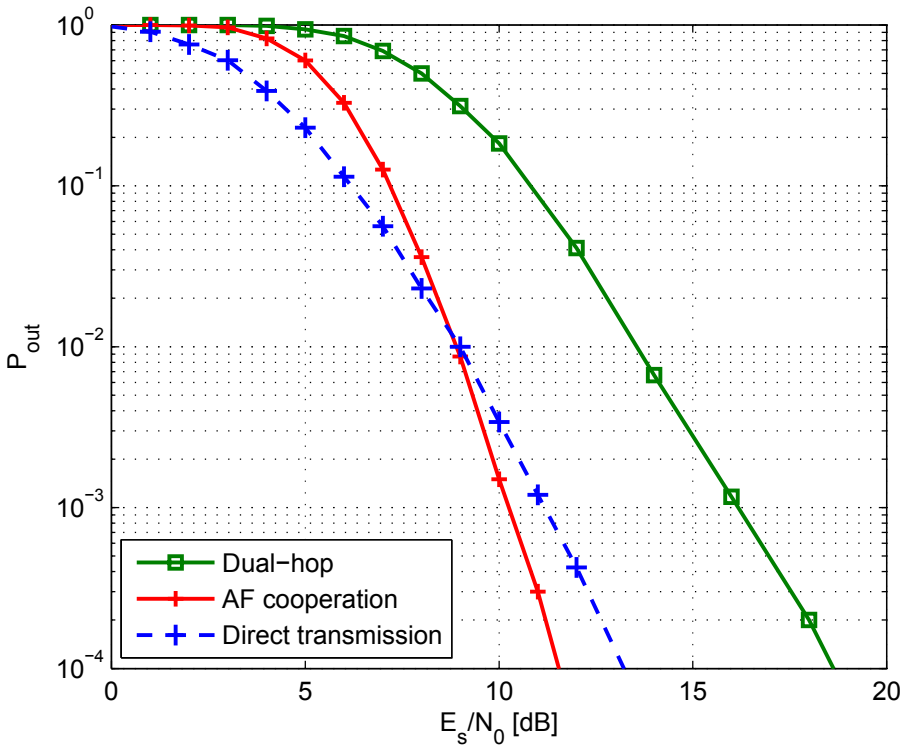

Figure 3.10: Outage probability for cooperative OFDM UWA communication system with AF relaying.

In Figure 3.10, we have investigated the outage performance of dual-hop OFDM UWA communication system in which there is no direct transmission between the source and the destination. As observed from Figure 3.10, we observe a loss in performance compared to the direct transmission although the average SNR per hop has increased. This is due to the decrease in spectral efficiency and the additional channel uses in half-duplex mode. In general, the reduction in spectral efficiency is observed by a scaling pre-log factor of the number of relays.

Chapter 4

Outage Performance of Cooperative Multicarrier UWA Communication with DF Relaying

In this chapter, we investigate the outage performance of DF cooperation over UWA channels. Specifically, we derive closed-form expressions for the outage probability under the assumptions of both unknown and known covariance of ambient noise. We analyze the effect of several system and environmental parameters on the outage probability. Furthermore, based on the derived expression, we determine the optimal relay location to minimize the outage probability.

4.1 System Model

In this section, we consider the same three-node model in Figure 3.1. Unlike the assumption of AF relaying in Chapter 3, we assume that the relay works in selective DF mode [104]. That is; if the relay successfully decodes the received signal, it re-encodes and transmits the signal to the destination node in the relaying phase. Otherwise, it remains idle. We adopt the aggregate channel model that takes into account large-scale path loss, small-scale fading effects, geometrical gains, and additive ambient noise model discussed in Chapter 3.

The source signal is first applied to a unitary linear constellation precoder $\mathbf{\Phi}$ satisfying $\mathrm{Tr}\{\mathbf{\Phi}\mathbf{\Phi}^H\} = N$ where N denotes the number of subcarriers. The resulting OFDM symbol is applied to a serial-to-parallel converter followed by the IFFT block. The parallel stream is converted back into a serial stream and a cyclic prefix is added to prevent interblock interference and ensure equal time duration in both phases. During the relaying phase, the received OFDM signal at the destination node after removing CP and applying FFT is given by

$$\mathbf{r}_{\mathrm{D},2}^{\mathrm{DF}} = \sqrt{G_{\mathrm{RD}}(f)E_s}\mathbf{D}_{\mathrm{RD}}\mathbf{\Phi}\,\mathbf{x} + \mathbf{n}_2. \tag{4.1}$$

The received signal in the broadcasting phase is obviously the same as $\mathbf{r}_{\mathrm{D},1}^{\mathrm{AF}}$ in (3.6).

4.2 Outage Analysis with Unknown Noise Covariance

As in Section 3.2, we assume the covariance matrix of ambient noise is unknown to the receiver. Under this assumption, the noise terms $\mathbf{n}_1$, $\mathbf{n}_{\mathrm{R}}$, and $\mathbf{n}_2$ are treated white Gaussian with zero mean and $N_0\mathbf{I}_N$ covariance matrix. Received signals can be written in compact matrix notation as

$$\underbrace{\begin{bmatrix} \mathbf{r}_{\mathrm{D},1}^{\mathrm{DF}} \\ \mathbf{r}_{\mathrm{D},2}^{\mathrm{DF}} \end{bmatrix}}_{\mathbf{r}_{\mathrm{u}}^{\mathrm{DF}}} = \underbrace{\begin{bmatrix} \sqrt{G_{\mathrm{SD}}(f)E_s}\mathbf{D}_{\mathrm{SD}}\mathbf{\Phi} \\ \sqrt{G_{\mathrm{RD}}(f)E_s}\mathbf{D}_{\mathrm{RD}}\mathbf{\Phi} \end{bmatrix}}_{\mathbf{H}_{\mathrm{u}}^{\mathrm{DF}}} \mathbf{x} + \underbrace{\begin{bmatrix} \mathbf{n}_1 \\ \mathbf{n}_2 \end{bmatrix}}_{\mathbf{n}_{\mathrm{u}}^{\mathrm{DF}}} \tag{4.2}$$

where the subscript u is used to denote the assumption of unknown noise covariance. The signal $\mathbf{r}_{\mathrm{u}}^{\mathrm{DF}}$ is then fed to an ML detector. The outage probability under the assumption of unknown noise covariance is given by

$$\begin{aligned} P_{\mathrm{out,u}}^{\mathrm{DF}} =& \Pr\left(I\left(\mathbf{r}_{\mathrm{u}}^{\mathrm{DF}};\mathbf{x}\left|\mathbf{H}_{\mathrm{u}}^{\mathrm{DF}}\right.\right) \le R | I\left(\mathbf{r}_{\mathrm{R}};\mathbf{x}|\mathbf{H}_{\mathrm{SR}}\right) > R\right) \Pr\left(I\left(\mathbf{r}_{\mathrm{R}};\mathbf{x}|\mathbf{H}_{\mathrm{SR}}\right) > R\right) \\ &+ \Pr\left(I\left(\mathbf{r}_{\mathrm{D},1}^{\mathrm{DF}};\mathbf{x}\left|\mathbf{H}_{\mathrm{SD}}\right.\right) \le R | I\left(\mathbf{r}_{\mathrm{R}};\mathbf{x}|\mathbf{H}_{\mathrm{SR}}\right) \le R\right)\left(1 - \Pr\left(I\left(\mathbf{r}_{\mathrm{R}};\mathbf{x}|\mathbf{H}_{\mathrm{SR}}\right) > R\right)\right) \end{aligned} \tag{4.3}$$

where $I\left(\mathbf{r}_{\mathrm{D},1}^{\mathrm{DF}};\mathbf{x}\left|\mathbf{H}_{\mathrm{SD}}\right.\right)$ is the instantaneous mutual information between $\mathbf{r}_{\mathrm{D},1}^{\mathrm{DF}}$ and $\mathbf{x}$ conditioned on $\mathbf{H}_{\mathrm{SD}}$, $I\left(\mathbf{r}_{\mathrm{R}};\mathbf{x}|\mathbf{H}_{\mathrm{SR}}\right)$ is the instantaneous mutual information between $\mathbf{r}_{\mathrm{R}}$ (after CP removal and FFT) and $\mathbf{x}$ conditioned on $\mathbf{H}_{\mathrm{SR}}$, and $I\left(\mathbf{r}_{\mathrm{u}}^{\mathrm{DF}};\mathbf{x}\left|\mathbf{H}_{\mathrm{u}}^{\mathrm{DF}}\right.\right)$ is the instantaneous mutual information between $\mathbf{r}_{\mathrm{u}}^{\mathrm{DF}}$ and $\mathbf{x}$ conditioned on $\mathbf{H}_{\mathrm{u}}^{\mathrm{DF}}$. Let I_{D}, I_{R}, and I_{C} respectively denote $I\left(\mathbf{r}_{\mathrm{D},1}^{\mathrm{DF}};\mathbf{x}\left|\mathbf{H}_{\mathrm{SD}}\right.\right)$, $I\left(\mathbf{r}_{\mathrm{R}};\mathbf{x}|\mathbf{H}_{\mathrm{SR}}\right)$, and $I\left(\mathbf{r}_{\mathrm{u}}^{\mathrm{DF}};\mathbf{x}\left|\mathbf{H}_{\mathrm{u}}^{\mathrm{DF}}\right.\right)$. They are respectively

given by

$$I_{\mathrm{D}} = \frac{1}{2\left(N+L_c\right)}\log_2 \det\left(\mathbf{I}_N + G_{\mathrm{SD}}(f)\gamma\mathbf{\Gamma}_{\mathrm{SD}}\right), \tag{4.4}$$

$$I_{\mathrm{R}} = \frac{1}{2\left(N+L_c\right)}\log_2 \det\left(\mathbf{I}_N + G_{\mathrm{SR}}(f)\gamma\mathbf{\Gamma}_{\mathrm{SR}}\right), \tag{4.5}$$

$$I_{\mathrm{C}} = \frac{1}{2\left(N+L_c\right)}\log_2 \det\left(\mathbf{I}_{2N} + N_0^{-1}\mathbf{H}_{\mathrm{u}}^{\mathrm{DF}}\left(\mathbf{H}_{\mathrm{u}}^{\mathrm{DF}}\right)^H\right) \tag{4.6}$$

where I_{C} can be further expressed as

$$I_{\mathrm{C}} = \frac{1}{2\left(N+L_c\right)}\log_2 \det\left(\left[\begin{array}{cc} G_{\mathrm{SD}}(f)\gamma\mathbf{\Gamma}_{\mathrm{SD}} + \mathbf{I}_N & \gamma\sqrt{G_{\mathrm{SD}}(f)G_{\mathrm{RD}}(f)}\mathbf{D}_{\mathrm{SD}}\mathbf{D}_{\mathrm{RD}}^H \\ \gamma\sqrt{G_{\mathrm{SD}}(f)G_{\mathrm{RD}}(f)}\mathbf{D}_{\mathrm{RD}}\mathbf{D}_{\mathrm{SD}}^H & G_{\mathrm{RD}}(f)\gamma\mathbf{\Gamma}_{\mathrm{RD}} + \mathbf{I}_N \end{array}\right]\right). \tag{4.7}$$

After some mathematical manipulations, (4.7) is given by

$$I_{\mathrm{C}} = \frac{1}{2\left(N+L_c\right)}\sum_{k=0}^{N-1}\log_2\left(1 + \gamma G_{\mathrm{SD}}(f)\mathbf{\Gamma}_{\mathrm{SD}}(k) + \gamma G_{\mathrm{RD}}(f)\mathbf{\Gamma}_{\mathrm{RD}}(k)\right). \tag{4.8}$$

The exact outage capacity is given by

$$\begin{aligned}\widetilde{C}_{\mathrm{out}}(\gamma) = &\sup\left\{R : \Pr\left(I_{\mathrm{C}} \le R | I_{\mathrm{R}} > R\right)\Pr(I_{\mathrm{R}} > R)\right. \\ &\left. + \Pr\left(I_{\mathrm{D}} \le R | I_{\mathrm{R}} \le R\right)\left(1 - \Pr(I_{\mathrm{R}} > R)\right) \le P_{\mathrm{out}}^{\mathrm{DF}}\right\}.\end{aligned} \tag{4.9}$$

Eqs. (4.4)-(4.6) can be upper bounded using Jensen's inequality to obtain

$$I_{\mathrm{D,U}} = \frac{N}{2\left(N+L_c\right)}\log_2\left(1 + \frac{1}{N}\sum_{k=0}^{N-1} G_{\mathrm{SD}}(f)\gamma\mathbf{\Gamma}_{\mathrm{SD}}(k)\right), \tag{4.10}$$

$$I_{\mathrm{R,U}} = \frac{N}{2\left(N+L_c\right)}\log_2\left(1 + \frac{1}{N}\sum_{k=0}^{N-1} G_{\mathrm{SR}}(f)\gamma\mathbf{\Gamma}_{\mathrm{SR}}(k)\right), \tag{4.11}$$

$$I_{\mathrm{C,U}} = \frac{N}{2\left(N+L_c\right)}\log_2\left(1 + \frac{1}{N}\sum_{k=0}^{N-1} \left[\gamma G_{\mathrm{SD}}(f)\mathbf{\Gamma}_{\mathrm{SD}}(k) + \gamma G_{\mathrm{RD}}(f)\mathbf{\Gamma}_{\mathrm{RD}}(k)\right]\right). \tag{4.12}$$

Due to the upper bound deployed in (4.10)-(4.12) on mutual information, these expressions result in a lower bound on CDFs, i.e., $F_{I_{\mathrm{D}}}(R) = \Pr\left(I_{\mathrm{D}} \le R\right)$, $F_{I_{\mathrm{R}}}(R) = \Pr\left(I_{\mathrm{R}} \le R\right)$, and $F_{I_{\mathrm{C}}}(R) = \Pr\left(I_{\mathrm{C}} \le R\right)$. The exact outage probability in (4.3) can be lower bounded by

$$P_{\mathrm{out,u}}^{\mathrm{DF}} \ge F_{I_{\mathrm{C,U}}}(R)\left(1 - F_{I_{\mathrm{R,U}}}(R)\right) + F_{I_{\mathrm{D,U}}}(R)F_{I_{\mathrm{R,U}}}(R). \tag{4.13}$$

The CDFs of $I_{\mathrm{D,U}}$ and $I_{\mathrm{R,U}}$ have a similar form and are derived in Appendix C.2. The CDF of $I_{\mathrm{C,U}}$ is derived in Appendix C.3. Replacing the results from Appendices C.2 and

C.3 in (4.13), we have the outage probability as

$$
\begin{aligned}
P_{\text{out,u}}^{\text{DF}} \geq & \frac{e^{-\frac{x_1}{2\mu_1}} x_1^{L_{\text{SD}}+L_{\text{RD}}+2}}{(2\mu_1)^{L_{\text{SD}}+L_{\text{RD}}+3}\Gamma(L_{\text{SD}}+L_{\text{RD}}+3)} \\
& \times \sum_{k_1=0}^{K_t-1} \frac{k_1!\widetilde{m}_{k_1}}{(L_{\text{SD}}+L_{\text{RD}}+3)_{k_1}} L_{k_1}^{(L_{\text{SD}}+L_{\text{RD}}+2)}\left(\frac{(L_{\text{SD}}+L_{\text{RD}}+3)x_1}{2\mu_0\mu_1}\right) \\
& - \frac{(G_{\text{SR}}(f)\gamma)^{-(L_{SR}+1)} e^{-\frac{(G_{\text{SR}}(f)\gamma+1)x_1}{2\mu_1 G_{\text{SR}}(f)\gamma}} x_1^{L_{\text{SD}}+L_{\text{SR}}+L_{\text{RD}}+3}}{(2\mu_1)^{L_{\text{SD}}+L_{\text{SR}}+L_{\text{RD}}+5}\Gamma(L_{\text{SD}}+L_{\text{RD}}+3)\Gamma(L_{\text{SR}}+2)} \\
\times & \sum_{k_1=0}^{K_t-1}\sum_{k_2=0}^{K_t-1} \left\{ \frac{k_1!k_2!\widetilde{m}_{k_1}c_{1,k_2}}{(L_{\text{SD}}+L_{\text{RD}}+3)_{k_1}(L_{\text{SR}}+2)_{k_2}} \; L_{k_1}^{(L_{\text{SD}}+L_{\text{RD}}+2)}\left(\frac{(L_{\text{SD}}+L_{\text{RD}}+3)x_1}{2\mu_0\mu_1}\right) L_{k_2}^{(L_{\text{SR}}+1)}\left(\frac{(L_{\text{SR}}+2)x_1}{2\mu_0\mu_1 G_{\text{SR}}(f)\gamma}\right)\right\} \\
& + \frac{\gamma^{-(L_{\text{SD}}+L_{\text{SR}}+2)} e^{-\frac{(G_{\text{SR}}(f)+G_{\text{SD}}(f))x_1}{2\mu_1 G_{\text{SR}}(f)G_{\text{SD}}(f)\gamma}} x_1^{L_{\text{SD}}+L_{\text{SR}}+2}}{(2\mu_1)^{L_{\text{SR}}+L_{\text{SD}}+4}(G_{\text{SR}}(f))^{L_{\text{SR}}+1}(G_{\text{SD}}(f))^{L_{\text{SD}}+1}\Gamma(L_{\text{SR}}+2)\Gamma(L_{\text{SD}}+2)} \\
\times & \sum_{k_3=0}^{K_t-1}\sum_{k_4=0}^{K_t-1} \left\{ \frac{k_3!k_4!c_{1,k_4}c_{2,k_3}}{(L_{\text{SD}}+2)_{k_3}(L_{\text{SR}}+2)_{k_4}} \; L_{k_3}^{(L_{\text{SD}}+1)}\left(\frac{(L_{\text{SD}}+2)x_1}{2\mu_0\mu_1 G_{\text{SD}}(f)\gamma}\right) L_{k_4}^{(L_{\text{SR}}+1)}\left(\frac{(L_{\text{SR}}+2)x_1}{2\mu_0\mu_1 G_{\text{SR}}(f)\gamma}\right)\right\}
\end{aligned}
\tag{4.14}
$$

where $x_1 = 2^{2(N+L_c)R/N} - 1$, $\mu_0, \mu_1 > 0$, $(.)_k$ is the rising factorial power (Pochhammer symbol), $\Gamma(.)$ is the complete Gamma function, and $L_k^{(\alpha)}$ is the k^{th} generalized Leguerre polynomial (defined in Appendix C.2). $\widetilde{m}_{k_1}$ is obtained by the recurrence relations in Appendix C.3, and c_{1,k_2} takes the form of m_k in the recurrence relations in Appendix C.2 with replacing L_{XY}, $\Omega_{\text{XY},i}$, $k_{\text{XY},i}$, $\sigma^2_{\text{XY},i}$,$\mu^2_{\text{XY},i}$ by L_{SR}, $\Omega_{\text{SR},i}$, $k_{\text{SR},i}$, $\sigma^2_{\text{SR},i}$, and $\mu^2_{\text{SR},i}$, respectively. Similarly, c_{2,k_3} takes the form of m_k in the recurrence relations in Appendix C.2 with replacing L_{XY}, $\Omega_{\text{XY},i}$, $k_{\text{XY},i}$, $\sigma^2_{\text{XY},i}$, $\mu^2_{\text{XY},i}$ by L_{SD}, $\Omega_{\text{SD},i}$, $k_{\text{SD},i}$, $\sigma^2_{\text{SD},i}$, $\mu^2_{\text{SD},i}$, respectively.

Under high SNR assumption, the lower bound in (4.14), is simplified to

$$
\lim_{\gamma\to\infty} P_{\text{out,u}}^{\text{DF}} \geq G_{c,0}\gamma^{-(L_{\text{SD}}+L_{\text{RD}}+2)}\left(1 - G_{c,1}\gamma^{-(L_{\text{SR}}+1)}\right) + G_{c,1}G_{c,2}\gamma^{-(L_{\text{SD}}+L_{\text{SR}}+2)} \tag{4.15}
$$

where $G_{c,0}$, $G_{c,1}$, and $G_{c,2}$ are respectively given by

$$
\begin{aligned}
G_{c,0} = & \frac{\left(2^{2(N+L_c)R/N}-1\right)^{L_{\text{SD}}+L_{\text{RD}}+2}}{(2\mu_1)^{L_{\text{SD}}+L_{\text{RD}}+3}\Gamma\left(L_{\text{SD}}+L_{\text{RD}}+3\right)} \\
& \times \sum_{k_1=0}^{K_t-1} \frac{k_1!\widetilde{m}_{k_1}}{\left(L_{\text{SD}}+L_{\text{RD}}+3\right)_{k_1}} \begin{pmatrix} L_{\text{SD}}+L_{\text{RD}}+2+k_1 \\ k_1 \end{pmatrix},
\end{aligned}
\tag{4.16}
$$

$$
G_{c,1} = \frac{\left(\left(2^{2(N+L_c)R/N}-1\right)/G_{\text{SR}}(f)\right)^{L_{\text{SR}}+1}}{(2\mu_1)^{L_{\text{SR}}+2}\Gamma\left(L_{\text{SR}}+2\right)} \sum_{k_2=0}^{K_t-1} \frac{k_2!c_{1,k_2}}{\left(L_{\text{SR}}+2\right)_{k_2}} \begin{pmatrix} L_{\text{SR}}+2+k_2 \\ k_2 \end{pmatrix}, \tag{4.17}
$$

$$
G_{c,2} = \frac{\left(\left(2^{2(N+L_c)R/N}-1\right)/G_{\text{SD}}(f)\right)^{L_{\text{SD}}+1}}{(2\mu_1)^{L_{\text{SD}}+2}\Gamma\left(L_{\text{SD}}+2\right)} \sum_{k_3=0}^{K_t-1} \frac{k_3!c_{2,k_3}}{\left(L_{\text{SD}}+2\right)_{k_3}} \begin{pmatrix} L_{\text{SD}}+2+k_3 \\ k_3 \end{pmatrix}. \tag{4.18}
$$

Detailed lower bound derivation of (4.15) is given in Appendix C.5. As the relay node moves closer to the source, i.e. $\beta \gg 1$, then $G_{c,1} \to 0$ and the expression in (4.15) simplifies to $G_{c,0}\gamma^{-(L_{\mathrm{SD}}+L_{\mathrm{RD}}+2)}$. Furthermore, as the relay node moves towards the destination, i.e. $\beta \ll 1$, then $G_{c,0} \to 0$ and the expression in (4.15) simplifies to $G_{c,1}G_{c,2}\gamma^{-(L_{\mathrm{SD}}+L_{\mathrm{SR}}+2)}$.

4.3 Outage Analysis with Known Noise Covariance

Under the assumption that noise covariance matrix is known at the receiver in DF relaying, the received signals are first applied to a whitening filter. The output of the whitening filter is given by

$$\underbrace{\begin{bmatrix} \overline{\mathbf{r}}_{\mathrm{D},1}^{\mathrm{DF}} \\ \overline{\mathbf{r}}_{\mathrm{D},2}^{\mathrm{DF}} \end{bmatrix}}_{\mathbf{r}_{\mathrm{k}}^{\mathrm{DF}}} = \underbrace{\begin{bmatrix} \sqrt{G_{\mathrm{SD}}(f)E_s}(\mathbf{W}_1)^{-1/2}\mathbf{D}_{\mathrm{SD}}\mathbf{\Phi} \\ \sqrt{G_{\mathrm{RD}}(f)E_s}(\mathbf{W}_1)^{-1/2}\mathbf{D}_{\mathrm{RD}}\mathbf{\Phi} \end{bmatrix}}_{\mathbf{H}_{\mathrm{k}}^{\mathrm{DF}}} \mathbf{x} + \underbrace{\begin{bmatrix} \overline{\mathbf{n}}_1 \\ \overline{\mathbf{n}}_2 \end{bmatrix}}_{\mathbf{n}_{\mathrm{k}}^{\mathrm{DF}}} \tag{4.19}$$

where the subscript k denotes the assumption of known noise covariance. The signal at destination node is then fed to a ML detector.

The outage probability under the assumption of known noise covariance is given by

$$\begin{aligned} P_{\mathrm{out,k}}^{\mathrm{DF}} =& \Pr\left(I\left(\mathbf{r}_{\mathrm{k}}^{\mathrm{DF}};\mathbf{x}\left|\mathbf{H}_{\mathrm{k}}^{\mathrm{DF}}\right.\right) \le R | I\left(\mathbf{r}_{\mathrm{R}};\mathbf{x}|\mathbf{H}_{\mathrm{SR}}\right) > R\right) \Pr\left(I\left(\mathbf{r}_{\mathrm{R}};\mathbf{x}|\mathbf{H}_{\mathrm{SR}}\right) > R\right) \\ &+ \Pr\left(I\left(\overline{\mathbf{r}}_{\mathrm{D},1}^{\mathrm{DF}};\mathbf{x}\left|\mathbf{H}_{\mathrm{SD}}\right.\right) \le R | I\left(\mathbf{r}_{\mathrm{R}};\mathbf{x}|\mathbf{H}_{\mathrm{SR}}\right) \le R\right)\left(1 - \Pr\left(I\left(\mathbf{r}_{\mathrm{R}};\mathbf{x}|\mathbf{H}_{\mathrm{SR}}\right) > R\right)\right) \end{aligned} \tag{4.20}$$

where $I\left(\overline{\mathbf{r}}_{\mathrm{D},1}^{\mathrm{DF}};\mathbf{x}\left|\mathbf{H}_{\mathrm{SD}}\right.\right)$ is the instantaneous mutual information between $\overline{\mathbf{r}}_{\mathrm{D},1}^{\mathrm{DF}}$ and $\mathbf{x}$ conditioned on $\mathbf{H}_{\mathrm{SD}}$, $I\left(\mathbf{r}_{\mathrm{R}};\mathbf{x}|\mathbf{H}_{\mathrm{SR}}\right)$ is the instantaneous mutual information between $\mathbf{r}_{\mathrm{R}}$ (after CP removal and FFT) and $\mathbf{x}$ conditioned on $\mathbf{H}_{\mathrm{SR}}$, and $I\left(\mathbf{r}_{\mathrm{k}}^{\mathrm{DF}};\mathbf{x}\left|\mathbf{H}_{\mathrm{k}}^{\mathrm{DF}}\right.\right)$ is the instantaneous mutual information between $\mathbf{r}_{\mathrm{k}}^{\mathrm{DF}}$ and $\mathbf{x}$ conditioned on $\mathbf{H}_{\mathrm{k}}^{\mathrm{DF}}$. $I\left(\overline{\mathbf{r}}_{\mathrm{D},1}^{\mathrm{DF}};\mathbf{x}\left|\mathbf{H}_{\mathrm{SD}}\right.\right)$, $I\left(\mathbf{r}_{\mathrm{R}};\mathbf{x}|\mathbf{H}_{\mathrm{SR}}\right)$, and $I\left(\mathbf{r}_{\mathrm{k}}^{\mathrm{DF}};\mathbf{x}\left|\mathbf{H}_{\mathrm{k}}^{\mathrm{DF}}\right.\right)$ are respectively given by

$$I\left(\overline{\mathbf{r}}_{\mathrm{D},1}^{\mathrm{DF}};\mathbf{x}\left|\mathbf{H}_{\mathrm{SD}}\right.\right) = \frac{1}{2\left(N+L_c\right)}\left\{\log_2\det\left(\mathbf{I}_N + G_{\mathrm{SD}}(f)\gamma\left(\mathbf{F}\mathbf{\Sigma}_n\mathbf{F}^H\right)^{-1}\mathbf{\Gamma}_{\mathrm{SD}}\right)\right\}, \tag{4.21}$$

$$I\left(\mathbf{r}_{\mathrm{R}};\mathbf{x}|\mathbf{H}_{\mathrm{SR}}\right) = \frac{1}{2\left(N+L_c\right)}\left\{\log_2\det\left(\mathbf{I}_N + G_{\mathrm{SR}}(f)\gamma\left(\mathbf{F}\mathbf{\Sigma}_n\mathbf{F}^H\right)^{-1}\mathbf{\Gamma}_{\mathrm{SR}}\right)\right\}, \tag{4.22}$$

$$I\left(\mathbf{r}_{\mathrm{k}}^{\mathrm{DF}};\mathbf{x}\left|\mathbf{H}_{\mathrm{k}}^{\mathrm{DF}}\right.\right) = \frac{1}{2\left(N+L_c\right)}\log_2\det\left(\mathbf{I}_{2N} + \begin{bmatrix} \mathbf{C}_{11} & \mathbf{C}_{12} \\ \mathbf{C}_{21} & \mathbf{C}_{22} \end{bmatrix}\right) \tag{4.23}$$

where

$$\mathbf{C}_{11} = G_{\mathrm{SD}}(f)\gamma \mathbf{U}\Lambda_1^{-1/2}\mathbf{U}^H \mathbf{\Gamma}_{\mathrm{SD}} \mathbf{U}\Lambda_1^{-1/2}\mathbf{U}^H, \tag{4.24}$$

$$\mathbf{C}_{12} = \sqrt{G_{\mathrm{SD}}(f)G_{\mathrm{RD}}(f)}\gamma \mathbf{U}\Lambda_1^{-1/2}\mathbf{U}^H \mathbf{D}_{\mathrm{SD}}\mathbf{D}_{\mathrm{RD}}^H \mathbf{U}\Lambda_1^{-1/2}\mathbf{U}^H, \tag{4.25}$$

$$\mathbf{C}_{21} = \sqrt{G_{\mathrm{SD}}(f)G_{\mathrm{RD}}(f)}\gamma \mathbf{U}\Lambda_1^{-1/2}\mathbf{U}^H \mathbf{D}_{\mathrm{RD}}\mathbf{D}_{\mathrm{SD}}^H \mathbf{U}\Lambda_1^{-1/2}\mathbf{U}^H, \tag{4.26}$$

$$\mathbf{C}_{22} = G_{\mathrm{RD}}(f)\gamma \mathbf{U}\Lambda_1^{-1/2}\mathbf{U}^H \mathbf{\Gamma}_{\mathrm{RD}} \mathbf{U}\Lambda_1^{-1/2}\mathbf{U}^H. \tag{4.27}$$

As in Section 3.3, one needs to use Monte Carlo simulations to numerically compute (4.22).

4.4 Numerical Results

In this section, we present numerical results on the outage performance of multicarrier DF cooperative UWA OFDM systems based on the derived expressions. We consider the system and environmental parameters of Section 3.5.

In Figure 4.1, we demonstrate the outage performance for a cooperative OFDM UWA

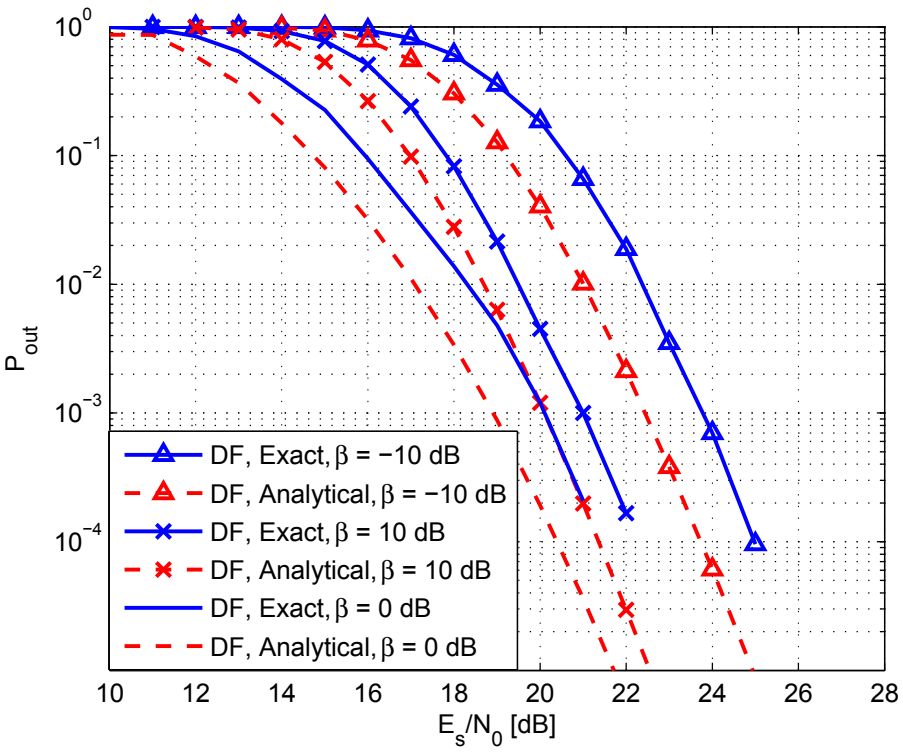

Figure 4.1: Outage probability for DF cooperative OFDM UWA system where noise covariance is unknown at the receiver.

system with DF relaying assuming unknown noise covariance at receiver. We consider three scenarios based on the relay location: $\beta = -10$, 0, and 10 dB. We compare the exact outage probability in (4.3) and the derived lower bound in (4.14) where the truncation is up to 5 terms (i.e., $K_t = 5$) and $\mu_0 = 1.5, \quad \mu_1 = 0.3$. We observe a close match between the exact expression and the derived bound. Specifically, at an outage probability of 10^{-3}, the SNR gap between derived lower bounds and exact outage probability is 0.9-1.3 dB for various relay locations. It is worth noting that the effect of relay location on the performance of DF relaying is different compared to the AF case. For $\beta = -10$ dB, i.e. the relay is closer to destination node in DF cooperation, the performance degrades compared to other relay locations. This is a result of high probability of unsuccessful decoding at the relay node due to the deterioration in quality in S $\rightarrow$ R channel link.

In analyzing the effect of carrier frequency, three operating carrier frequencies are considered: 15, 20, and 25 kHz. It is assumed that the relay is placed in the middle. We have similar observations for DF relaying to Figure 3.7. The SNR requirement to maintain an outage probability $P_{\text{out,u}}^{\text{DF}} = 10^{-3}$ for 15-kHz system is 1.75 dB and 3.65 dB less than the amount required for 20-kHz and 25-kHz systems respectively. This increase in SNR requirement is due to the dependency of absorption coefficient in underwater path loss on operating carrier frequency.

In Figure 4.2, we assume that noise covariance is known at the receiver and present the outage probability for cooperative OFDM UWA system with DF relaying. From Figure 4.2, we observe similar relay location effect on outage performance to the unknown noise covariance case in Figure 4.1; however, the SNR requirements (gains) for different relay locations are not the same. Specifically, we observe that at an outage probability of 10^{-3}, the SNR gain of $\beta = 0$ dB compared to $\beta = 10$ dB increases from 0.9 dB (see Figure 4.1) to 3.49 dB under known noise covariance assumption. However, the SNR gain of $\beta = 10$ dB compared to $\beta = -10$ dB decreases from 2.78 dB in Figure 4.1 to 1.19 dB in correlated ambient noise.

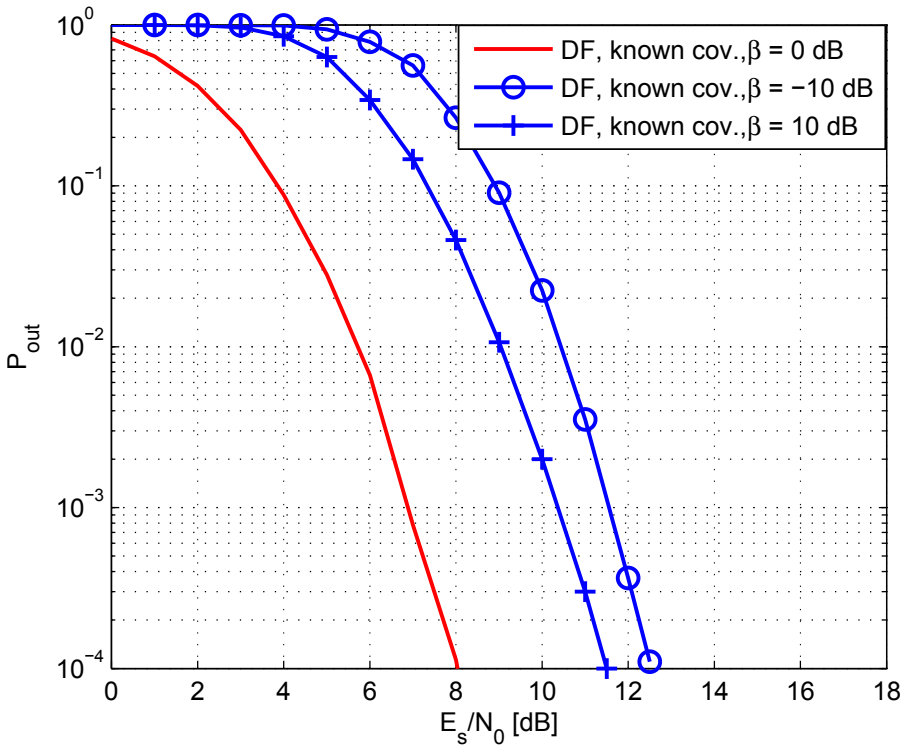

Figure 4.2: Effect of relay location on the outage probability of cooperative OFDM UWA system with DF relaying where noise covariance is known at the receiver.

4.5 Optimal Relay Location

The relay location is indicated by $\beta = d_{\mathrm{RD}}/d_{\mathrm{SR}}$. Recall that, in Section 4.2, we have derived a bound based on high SNR assumption for the lower bound on outage probability, $P^{\mathrm{DF}}_{\mathrm{out,u}}$. Let $P^{\mathrm{H}}_{\mathrm{out,u}}(\gamma, \beta)$ denotes the bound derived in (4.15) which depends on SNR, γ, and relay location β. The optimal relay location is given by

$$\beta_{\mathrm{opt}} = \arg\min_{\beta} P^{\mathrm{H}}_{\mathrm{out,u}}(\gamma, \beta) \tag{4.28}$$

where the objective functions $P^{\mathrm{H}}_{\mathrm{out,u}}(\gamma, \beta)$ defined in (4.15) is convex for various values of β in different SNR conditions.

Some terms that depend on the optimization parameter β in $P^{\mathrm{H}}_{\mathrm{out,u}}(\gamma, \beta)$ are $G_{c,0}$ and $G_{c,1}$ given in (4.16) and (4.17), respectively. Furthermore, $\widetilde{m}_{k_1}$ and ϕ_i, i.e. i^{th} element of $\boldsymbol{\Xi}$, in the recurrence relations in Appendix C.3 appear in many expressions and complicate the derivation due to the dependency on β. Let $\widetilde{c}_1 = \gamma^{-(L_{\mathrm{SD}}+L_{\mathrm{RD}}+2)}$, $\widetilde{c}_2 = \gamma^{-(L_{\mathrm{SR}}+1)}$, and

$\widetilde{c}_3 = G_{c,2}\gamma^{-(L_{\rm SD}+L_{\rm SR}+2)}$ where $G_{c,2}$ is defined in (4.18). The optimal relay location in terms of $\widetilde{c}_1$, $\widetilde{c}_2$, $\widetilde{c}_3$, $G_{c,0}$, $G_{c,1}$, and $G_{c,2}$ is given by

$$\beta_{\rm opt} = \arg\min_{\beta} \ \widetilde{c}_1 G_{c,0} - \widetilde{c}_1\widetilde{c}_2 G_{c,0}G_{c,1} + \widetilde{c}_2\widetilde{c}_3 G_{c,1}. \tag{4.29}$$

To simplify $G_{c,0}$ in (4.29), we approximate $\boldsymbol{\Xi}$ in Appendix C.3 by

$$\widetilde{\boldsymbol{\Xi}} = \left[\ \frac{\widetilde{G}_a(f)\Omega_{{\rm SD},0}}{k_{{\rm SD},0}+1} \cdots \frac{\widetilde{G}_a(f)\Omega_{{\rm SD},L_{\rm SD}}}{k_{{\rm SD},L_{\rm SD}}+1} \frac{\Omega_{{\rm RD},0}}{k_{{\rm RD},0}+1} \cdots \frac{\Omega_{{\rm RD},L_{\rm RD}}}{k_{{\rm RD},L_{\rm RD}}+1} \ \right] \tag{4.30}$$

where $\widetilde{G}_a(f) = 2^{-s}a(f)^{-(d_{\rm SD}/2)}$. The optimal β, i.e. $\beta_{\rm opt}$, is based on $\partial P^{\rm H}_{{\rm out,u}}(\gamma,\beta)/\partial\beta$ and then finding β such that $\partial P^{\rm H}_{{\rm out,u}}(\gamma,\beta)/\partial\beta = 0$. Manipulation of $G_{c,0}$ leads to the term that depends on β defined as

$$\overline{G}_0 = \left\{ \left(\frac{1+\beta^{-2}-2\cos\theta\beta^{-1}}{d_{\rm SD}^2} \right)^{s/2} a(f)^{-d_{\rm SD}/\sqrt{1+\beta^{-2}-2\beta^{-1}\cos\theta}} \right\}^{-(L_{\rm SD}+L_{\rm RD}+2)} \tag{4.31}$$

We take the derivative of $\overline{G}_0$ with respect to β and after some mathematical manipulations, it is given by

$$\begin{aligned}\frac{\partial\overline{G}_0}{\partial\beta} &= (L_{\rm SD}+L_{\rm RD}+2)\, d_{\rm SD}^{-2} \left(\beta^{-3}-\cos\theta\beta^{-2}\right) a(f)^{\left(d_{\rm SD}(L_{\rm SD}+L_{\rm RD}+2)/\sqrt{1+\beta^{-2}-2\beta^{-1}\cos\theta}\right)} \\ &\times \left(\frac{1+\beta^{-2}-2\cos\theta\beta^{-1}}{d_{\rm SD}^2} \right)^{-\left(\frac{(L_{\rm SD}+L_{\rm RD}+2)s+2}{2}\right)} \left\{ s + \log_e a(f) \left(\frac{1+\beta^{-2}-2\cos\theta\beta^{-1}}{d_{\rm SD}^2} \right)^{-1/2} \right\}\end{aligned} \tag{4.32}$$

In a similar manner, we define a term based on $G_{c,1}$ that depends on β as

$$\overline{G}_1 = \left\{ \left(\frac{1+\beta^2-2\beta\cos\theta}{d_{\rm SD}^2} \right)^{s/2} a(f)^{-d_{\rm SD}/\sqrt{1+\beta^2-2\beta\cos\theta}} \right\}^{-(L_{\rm SR}+1)} \tag{4.33}$$

Taking the derivative of $\overline{G}_1$ with respect to β and after some mathematical manipulations, it is given by

$$\begin{aligned}\frac{\partial\overline{G}_1}{\partial\beta} =& -(L_{\rm SR}+1)\, d_{\rm SD}^{-2} (\beta-\cos\theta)\, a(f)^{\frac{(L_{\rm SR}+1)d_{\rm SD}}{\sqrt{1+\beta^2-2\beta\cos\theta}}} \left(\frac{1+\beta^2-2\beta\cos\theta}{d_{\rm SD}^2} \right)^{-\left(\frac{(L_{\rm SR}+1)s+2}{2}\right)} \\ &\times \left\{ s + \log_e a(f) \left(\frac{1+\beta^2-2\beta\cos\theta}{d_{\rm SD}^2} \right)^{-1/2} \right\}.\end{aligned} \tag{4.34}$$

Therefore, $\partial P^{\rm H}_{{\rm out,u}}(\gamma,\beta)/\partial\beta$ is given by

$$\frac{\partial P^{\rm H}_{{\rm out,u}}(\gamma,\beta)}{\partial\beta} = \widetilde{c}_1\widetilde{G}_{c,0}\frac{\partial\overline{G}_0}{\partial\beta} - \widetilde{a}\widetilde{c}_1\widetilde{G}_{c,0}\left[\overline{G}_0\frac{\partial\overline{G}_1}{\partial\beta} + \overline{G}_1\frac{\partial\overline{G}_0}{\partial\beta}\right] + \widetilde{a}G_{c,2}\frac{\partial\overline{G}_1}{\partial\beta} \tag{4.35}$$

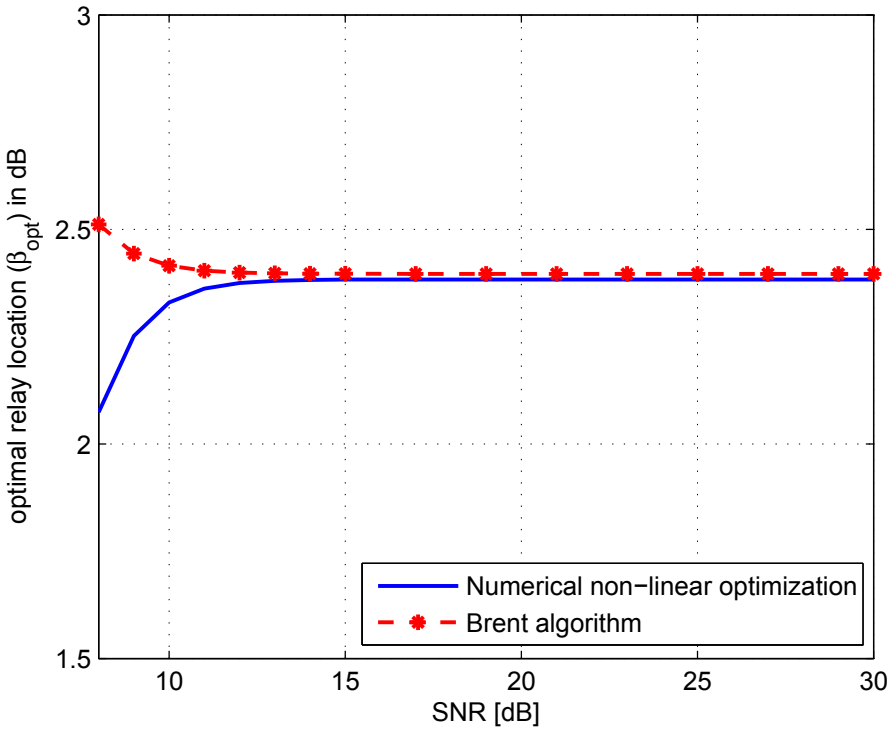

Figure 4.3: Optimal relay location in DF cooperative UWA communication system.

where $\widetilde{G}_{c,0}$ is defined based on the approximation in (4.30) and

$$\widetilde{a} = \frac{\left(2^{2(N+L_c)R/N}-1\right)^{L_{\rm SR}+1}\gamma^{-(L_{\rm SR}+1)}}{(2\mu_1)^{L_{\rm SR}+2}\Gamma\left(L_{\rm SR}+2\right)}\sum_{k_2=0}^{K_t-1}\frac{k_2!c_{1,k_2}}{(L_{\rm SR}+2)_{k_2}}\begin{pmatrix} L_{\rm SR}+2+k_2 \\ k_2 \end{pmatrix} \tag{4.36}$$

Substituting (4.32) and (4.34) in (4.35), we obtain the optimal relay location by setting to zero and solving for β in (4.35). Unfortunately, a closed-form expression for the optimal relay location based on the roots of the nonlinear equation of (4.35) is complicated. Therefore, an efficient root-finding algorithm for nonlinear equation, e.g. Brent algorithm [107], can be applied to find the optimal relay location.

In Figure 4.3, we compare the optimal relay location based on Brent algorithm applied in (4.35), and non-linear optimization in (4.28) for selective DF cooperative UWA communication system with system and environmental parameters of Section 3.5. We observe from Figure 4.3 that the optimal relay location based on approximate derived expression evaluated by Brent algorithm is approaching the optimal value based on minimizing (4.28)

as the SNR increases. This convergence is noticed at relatively low SNR values, i.e. ∼10 dB, and continues at higher SNRs.

We further analyze the effect of Rician k-factors in the different underwater links on the optimal relay location. Assume that the cooperative links may experience different Rician k-factors. We define the following cases: 1) no line-of-sight in the S $\rightarrow$ D underwater link, 2) no-line-of-sight in the S $\rightarrow$ R underwater link, and 3) there is no-line-of-sight in the R $\rightarrow$ D underwater link. In Table 4.1, the optimal relay location for corresponding cases of different Rician k-factors along the cooperative links is presented.

Table 4.1: Effect of Rician k-factor on optimal relay location.

Rician k-factor	**Optimal relay location β_{opt} [dB]**
Case 1: $\mathbf{k}_{\text{SD}} = 0, \mathbf{k}_{\text{SR}} = 2, \mathbf{k}_{\text{RD}} = 2$	2.4183
Case 2: $\mathbf{k}_{\text{SD}} = 2, \mathbf{k}_{\text{SR}} = 0, \mathbf{k}_{\text{RD}} = 2$	3.9450
Case 3: $\mathbf{k}_{\text{SD}} = 2, \mathbf{k}_{\text{SR}} = 2, \mathbf{k}_{\text{RD}} = 0$	0.9798

Comparing cases 1 and 2, we observe that the optimal relay location, β_{opt}, has increased to 3.95 dB in case 2. The limiting outage performance of the system as the relay moves closer to the source, i.e. $\beta \gg 1$, is $\widetilde{c}_1 G_{c,0}$. This term in case 2 is less than the corresponding one in case 1 due to larger $\mathbf{k}_{\text{SD}}$. Hence, case 1 approaches $\widetilde{c}_1 G_{c,0}$ rapidly compared to case 2 and the optimal relay location in case 2 is larger.

As for comparing optimal relay location in cases 1 and 3, we observe that it has decreased to 0.98 dB. The limiting outage performance of the cooperative system for $\beta \ll 1$ is $\widetilde{a} G_{c,2} \overline{G}_1$. This term depends on $\mathbf{k}_{\text{SD}}$ which is larger in case 3. In case 1, the term $\widetilde{a} G_{c,2} \overline{G}_1$ is approached faster than case 3 due to larger $\mathbf{k}_{\text{SD}}$. This leads to the optimal relay location of case 3 to be less than case 1.

Table 4.2: Effect of carrier frequency on optimal relay location.

Carrier frequency f_c **[kHz]**	**Optimal relay location** β_{opt} **[dB]**
10	3.4935
15	2.3964
20	1.4317
25	0.6604

We study the effect of carrier frequency, f_c, on the optimal relay location for the case $\mathbf{k}_{\text{SD}} = \mathbf{k}_{\text{SR}} = \mathbf{k}_{\text{RD}} = 2$. In Table 4.2, we observe the decrease of optimal relay location β_{opt} as the carrier frequency increases. The changes in optimal relay location are due to the frequency-dependent underwater absorption coefficient in $\overline{G}_0$, $\partial\overline{G}_0/\partial\beta$, $\overline{G}_1$, and $\partial\overline{G}_1/\partial\beta$ in (4.35).

Chapter 5

Outage Capacity Regions of Cooperative Multicarrier UWA Communication with DF Relaying

In this chapter, we investigate the common/individual outage capacity regions for multicarrier UWA communication in correlated ambient noise. Specifically, we derive the maximum achievable sum-rate expressions for various DF cooperation protocols that vary in degrees of broadcasting and collision. We further study the effect of several system and environmental parameters such as underwater temperature, carrier frequency, noise correlation, etc. on the outage capacity regions.

5.1 System Model

In this section, we consider the same three-node model in Figure 3.1 similar to Chapter 4. However, unlike the assumption of orthogonal cooperation protocol in Chapter 4, we consider three cooperation protocols that vary in degrees of broadcasting and collision (see Table 5.1). These are named as Protocol I, II and III using the terminology in [100]. Note that Protocol II is identical to orthogonal cooperation protocol.

Protocol I: Let the source signal vectors transmitted during the first and second phases be $\mathbf{x}_1$ and $\mathbf{x}_2$. As explained in Section 4.1, the source node applies precoding, serial-to-

Table 5.1: DF cooperation protocols [100].

Phase	Protocol I	Protocol II	Protocol III
Broadcasting	S $\rightarrow$ D , R	S $\rightarrow$ D , R	S $\rightarrow$ R
Relaying	S $\rightarrow$ D,R $\rightarrow$ D	R $\rightarrow$ D	S $\rightarrow$ D , R $\rightarrow$ D

parallel conversion, IFFT, and cyclic prefix on both signal vectors. At the relay node, the received signals corrupted by small-scale fading and ambient noise after CP removal is given by $\mathbf{r}_{\mathrm{R}} = \sqrt{G_{\mathrm{SR}}(f)E_s}\mathbf{H}_{\mathrm{SR}}\mathbf{F}^H\mathbf{\Phi}\mathbf{x}_1 + \mathbf{n}_{\mathrm{R}}$ where E_s is the average energy per symbol. Here, $\mathbf{n}_{\mathrm{R}}$ is complex additive non-white Gaussian noise with zero mean and covariance matrix $\mathbf{F}(N_0\mathbf{\Sigma}_n)\mathbf{F}^H$ where $\mathbf{\Sigma}_n$ is the normalized noise covariance matrix and N_0 is the variance of noise. The relay node demodulates and decodes the received signal and transmits the re-encoded and re-modulated signal to the destination while the source transmits $\mathbf{x}_2$. After CP removal and FFT processing, the received signals at the destination can be written as $\mathbf{r}_{\mathrm{D},1}^{\mathrm{P-I}} = \sqrt{G_{\mathrm{SD}}(f)E_s}\mathbf{D}_{\mathrm{SD}}\mathbf{\Phi}\mathbf{x}_1 + \mathbf{n}_{\mathrm{D},1}$, and $\mathbf{r}_{\mathrm{D},2}^{\mathrm{P-I}} = \sqrt{G_{\mathrm{RD}}(f)\,(E_s/2)}\mathbf{D}_{\mathrm{RD}}\mathbf{\Phi}\mathbf{x}_1 + \sqrt{G_{\mathrm{SD}}(f)\,(E_s/2)}\mathbf{D}_{\mathrm{SD}}\mathbf{\Phi}\mathbf{x}_2 + \mathbf{n}_{\mathrm{D},2}$ where $\mathbf{n}_{\mathrm{D},1}$ and $\mathbf{n}_{\mathrm{D},2}$ are complex additive non-white Gaussian noise random vectors with zero mean and covariance matrix $\mathbf{F}(N_0\mathbf{\Sigma}_n)\mathbf{F}^H$. Under the assumption that covariance matrix is known at the receiver, the received signals $\mathbf{r}_{\mathrm{D},1}^{\mathrm{P-I}}$ and $\mathbf{r}_{\mathrm{D},2}^{\mathrm{P-I}}$ are first applied to a whitening filter to remove the effects of correlated ambient noise. Then they are fed to a maximum likelihood detector. For the ensuing outage performance analysis, we can rewrite $\mathbf{r}_{\mathrm{D},1}^{\mathrm{P-I}}$ and $\mathbf{r}_{\mathrm{D},2}^{\mathrm{P-I}}$ in a compact matrix form as $\mathbf{r}_{\mathrm{P-I}} = \mathbf{H}_{\mathrm{P-I}}\widetilde{\mathbf{x}} + \mathbf{n}$ where $\widetilde{\mathbf{x}} = [\mathbf{x}_1^T \quad \mathbf{x}_2^T]^T$, $\mathbf{n} = [\mathbf{n}_{\mathrm{D},1}^T \quad \mathbf{n}_{\mathrm{D},2}^T]^T$, and the channel matrix $\mathbf{H}_{\mathrm{P-I}}$ is given by

$$\mathbf{H}_{\mathrm{P-I}} = \begin{bmatrix} \sqrt{G_{\mathrm{SD}}(f)E_s}\mathbf{D}_{\mathrm{SD}}\mathbf{\Phi} & \mathbf{0} \\ \sqrt{G_{\mathrm{RD}}(f)\,(E_s/2)}\mathbf{D}_{\mathrm{RD}}\mathbf{\Phi} & \sqrt{G_{\mathrm{SD}}(f)\,(E_s/2)}\mathbf{D}_{\mathrm{SD}}\mathbf{\Phi} \end{bmatrix}. \tag{5.1}$$

Protocol II: In this protocol, the source broadcasts to the destination as in Protocol I; however, in the second phase the source remains silent (idle) and the relay communicates with the destination node. For Protocol II, using similar steps above, the received OFDM blocks at the destination node are obtained in a matrix form as $\mathbf{r}_{\mathrm{P-II}} = \mathbf{H}_{\mathrm{P-II}}\mathbf{x}_1 + \mathbf{n}$ where the channel matrix $\mathbf{H}_{\mathrm{P-II}}$ is given by

$$\mathbf{H}_{\mathrm{P-II}} = \begin{bmatrix} \sqrt{G_{\mathrm{SD}}(f)E_s}\mathbf{D}_{\mathrm{SD}}\mathbf{\Phi} \\ \sqrt{G_{\mathrm{RD}}(f)E_s}\mathbf{D}_{\mathrm{RD}}\mathbf{\Phi} \end{bmatrix}. \tag{5.2}$$

Protocol III: This protocol is identical to Protocol I apart from the fact that the destination terminal chooses not to receive the direct S→D transmission during the first phase for reasons which are possibly imposed from the upper-layer networking protocols (e.g.. the destination node may be engaged in data transmission to another terminal). The received OFDM blocks over broadcasting and relaying phases at the destination node are given in a matrix form as $\mathbf{r}_{\mathrm{P-III}} = \mathbf{H}_{\mathrm{P-III}}\widetilde{\mathbf{x}} + \mathbf{n}_{\mathrm{D},2}$ where the channel matrix $\mathbf{H}_{\mathrm{P-III}}$ is

$$\mathbf{H}_{\mathrm{P-III}} = \left[\begin{array}{cc} \sqrt{G_{\mathrm{RD}}(f)\,(E_s/2)}\mathbf{D}_{\mathrm{RD}}\mathbf{\Phi} & \sqrt{G_{\mathrm{SD}}(f)\,(E_s/2)}\mathbf{D}_{\mathrm{SD}}\mathbf{\Phi} \end{array} \right]. \tag{5.3}$$

5.2 Derivation of Maximum Achievable Sum-Rate

The maximum achievable sum-rate in a multi-user system is defined as [13, 106] the maximum sum of transmission rates of individual users at which users can jointly reliably communicate under a certain power allocation policy. The cooperation protocols under consideration can be interpreted as a two-user system in which the source and the relay nodes are the individual users. Under this interpretation, we derive the maximum achievable sum-rate for Protocols I, II and III over frequency-selective UWA channel assuming equal power allocation.

Protocol I: Let R_1 and R_2 denote the transmission rates (in bps/Hz) associated respectively with the signal vectors $\mathbf{x}_1$ and $\mathbf{x}_2$. $R_1 + R_2$ therefore denotes the sum-rate for Protocol I. For reliable decoding at the destination, R_1 and R_2 must satisfy the following inequalities

$$R_1 \leq I\left(\mathbf{r}_{\mathrm{R}}; \mathbf{x}_1 | \mathbf{H}_{\mathrm{SR}}\right), \tag{5.4}$$

$$R_1 \leq I\left(\mathbf{r}_{\mathrm{P-I}}; \mathbf{x}_1 | \mathbf{x}_2, \mathbf{H}_{\mathrm{SD}}, \mathbf{H}_{\mathrm{RD}}\right), \tag{5.5}$$

$$R_2 \leq I\left(\mathbf{r}_{\mathrm{P-I}}; \mathbf{x}_2 | \mathbf{x}_1, \mathbf{H}_{\mathrm{SD}}, \mathbf{H}_{\mathrm{RD}}\right), \tag{5.6}$$

$$R_1 + R_2 \leq I\left(\mathbf{r}_{\mathrm{P-I}}; \mathbf{x}_1, \mathbf{x}_2 | \mathbf{H}_{\mathrm{SD}}, \mathbf{H}_{\mathrm{RD}}\right). \tag{5.7}$$

The transmission rate R_1 must satisfy (5.4) for reliably decoding $\mathbf{x}_1$ at the relay and (5.5) to reliably communicate $\mathbf{x}_1$ to the destination node. Hence, from (5.4) and (5.5), we

have $R_1 \leq \min\left\{I\left(\mathbf{r}_{\mathrm{R}};\mathbf{x}_1|\mathbf{H}_{\mathrm{SR}}\right), I\left(\mathbf{r}_{\mathrm{P-I}};\mathbf{x}_1|\mathbf{x}_2,\mathbf{H}_{\mathrm{SD}},\mathbf{H}_{\mathrm{RD}}\right)\right\}$ where

$$I\left(\mathbf{r}_{\mathrm{R}};\mathbf{x}_1|\mathbf{H}_{\mathrm{SR}}\right) = \frac{1}{2\left(N+L_c\right)}\log\det\left(\mathbf{I}_N + G_{\mathrm{SR}}(f)\gamma\big(\mathbf{F}\boldsymbol{\Sigma}_n\mathbf{F}^H\big)^{-1}\boldsymbol{\Gamma}_{\mathrm{SR}}\right), \tag{5.8}$$

$$I\left(\mathbf{r}_{\mathrm{P-I}};\mathbf{x}_1|\mathbf{x}_2,\mathbf{H}_{\mathrm{SD}},\mathbf{H}_{\mathrm{RD}}\right) = \frac{1}{2\left(N+L_c\right)}\log\det\left(\mathbf{I}_{2N} + \left(\mathbf{I}_2\otimes\left(\mathbf{F}(N_0\boldsymbol{\Sigma}_n)\mathbf{F}^H\right)\right)^{-1}\mathbf{P}_1\mathbf{P}_1^H\right) \tag{5.9}$$

where $\otimes$ denotes the kronecker product. In (5.8) and (5.9), we have $\gamma = E_s/N_0$, $\boldsymbol{\Gamma}_{\mathrm{XY}} = \mathbf{F}\mathbf{H}_{\mathrm{XY}}\mathbf{H}_{\mathrm{XY}}^H\mathbf{F}^H$ for X $\rightarrow$ Y link and $\mathbf{P}_1\mathbf{P}_1^H$ is given by

$$\mathbf{P}_1\mathbf{P}_1^H = \begin{bmatrix} G_{\mathrm{SD}}(f)E_s\boldsymbol{\Gamma}_{\mathrm{SD}} & \sqrt{G_{\mathrm{SD}}(f)G_{\mathrm{RD}}(f)(E_s^2/2)}\mathbf{D}_{\mathrm{SD}}\mathbf{D}_{\mathrm{RD}}^H \\ \sqrt{G_{\mathrm{SD}}(f)G_{\mathrm{RD}}(f)(E_s^2/2)}\mathbf{D}_{\mathrm{RD}}\mathbf{D}_{\mathrm{SD}}^H & G_{\mathrm{RD}}(f)\left(E_s/2\right)\boldsymbol{\Gamma}_{\mathrm{RD}} \end{bmatrix}. \tag{5.10}$$

For reliably decoding $\mathbf{x}_2$ at the destination, the transmission rate R_2 must satisfy (5.6). This assumes that $\mathbf{x}_1$ is known at destination. Due to the knowledge of $\mathbf{x}_1$, $\mathbf{r}_{\mathrm{D},1}^{\mathrm{P-I}}$ has no additional information and therefore $I\left(\mathbf{r}_{\mathrm{P-I}};\mathbf{x}_2|\mathbf{x}_1,\mathbf{H}_{\mathrm{SD}},\mathbf{H}_{\mathrm{RD}}\right)$ simplifies to $I\left(\mathbf{r}_{\mathrm{D},2}^{\mathrm{P-I}};\mathbf{x}_2|\mathbf{x}_1,\mathbf{H}_{\mathrm{P-I}}\right)$. Therefore, we have (5.6) as

$$R_2 \leq \frac{1}{2\left(N+L_c\right)}\log\det\left(\mathbf{I}_N + \frac{1}{2}G_{\mathrm{SD}}(f)\gamma\big(\mathbf{F}\boldsymbol{\Sigma}_n\mathbf{F}^H\big)^{-1}\boldsymbol{\Gamma}_{\mathrm{SD}}\right). \tag{5.11}$$

Eq. (5.7) refers to the maximum information that can be reliably communicated in the two phases and it is given by

$$\begin{aligned} R_1 + R_2 \leq & I\left(\mathbf{r}_{\mathrm{P-I}};\mathbf{x}_1,\mathbf{x}_2|\mathbf{H}_{\mathrm{SD}},\mathbf{H}_{\mathrm{RD}}\right) = \frac{1}{2\left(N+L_c\right)} \\ & \times\log\det\left(\mathbf{I}_{2N} + \left(\mathbf{I}_2\otimes\left(\mathbf{F}(N_0\boldsymbol{\Sigma}_n)\mathbf{F}^H\right)\right)^{-1}\mathbf{P}_2\mathbf{P}_2^H\right) \end{aligned} \tag{5.12}$$

where

$$\mathbf{P}_2\mathbf{P}_2^H = \begin{bmatrix} G_{\mathrm{SD}}(f)E_s\boldsymbol{\Gamma}_{\mathrm{SD}} & \sqrt{G_{\mathrm{SD}}(f)G_{\mathrm{RD}}(f)(E_s^2/2)}\mathbf{D}_{\mathrm{SD}}\mathbf{D}_{\mathrm{RD}}^H \\ \sqrt{G_{\mathrm{SD}}(f)G_{\mathrm{RD}}(f)(E_s^2/2)}\mathbf{D}_{\mathrm{RD}}\mathbf{D}_{\mathrm{SD}}^H & G_{\mathrm{SD}}(f)\left(E_s/2\right)\boldsymbol{\Gamma}_{\mathrm{SD}} + G_{\mathrm{RD}}(f)\left(E_s/2\right)\boldsymbol{\Gamma}_{\mathrm{RD}} \end{bmatrix}. \tag{5.13}$$

R_1 depends on the quality of the S$\rightarrow$R underwater channel condition. In the case that the channel conditions does not enable correct decoding at the relay, the bound in (5.12) might not be achievable. Therefore, based on (5.8), (5.11), and (5.12), the maximum achievable

sum-rate for Protocol I of cooperative OFDM UWA system is expressed as

$$R_{\text{sum}}^{\text{P-I}} = R_1 + R_2 = \begin{cases} \frac{1}{2(N+L_c)} \log\det\left(\mathbf{I}_{2N} + \left(\mathbf{I}_2 \otimes \left(\mathbf{F}(N_0\mathbf{\Sigma}_n)\mathbf{F}^H\right)\right)^{-1}\mathbf{P}_2\mathbf{P}_2^H\right) \\ if\ I\left(\mathbf{r}_{\text{R}};\mathbf{x}_1|\mathbf{H}_{\text{SR}}\right) \geq I\left(\mathbf{r}_{\text{P-I}};\mathbf{x}_1,\mathbf{x}_2|\mathbf{H}_{\text{P-I}}\right) - I\left(\mathbf{r}_{\text{P-I}};\mathbf{x}_2|\mathbf{x}_1,\mathbf{H}_{\text{P-I}}\right), \\ \\ \frac{1}{2(N+L_c)} \log\det\Big(\mathbf{I}_N + G_{\text{SR}}(f)\gamma\big(\mathbf{F}\mathbf{\Sigma}_n\mathbf{F}^H\big)^{-1}\mathbf{\Gamma}_{\text{SR}} \\ \qquad\qquad + \frac{1}{2}G_{\text{SD}}(f)\gamma\big(\mathbf{F}\mathbf{\Sigma}_n\mathbf{F}^H\big)^{-1}\mathbf{\Gamma}_{\text{SD}} \\ \qquad\qquad + \frac{1}{2}G_{\text{SD}}(f)G_{\text{SR}}(f)\gamma^2\big(\mathbf{F}\mathbf{\Sigma}_n\mathbf{F}^H\big)^{-1}\ \mathbf{\Gamma}_{\text{SR}}\big(\mathbf{F}\mathbf{\Sigma}_n\mathbf{F}^H\big)^{-1}\mathbf{\Gamma}_{\text{SD}}\Big) \\ if\ I\left(\mathbf{r}_{\text{R}};\mathbf{x}_1|\mathbf{H}_{\text{SR}}\right) < I\left(\mathbf{r}_{\text{P-I}};\mathbf{x}_1,\mathbf{x}_2|\mathbf{H}_{\text{P-I}}\right) - I\left(\mathbf{r}_{\text{P-I}};\mathbf{x}_2|\mathbf{x}_1,\mathbf{H}_{\text{P-I}}\right). \end{cases} \tag{5.14}$$

Protocol II: In this protocol, the transmission rate R_2 is simply equal to zero since there is no transmission from the source node in the second phase. Hence, the maximum achievable sum-rate for Protocol II is

$$R_{\text{sum}}^{\text{P-II}} = \min\left\{ I\left(\mathbf{r}_{\text{R}};\mathbf{x}_1|\mathbf{H}_{\text{SR}}\right), I\left(\mathbf{r}_{\text{P-II}};\mathbf{x}_1|\mathbf{H}_{\text{P-II}}\right)\right\} \tag{5.15}$$

where $I\left(\mathbf{r}_{\text{R}};\mathbf{x}_1|\mathbf{H}_{\text{SR}}\right)$ has been already defined in (5.8) and $I\left(\mathbf{r}_{\text{P-II}};\mathbf{x}_1|\mathbf{H}_{\text{P-II}}\right)$ is given by

$$I\left(\mathbf{r}_{\text{P-II}};\mathbf{x}_1|\mathbf{H}_{\text{P-II}}\right) = \frac{1}{2\left(N+L_c\right)} \log\det\left(\mathbf{I}_{2N} + \left(\mathbf{I}_2 \otimes \left(\mathbf{F}(N_0\mathbf{\Sigma}_n)\mathbf{F}^H\right)\right)^{-1}\mathbf{P}_3\mathbf{P}_3^H\right) \tag{5.16}$$

with

$$\mathbf{P}_3\mathbf{P}_3^H = \begin{bmatrix} G_{\text{SD}}(f)E_s\mathbf{\Gamma}_{\text{SD}} & \sqrt{G_{\text{SD}}(f)G_{\text{RD}}(f)E_s^2}\mathbf{D}_{\text{SD}}\mathbf{D}_{\text{RD}}^H \\ \sqrt{G_{\text{SD}}(f)G_{\text{RD}}(f)E_s^2}\mathbf{D}_{\text{RD}}\mathbf{D}_{\text{SD}}^H & G_{\text{RD}}(f)E_s\mathbf{\Gamma}_{\text{RD}} \end{bmatrix}. \tag{5.17}$$

Protocol III: The transmission rate R_1 is constrained by

$$R_1 \leq \min\left\{ I\left(\mathbf{r}_{\text{R}};\mathbf{x}_1|\mathbf{H}_{\text{SR}}\right), I\left(\mathbf{r}_{\text{P-III}};\mathbf{x}_1|\mathbf{x}_2,\mathbf{H}_3\right)\right\} \tag{5.18}$$

where $I\left(\mathbf{r}_{\text{R}};\mathbf{x}_1|\mathbf{H}_{\text{SR}}\right)$ has been already defined in (5.8) and $I\left(\mathbf{r}_{\text{P-III}};\mathbf{x}_1|\mathbf{x}_2,\mathbf{H}_{\text{SD}},\mathbf{H}_{\text{RD}}\right)$ is given by

$$I\left(\mathbf{r}_{\text{P-III}};\mathbf{x}_1|\mathbf{x}_2,\mathbf{H}_{\text{SD}},\mathbf{H}_{\text{RD}}\right) = \frac{1}{2\left(N+L_c\right)} \log\det\left(\mathbf{I}_N + \frac{1}{2}G_{\text{RD}}(f)\gamma\big(\mathbf{F}\mathbf{\Sigma}_n\mathbf{F}^H\big)^{-1}\mathbf{\Gamma}_{\text{RD}}\right). \tag{5.19}$$

The maximum information that can be reliably communicated in the two phases, $I\left(\mathbf{r}_{\text{P-III}};\mathbf{x}_1,\mathbf{x}_2|\mathbf{H}_{\text{P-III}}\right)$, is given by

$$I\left(\mathbf{r}_{\text{P-III}};\mathbf{x}_1,\mathbf{x}_2|\mathbf{H}_{\text{P-III}}\right) = \frac{1}{2\left(N+L_c\right)} \times \log\det\left(\mathbf{I}_N + \frac{G_{\text{SD}}(f)\gamma}{2}\big(\mathbf{F}\mathbf{\Sigma}_n\mathbf{F}^H\big)^{-1}\mathbf{\Gamma}_{\text{SD}} + \frac{G_{\text{RD}}(f)\gamma}{2}\big(\mathbf{F}\mathbf{\Sigma}_n\mathbf{F}^H\big)^{-1}\mathbf{\Gamma}_{\text{RD}}\right). \tag{5.20}$$

The mutual information between $\mathbf{r}_{\mathrm{P-III}}$ and $\mathbf{x}_2$ conditioned on $\mathbf{x}_1$ and channel conditions, $I\left(\mathbf{r}_{\mathrm{P-III}};\mathbf{x}_2|\mathbf{x}_1,\mathbf{H}_{\mathrm{SD}},\mathbf{H}_{\mathrm{RD}}\right)$, is given by

$$I\left(\mathbf{r}_{\mathrm{P-III}};\mathbf{x}_2|\mathbf{x}_1,\mathbf{H}_{\mathrm{SD}},\mathbf{H}_{\mathrm{RD}}\right)=\frac{1}{2\left(N+L_c\right)}\log\det\left(\mathbf{I}_N+\frac{1}{2}G_{\mathrm{SD}}(f)\gamma\big(\mathbf{F}\mathbf{\Sigma}_n\mathbf{F}^H\big)^{-1}\mathbf{\Gamma}_{\mathrm{SD}}\right). \tag{5.21}$$

Therefore, based on (5.8), (5.20), and (5.21), the maximum achievable sum-rate for Protocol III is given by

$$R_{\mathrm{sum}}^{\mathrm{P-III}}=R_1+R_2=\begin{cases}\frac{1}{2(N+L_c)}\log\det\Big(\mathbf{I}_N+\frac{1}{2}G_{\mathrm{SD}}(f)\gamma\big(\mathbf{F}\mathbf{\Sigma}_n\mathbf{F}^H\big)^{-1}\mathbf{\Gamma}_{\mathrm{SD}} \\ \qquad\qquad +\frac{1}{2}G_{\mathrm{RD}}(f)\gamma\big(\mathbf{F}\mathbf{\Sigma}_n\mathbf{F}^H\big)^{-1}\mathbf{\Gamma}_{\mathrm{RD}}\Big) \\ if I\left(\mathbf{r}_{\mathrm{R}};\mathbf{x}_1|\mathbf{H}_{\mathrm{SR}}\right)\geq I\left(\mathbf{r}_{\mathrm{P-III}};\mathbf{x}_1,\mathbf{x}_2|\mathbf{H}_{\mathrm{P-III}}\right)-I\left(\mathbf{r}_{\mathrm{P-III}};\mathbf{x}_2|\mathbf{x}_1,\mathbf{H}_{\mathrm{P-III}}\right), \\ \\ \frac{1}{2(N+L_c)}\log\det\Big(\mathbf{I}_N+\frac{1}{2}G_{\mathrm{SD}}(f)\gamma\big(\mathbf{F}\mathbf{\Sigma}_n\mathbf{F}^H\big)^{-1}\mathbf{\Gamma}_{\mathrm{SD}} \\ \qquad +G_{\mathrm{SR}}(f)\gamma\big(\mathbf{F}\mathbf{\Sigma}_n\mathbf{F}^H\big)^{-1}\mathbf{\Gamma}_{\mathrm{SR}} \\ \qquad +\frac{1}{2}G_{\mathrm{SD}}(f)G_{\mathrm{SR}}(f)\gamma^2\big(\mathbf{F}\mathbf{\Sigma}_n\mathbf{F}^H\big)^{-1}\mathbf{\Gamma}_{\mathrm{SR}}\big(\mathbf{F}\mathbf{\Sigma}_n\mathbf{F}^H\big)^{-1}\mathbf{\Gamma}_{\mathrm{SD}}\Big) \\ if I\left(\mathbf{r}_{\mathrm{R}};\mathbf{x}_1|\mathbf{H}_{\mathrm{SR}}\right)<I\left(\mathbf{r}_{\mathrm{P-III}};\mathbf{x}_1,\mathbf{x}_2|\mathbf{H}_{\mathrm{P-III}}\right)-I\left(\mathbf{r}_{\mathrm{P-III}};\mathbf{x}_2|\mathbf{x}_1,\mathbf{H}_{\mathrm{P-III}}\right).\end{cases} \tag{5.22}$$

5.3 Common and Individual Outage Capacity Regions

Outage capacity region is defined as [13] the set of fixed achievable individual rate vectors that can be maintained in all fading states subject to a given non-zero outage probability. It is analogous to outage capacity in single-user systems. It is possible to define these regions based on common or individual outage probability for the different cooperation phases [107]. In this section, based on the derived sum-rate expressions in the previous section, $R_{\mathrm{sum}}^{\mathrm{P-I}}$, $R_{\mathrm{sum}}^{\mathrm{P-II}}$, and $R_{\mathrm{sum}}^{\mathrm{P-III}}$ are substituted for the upper bounds on R_1+R_2 in corresponding achievable rate regions for Protocols I, II, and III respectively. We derive the common and individual outage capacity regions cooperation protocols under consideration over frequency-selective UWA channel assuming equal power allocation.

Protocol I: In this protocol, the set of achievable positive rate vectors $\mathbf{R}=\left(R_1,R_2\right),\ R_1,\ R_2\in\mathbb{R}$, conditioned on $\mathbf{H}_{\mathrm{SD}}$, $\mathbf{H}_{\mathrm{SR}}$, and $\mathbf{H}_{\mathrm{RD}}$ is denoted by $\Psi_{\mathrm{P-I}}(\gamma)$. If the transmission

rate R_1 satisfies $R_1 \leq I\left(\mathbf{r}_{\mathrm{R}}; \mathbf{x}_1 | \mathbf{H}_{\mathrm{SR}}\right)$, then the achievable region is

$$\widetilde{\Psi}_{\mathrm{P-I}}(\gamma) = \{\mathbf{R} : R_1 \leq I\left(\mathbf{r}_{\mathrm{P-I}}; \mathbf{x}_1 | \mathbf{x}_2, \mathbf{H}_{\mathrm{SD}}, \mathbf{H}_{\mathrm{RD}}\right), R_2 \leq I\left(\mathbf{r}_{\mathrm{P-I}}; \mathbf{x}_2 | \mathbf{x}_1, \mathbf{H}_{\mathrm{SD}}, \mathbf{H}_{\mathrm{RD}}\right), \\ R_1 + R_2 \leq I\left(\mathbf{r}_{\mathrm{P-I}}; \mathbf{x}_1, \mathbf{x}_2 | \mathbf{H}_{\mathrm{SD}}, \mathbf{H}_{\mathrm{RD}}\right)\}. \quad (5.23)$$

Based on the quality of the S $\rightarrow$ R underwater channel, the achievable region in (5.23) can be affected and have a smaller region. The set of achievable rates $\Psi_{\mathrm{P-I}}(\gamma) \subseteq \widetilde{\Psi}_{\mathrm{P-I}}$ conditioned on the channel states is

$$\Psi_{\mathrm{P-I}}(\gamma) = \begin{cases} \Psi^1_{\mathrm{P-I}}(\gamma), & I\left(\mathbf{r}_{\mathrm{R}}; \mathbf{x}_1 | \mathbf{H}_{\mathrm{SR}}\right) \geq I\left(\mathbf{r}_{\mathrm{P-I}}; \mathbf{x}_1, \mathbf{x}_2 | \mathbf{H}_1\right) - I\left(\mathbf{r}_{\mathrm{P-I}}; \mathbf{x}_2 | \mathbf{x}_1, \mathbf{H}_1\right) \\ \Psi^2_{\mathrm{P-I}}(\gamma), & I\left(\mathbf{r}_{\mathrm{R}}; \mathbf{x}_1 | \mathbf{H}_{\mathrm{SR}}\right) < I\left(\mathbf{r}_{\mathrm{P-I}}; \mathbf{x}_1, \mathbf{x}_2 | \mathbf{H}_1\right) - I\left(\mathbf{r}_{\mathrm{P-I}}; \mathbf{x}_2 | \mathbf{x}_1, \mathbf{H}_1\right) \end{cases} \quad (5.24)$$

where $\Psi^1_{\mathrm{P-I}}(\gamma)$ and $\Psi^2_{\mathrm{P-I}}(\gamma)$ $\left(\Psi^2_{\mathrm{P-I}}(\gamma) \subseteq \Psi^1_{\mathrm{P-I}}(\gamma)\right)$ are given by

$$\Psi^1_{\mathrm{P-I}}(\gamma) = \{\mathbf{R} : \quad R_1 \leq \min\left\{I\left(\mathbf{r}_{\mathrm{R}}; \mathbf{x}_1 | \mathbf{H}_{\mathrm{SR}}\right), I\left(\mathbf{r}_{\mathrm{P-I}}; \mathbf{x}_1 | \mathbf{x}_2, \mathbf{H}_{\mathrm{SD}}, \mathbf{H}_{\mathrm{RD}}\right)\right\} \\ R_2 \leq I\left(\mathbf{r}_{\mathrm{P-I}}; \mathbf{x}_2 | \mathbf{x}_1, \mathbf{H}_{\mathrm{SD}}, \mathbf{H}_{\mathrm{RD}}\right) \\ R_1 + R_2 \leq I\left(\mathbf{r}_{\mathrm{P-I}}; \mathbf{x}_1, \mathbf{x}_2 | \mathbf{H}_{\mathrm{SD}}, \mathbf{H}_{\mathrm{RD}}\right)\}, \quad (5.25)$$

$$\Psi^2_{\mathrm{P-I}}(\gamma) = \{\mathbf{R} : \quad R_1 \leq \min\left\{I\left(\mathbf{r}_{\mathrm{R}}; \mathbf{x}_1 | \mathbf{H}_{\mathrm{SR}}\right), I\left(\mathbf{r}_{\mathrm{P-I}}; \mathbf{x}_1 | \mathbf{x}_2, \mathbf{H}_{\mathrm{SD}}, \mathbf{H}_{\mathrm{RD}}\right)\right\} \\ R_2 \leq I\left(\mathbf{r}_{\mathrm{P-I}}; \mathbf{x}_2 | \mathbf{x}_1, \mathbf{H}_{\mathrm{SD}}, \mathbf{H}_{\mathrm{RD}}\right) \\ R_1 + R_2 \leq I\left(\mathbf{r}_{\mathrm{R}}; \mathbf{x}_1 | \mathbf{H}_{\mathrm{SR}}\right) + I\left(\mathbf{r}_{\mathrm{P-I}}; \mathbf{x}_2 | \mathbf{x}_1, \mathbf{H}_{\mathrm{SD}}, \mathbf{H}_{\mathrm{RD}}\right)\}. \quad (5.26)$$

Equality, $\Psi^2_{\mathrm{P-I}}(\gamma) = \Psi^1_{\mathrm{P-I}}(\gamma)$, holds if the mutual information $I\left(\mathbf{r}_{\mathrm{P-I}}; \mathbf{x}_1, \mathbf{x}_2 | \mathbf{H}_{\mathrm{P-I}}\right) = I\left(\mathbf{r}_{\mathrm{R}}; \mathbf{x}_1 | \mathbf{H}_{\mathrm{SR}}\right) + I\left(\mathbf{r}_{\mathrm{P-I}}; \mathbf{x}_2 | \mathbf{x}_1, \mathbf{H}_{\mathrm{P-I}}\right)$. Let ε denote the common outage probability. The common outage capacity region is given by

$$C^{\mathrm{P-I}}_{\mathrm{out}}(\gamma, \varepsilon) = \left\{\mathbf{R} : \Pr\left\{\mathbf{R} \in \Psi_{\mathrm{P-I}}(\gamma)\right\} \geq 1 - \varepsilon\right\}. \quad (5.27)$$

This represents all the rate pairs $\mathbf{R}$ that can be achieved with a probability of at least $1 - \varepsilon$. In other words, the rate pairs belonging to the outage capacity region will result in an outage, i.e., non-reliable communication, with a probability of at most ε. Maximum achievable rate pairs with outage probability of ε is the supremum of outage capacity regions defined in (5.27).

Similarly, the individual outage capacity region consists of all achievable rate vectors such that individual outage probabilities do not exceed elements of $\boldsymbol{\varepsilon}$ under average power constraint [107]. This outage capacity region reflects the effect of assigning various outage probability constraints for the cooperation phases. Let $\boldsymbol{\varepsilon} = [\ \varepsilon_1 \quad \varepsilon_2\ ]$ denote the individual

outage probability vector. The individual outage capacity region is given by

$$C_{\text{out}}^{\text{P-I}}(\gamma,\varepsilon)=\left\{\mathbf{R}:\forall\left(\widetilde{\alpha}_1,\widetilde{\alpha}_2\right)\in\Psi_{\text{P-I}}(\gamma),\Pr\left\{\widetilde{\alpha}_1\geq R_1\right\}\geq 1-\varepsilon_1,\Pr\left\{\widetilde{\alpha}_2\geq R_2\right\}\geq 1-\varepsilon_2\right\}. \tag{5.28}$$

This represents all the rate pairs R_1 and R_2 that can be achieved with a probability of at least ε_1 and ε_2 respectively. In other words, cooperation phases rate pairs belonging to the individual outage capacity region will result in an outage, i.e. non-reliable communication, with a probability of at most ε_1 and ε_2 respectively.

Protocol II: The set of achievable rates for Protocol II conditioned on the channel states ($R_2=0$) is denoted by $\Psi_{\text{P-II}}(\gamma)$ and given by

$$\Psi_{\text{P-II}}(\gamma)=\left\{\mathbf{R}:R_1\leq\min\left\{I\left(\mathbf{r}_{\text{R}};\mathbf{x}_1|\mathbf{H}_{\text{SR}}\right),I\left(\mathbf{r}_{\text{P-II}};\mathbf{x}_1|\mathbf{H}_{\text{P-II}}\right)\right\},R_2=0\right\}. \tag{5.29}$$

Common outage capacity region is then given by

$$C_{\text{out}}^{\text{P-II}}(\gamma,\varepsilon)=\left\{\mathbf{R}:\Pr\left\{\mathbf{R}\in\Psi_{\text{P-II}}(\gamma)\right\}\geq 1-\varepsilon\right\}. \tag{5.30}$$

Individual outage capacity region with individual outage vector $\boldsymbol{\varepsilon}$, is

$$C_{\text{out}}^{\text{P-II}}(\gamma,\varepsilon)=\left\{\mathbf{R}:\forall\left(\widetilde{\alpha}_1,0\right)\in\Psi_{\text{P-II}}(\gamma),\Pr\left\{\widetilde{\alpha}_1\geq R_1\right\}\geq 1-\varepsilon_1,\varepsilon_2\in[0,1]\right\}. \tag{5.31}$$

Protocol III: The set of achievable rates for Protocol III conditioned on channel states is denoted by $\Psi_{\text{P-III}}(\gamma)$. Based on the quality of the S→R underwater channel, the achievable region can be affected and have a smaller region. The set of achievable rates is then given by

$$\widetilde{\Psi}_{\text{P-III}}(\gamma)=\{\mathbf{R}:R_1\leq I\left(\mathbf{r}_{\text{P-III}};\mathbf{x}_1|\mathbf{x}_2,\mathbf{H}_{\text{SD}},\mathbf{H}_{\text{RD}}\right),R_2\leq I\left(\mathbf{r}_{\text{P-III}};\mathbf{x}_2|\mathbf{x}_1,\mathbf{H}_{\text{SD}},\mathbf{H}_{\text{RD}}\right),$$

$$R_1+R_2\leq I\left(\mathbf{r}_{\text{P-III}};\mathbf{x}_1,\mathbf{x}_2|\mathbf{H}_{\text{SD}},\mathbf{H}_{\text{RD}}\right)\}. \tag{5.32}$$

Based on the quality of the S → R underwater channel, the achievable region in (5.32) can be affected and have a smaller region. The set of achievable rates $\Psi_{\text{P-III}}(\gamma)\subseteq\widetilde{\Psi}_{\text{P-III}}$ is

then given by

$$\Psi_{\text{P-III}}(\gamma) = \begin{cases} \Psi^1_{\text{P-III}}(\gamma), & I\left(\mathbf{r}_{\text{R}};\mathbf{x}_1|\mathbf{H}_{\text{SR}}\right) \geq I\left(\mathbf{r}_{\text{P-III}};\mathbf{x}_1,\mathbf{x}_2|\mathbf{H}_{\text{P-III}}\right) \\ & \qquad -I\left(\mathbf{r}_{\text{P-III}};\mathbf{x}_2|\mathbf{x}_1,\mathbf{H}_{\text{P-III}}\right), \\ \Psi^2_{\text{P-III}}(\gamma), & I\left(\mathbf{r}_{\text{R}};\mathbf{x}_1|\mathbf{H}_{\text{SR}}\right) < I\left(\mathbf{r}_{\text{P-III}};\mathbf{x}_1,\mathbf{x}_2|\mathbf{H}_{\text{P-III}}\right) \\ & \qquad -I\left(\mathbf{r}_{\text{P-III}};\mathbf{x}_2|\mathbf{x}_1,\mathbf{H}_{\text{P-III}}\right) \end{cases} \tag{5.33}$$

where $\Psi^1_{\text{P-III}}(\gamma)$ and $\Psi^2_{\text{P-III}}(\gamma)$ $\left(\Psi^2_{\text{P-III}}(\gamma) \subseteq \Psi^1_{\text{P-III}}(\gamma)\right)$ are given by

$$\begin{aligned} \Psi^1_{\text{P-III}}(\gamma) = \{\mathbf{R}: \quad & R_1 \leq \min\left\{I\left(\mathbf{r}_{\text{R}};\mathbf{x}_1|\mathbf{H}_{\text{SR}}\right), I\left(\mathbf{r}_{\text{P-III}};\mathbf{x}_1|\mathbf{x}_2,\mathbf{H}_{\text{SD}},\mathbf{H}_{\text{RD}}\right)\right\} \\ & R_2 \leq I\left(\mathbf{r}_{\text{P-III}};\mathbf{x}_2|\mathbf{x}_1,\mathbf{H}_{\text{SD}},\mathbf{H}_{\text{RD}}\right) \\ & R_1+R_2 \leq I\left(\mathbf{r}_{\text{P-III}};\mathbf{x}_1,\mathbf{x}_2|\mathbf{H}_{\text{SD}},\mathbf{H}_{\text{RD}}\right)\}, \end{aligned} \tag{5.34}$$

$$\begin{aligned} \Psi^2_{\text{P-III}}(\gamma) = \{\mathbf{R}: \quad & R_1 \leq \min\left\{I\left(\mathbf{r}_{\text{R}};\mathbf{x}_1|\mathbf{H}_{\text{SR}}\right), I\left(\mathbf{r}_{\text{P-III}};\mathbf{x}_1|\mathbf{x}_2,\mathbf{H}_{\text{SD}},\mathbf{H}_{\text{RD}}\right)\right\} \\ & R_2 \leq I\left(\mathbf{r}_{\text{P-III}};\mathbf{x}_2|\mathbf{x}_1,\mathbf{H}_{\text{SD}},\mathbf{H}_{\text{RD}}\right) \\ & R_1+R_2 \leq I\left(\mathbf{r}_{\text{R}};\mathbf{x}_1|\mathbf{H}_{\text{SR}}\right)+I\left(\mathbf{r}_{\text{P-III}};\mathbf{x}_2|\mathbf{x}_1,\mathbf{H}_{\text{SD}},\mathbf{H}_{\text{RD}}\right)\}. \end{aligned} \tag{5.35}$$

Equality, $\Psi^2_{\text{P-III}}(\gamma) = \Psi^1_{\text{P-III}}(\gamma)$, holds if the mutual information $I\left(\mathbf{r}_{\text{P-III}};\mathbf{x}_1,\mathbf{x}_2|\mathbf{H}_{\text{P-III}}\right)$ $= I\left(\mathbf{r}_{\text{R}};\mathbf{x}_1|\mathbf{H}_{\text{SR}}\right)+I\left(\mathbf{r}_{\text{P-III}};\mathbf{x}_2|\mathbf{x}_1,\mathbf{H}_{\text{P-III}}\right)$ for Protocol III. Common outage capacity region for Protocol III is then given by

$$C^{\text{P-III}}_{\text{out}}(\gamma,\varepsilon) = \left\{\mathbf{R}: \Pr\left\{\mathbf{R} \in \Psi_{\text{P-III}}(\gamma)\right\} \geq 1-\varepsilon\right\}. \tag{5.36}$$

Individual outage capacity region with individual outage vector $\boldsymbol{\varepsilon}$, is

$$C^{\text{P-III}}_{\text{out}}(\gamma,\varepsilon) = \left\{\mathbf{R}: \forall\left(\widetilde{\alpha}_1,\widetilde{\alpha}_2\right) \in \Psi_{\text{P-III}}(\gamma), \Pr\left\{\widetilde{\alpha}_1 \geq R_1\right\} \geq 1-\varepsilon_1, \Pr\left\{\widetilde{\alpha}_2 \geq R_2\right\} \geq 1-\varepsilon_2\right\}. \tag{5.37}$$

5.4 Numerical Results and Discussions

In this section, we present numerical results for the outage capacity regions using derived sum-rate expressions for underwater DF-based cooperative protocols in colored non-white ambient noise. We consider the carrier frequency of 16 kHz, $d_{\text{SD}} = 1$ km, underwater temperature of 25 °C, and the rest of the system and environmental parameters of Section 3.5.

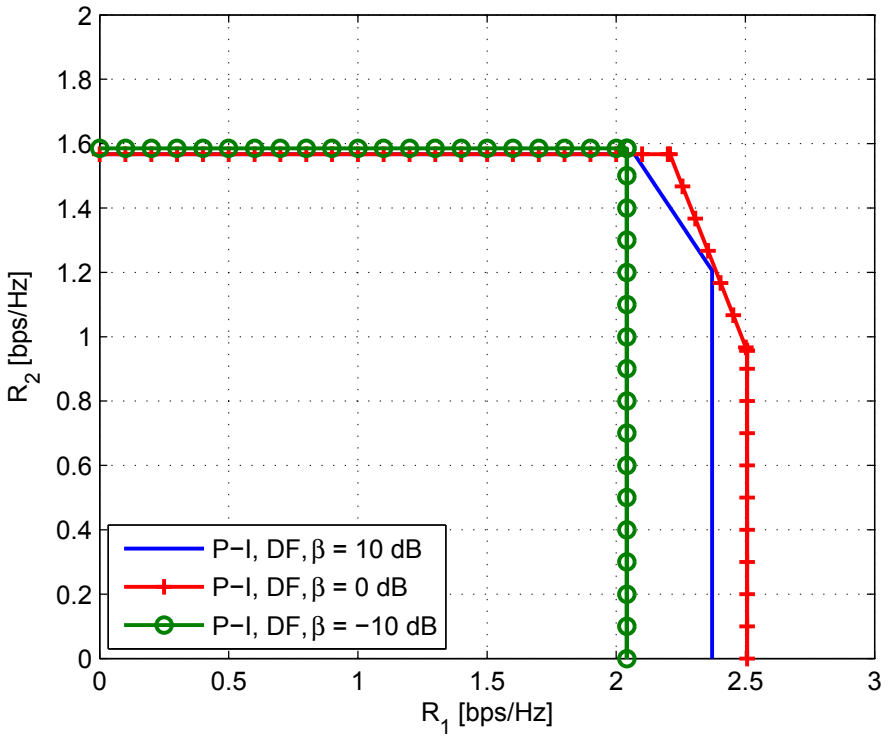

Figure 5.1: Common outage capacity region for Protocol I assuming different relay locations.

In Figure 5.1, we present the common outage capacity region of Protocol I for various relay locations at SNR of 10 dB and outage probability of $\varepsilon = 0.1$. Our results demonstrate the decrease in the area of outage capacity region as the relay node moves closer to the destination node. This is due to error propagation as a result of the poor channel quality of S $\rightarrow$ R link. We notice that the maximum outage capacity region is achieved when the relay is located in the middle ($\beta = 0$ dB) and smaller outage capacity region for the case of $\beta = 10$ dB. Specifically, at a transmission rate $R_2 = 0.6$ bps/Hz the transmission rate in broadcasting phase R_1 for $\beta = -10$ dB is less by 0.33 bps/Hz and 0.47 bps/Hz than the cases of $\beta = 10$ dB and $\beta = 0$ dB respectively.

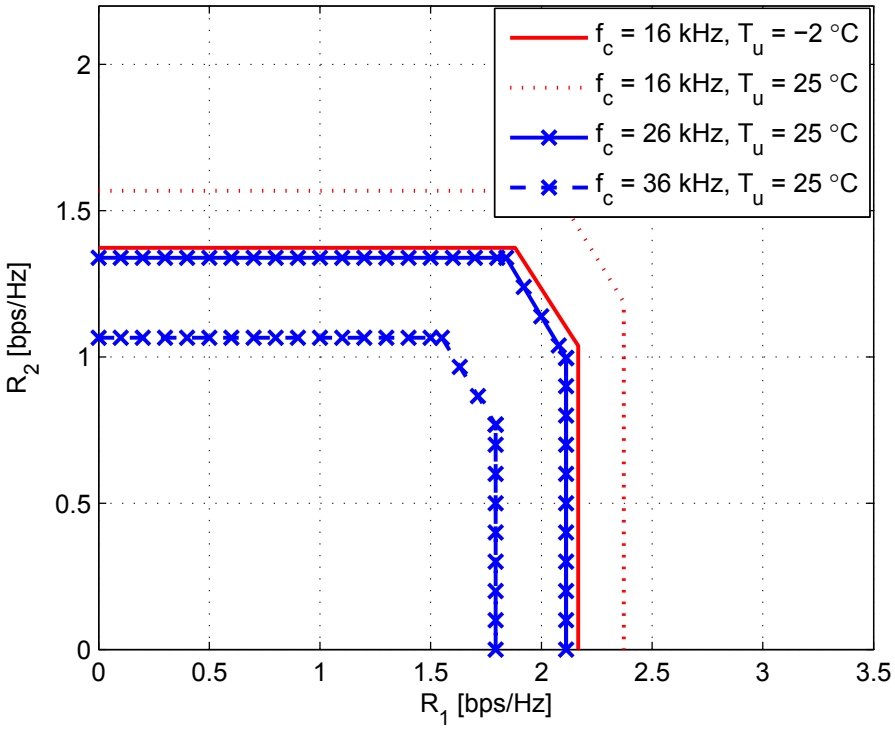

Figure 5.2: Effect of temperature (T_{u}) and carrier frequency (f_c) on common outage capacity region of Protocol I.

In Figure 5.2, we study the effect of carrier frequency and underwater temperature on the common outage capacity region. Specifically we consider three carrier frequencies, namely, 16 kHz, 26 kHz, and 36 kHz. We observe that for a targeted broadcasting phase transmission rate $R_1 = 0.5$ bps/Hz, the relaying phase transmission rate for a 16 kHz-system is, respectively, 0.23 bps/Hz and 0.5 bps/Hz more than R_2 for 26 kHz and 36 kHz-systems. This is as a result of the dependent nature of underwater path loss on the carrier frequency. As for the effect of underwater temperature, we consider two temperatures, namely, -2 °C and 25 °C. We observe that for a targeted relaying phase transmission rate $R_2 = 0.5$ bps/Hz, the broadcasting transmission rate in -2 °C is 0.21 bps/Hz less than R_1 in 25 °C. This reflects that higher underwater temperature is more favourable.

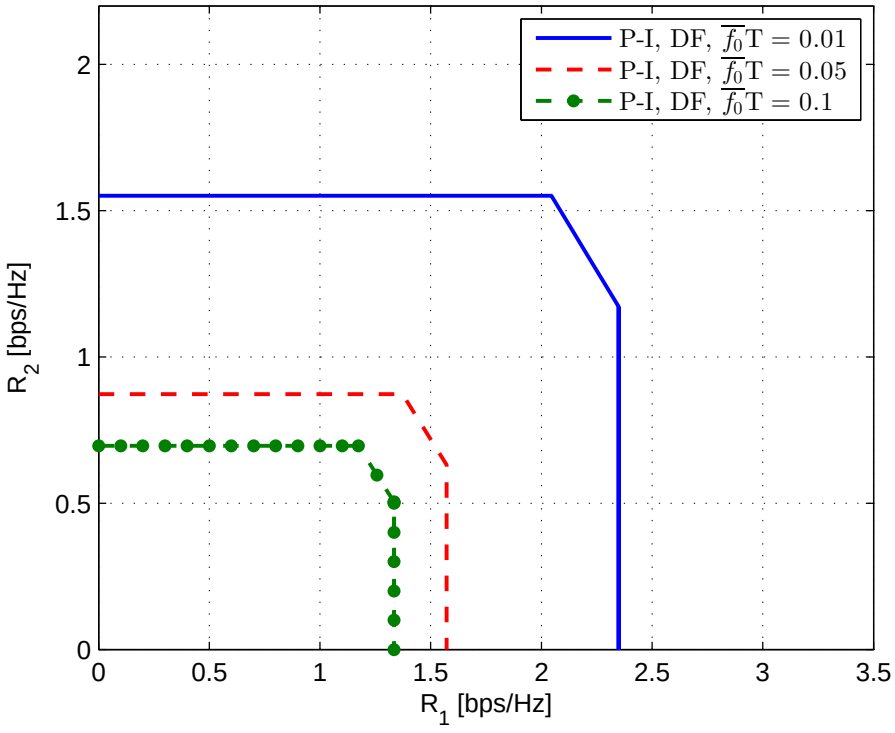

Figure 5.3: Effect of noise correlation on common outage capacity region of Protocol I ($\varepsilon = 0.1$ and $\beta = 10$ dB).

In Figure 5.3, we present the common outage capacity region for various values of ambient noise correlation when the relay is closer to the source node. For a targeted broadcasting phase transmission rate $R_1 = 0.5$ bps/Hz, the increase in relaying phase transmission rate R_2 for $\overline{f}_0 T = 0.01$ is 0.68 bps/Hz and 0.86 bps/Hz more than the cases of $\overline{f}_0 T = 0.05$ and 0.1 respectively. This is due to the increase in $\overline{f}_0 T$ that causes lower correlation between the noise samples, i.e. ambient noise becomes closer to white noise. Hence, the area of the outage capacity region decreases.

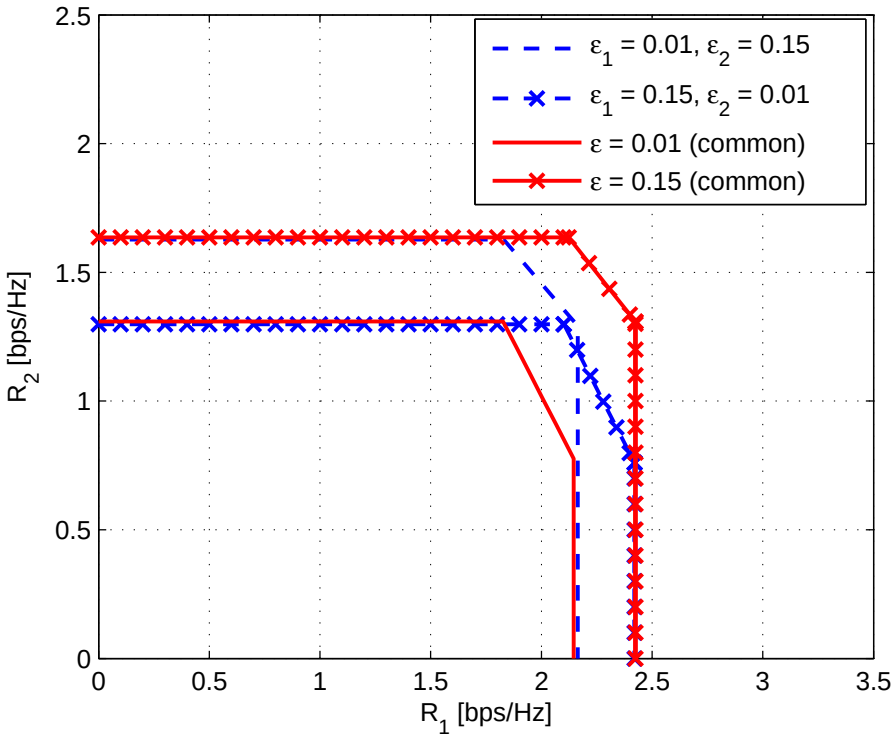

Figure 5.4: Individual and common outage capacity regions for Protocol I at $\gamma = 10$ dB.

In Figure 5.4, we study the individual and common outage capacity regions at SNR of 10 dB and $\beta = 10$ dB. We observe that for $R_1 = 1$ bps/Hz, R_2 decreases from 1.6 bps/Hz to 1.34 bps/Hz for individual outage probabilities $\varepsilon_2 = 0.15$ and 0.01 respectively. This decrease in the rate results from the decrease in the corresponding outage probability. Similarly, common outage capacity region increases as we increase ε from 0.01 to 0.15.

Chapter 6

Cooperative Multicarrier UWA Communication in the Presence of Non-Uniform Doppler-Distortion

In the previous chapters, we have assumed that the nodes are stationary leading to a quasi-static channel assumption. In this chapter, we consider a UWA channel with Doppler effects and investigate the performance of a multi-relay multi-carrier UWA system in the presence of Doppler distortion. Furthermore, we study resampling at the receiver and relay selection techniques, and then evaluate the BER performance for the system.

6.1 System Model

In this chapter, we consider the multi-relay system model in Figure 6.1 with K relays. For the following, we consider relay selection techniques for cooperative OFDM UWA system with AF relaying among K relays. The transmitted OFDM signal with cyclic prefix at the source node in the broadcasting phase is given by

$$\widetilde{s}(t) = \Re\left\{\sum_{n=0}^{N-1}\sqrt{E_s}x[n]\mathrm{e}^{j2\pi f_n t}p(t)\right\}, \quad t\in[-T_g,T] \tag{6.1}$$

where N is the number of subcarriers, $x[n]$ is the information symbol modulated on the $(n+1)^{\text{th}}$ subcarrier $f_n = f_0 + n\Delta f$, $B = N\Delta f$ is the total bandwidth, Δf is the subcarrier

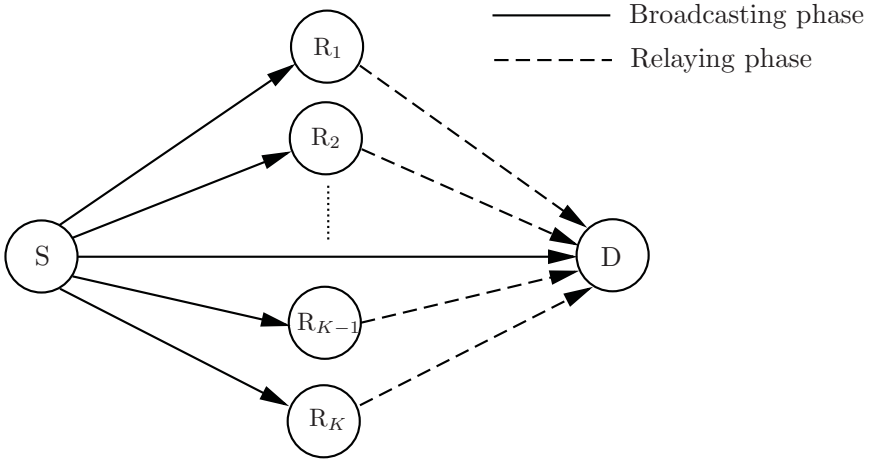

Figure 6.1: Multi-relay orthogonal cooperation model.

spacing, E_s is average energy per symbol, $T = 1/\Delta f$ is the OFDM symbol duration, T_g is cyclic prefix duration (or the guard duration), and $p(t)$ is the modulation pulse of duration $T + T_g$.

Let S, D, and R_k, $k = 1, \ldots, K$ respectively denote source, destination, and k^{th} relay nodes with intra-distances given by d_{SD}, d_{SR_k}, and $d_{\mathrm{R}_k\mathrm{D}}$. Defining $\beta_k = d_{\mathrm{R}_k\mathrm{D}}/d_{\mathrm{SR}_k}$, $\alpha_R^k = d_{\mathrm{SD}}/(1 + \beta_k^2 - 2\beta_k \cos\theta_k)^{-1/2}$, $\alpha_D^k = d_{\mathrm{SD}}/\left(1 + \beta_k^{-2} - 2\beta_k^{-1}\cos\theta_k\right)^{-1/2}$ and further using the law of cosines, geometrical gains are given by $G_{\mathrm{SD}}(f) = d_{\mathrm{SD}}^{-s} a(f)^{-d_{\mathrm{SD}}}$, $G_{\mathrm{SR}_k}(f) = ((1 + \beta_k^2 - 2\beta_k \cos\theta_k)/d_{\mathrm{SD}}^2)^{s/2}\ a(f)^{-\alpha_R^k}$ and $G_{\mathrm{R}_k\mathrm{D}}(f) = \left((1 + \beta_k^{-2} - 2\beta_k^{-1}\cos\theta_k)/d_{\mathrm{SD}}^2\right)^{s/2}$ $a(f)^{-\alpha_D^k}$. s and $a(f)$, respectively, denote the spreading factor and absorption coefficient. The absorption coefficient, which is based on Francois-Garrison model [72], is a function of frequency, pressure, temperature, salinity and acidity as introduced in Section 2.1. Channel impulse responses of the linear time-varying UWA channel for S $\to$ D, S $\to$ R_k, and $\mathrm{R}_k \to$ D links for $k = 1,\ \ldots\ , K$ are given, respectively, by

$$h_{\mathrm{SD}}(\tau, t) = \sum_{l=1}^{N_{\mathrm{S}}} h_{\mathrm{SD},l}\ \delta\left(\tau - (\tau_{\mathrm{SD},l} - a_l t)\right), \tag{6.2}$$

$$h_{\mathrm{SR}_k}(\tau, t) = \sum_{m=1}^{N_{\mathrm{R}}^k} h_{\mathrm{SR}_k,m}\, \delta\left(\tau - \left(\tau_{\mathrm{SR}_k,m} - b_m^k t\right)\right), \tag{6.3}$$

$$h_{\mathrm{R}_k\mathrm{D}}(\tau,t)=\sum_{p=1}^{N_{\mathrm{D}}^k}h_{\mathrm{R}_k\mathrm{D},p}\;\delta\left(\tau-\left(\tau_{\mathrm{R}_k\mathrm{D},p}-c_p^k t\right)\right) \tag{6.4}$$

where $\delta(.)$ is Dirac delta function and N_{S}, N_{R}^k, and N_{D}^k are the dominant discrete paths for the S $\rightarrow$ D, S $\rightarrow$ R_k, and R_k $\rightarrow$ D links respectively. $h_{\mathrm{SD},i}$, $h_{\mathrm{SR}_k,i}$, and $h_{\mathrm{R}_k\mathrm{D},i}$ and $\tau_{\mathrm{SD},i}$, $\tau_{\mathrm{SR}_k,i}$, and $\tau_{\mathrm{R}_k\mathrm{D},i}$ are the path gains and delays for i^{th} path in the S $\rightarrow$ D, S $\rightarrow$ R_k, and R_k $\rightarrow$ D links respectively. a_i, b_i^k, and c_i^k denote path-dependent Doppler scaling factors for i^{th} path of S $\rightarrow$ D, S $\rightarrow$ R_k, and R_k $\rightarrow$ D channel links respectively. In the case of stationary nodes, the UWA channel impulse response for S $\rightarrow$ D, S $\rightarrow$ R_k, and R_k $\rightarrow$ D links for $k=1,\ldots,K$ are assumed to be time-invariant during the OFDM symbol duration, i.e. $h_{\mathrm{XY}}(\tau,t)\approx h_{\mathrm{XY}}(\tau)$ for the link X $\rightarrow$ Y.

The continuous time bandpass received signals at k^{th} relay and destination nodes are, respectively, given by

$$\widetilde{y}_{\mathrm{R}_k}(t)=\Re\left\{\sum_{n=0}^{N-1}\sqrt{G_{\mathrm{SR}_k}(f)E_s}\,x[n]\right.$$
$$\left.\times\sum_{m=1}^{N_{\mathrm{R}}^k}h_{\mathrm{SR}_k,m}\mathrm{e}^{j2\pi f_n(t+b_m^k t-\tau_{\mathrm{SR}_k,m})}p(t+b_m^k t-\tau_{\mathrm{SR}_k,m})\right\}+\widetilde{z}_{\mathrm{R}_k}(t), \tag{6.5}$$

$$\widetilde{y}_{\mathrm{D},1}(t)=\Re\left\{\sum_{n=0}^{N-1}\sqrt{G_{\mathrm{SD}}(f)E_s}x[n]\sum_{l=1}^{N_{\mathrm{S}}}h_{\mathrm{SD},l}\mathrm{e}^{j2\pi f_n(t+a_l t-\tau_{\mathrm{SD},l})}\,p(t+a_l t-\tau_{\mathrm{SD},l})\right\}+\widetilde{z}_{\mathrm{D},1}(t) \tag{6.6}$$

where $\widetilde{z}_{\mathrm{R}_k}(t)$ and $\widetilde{z}_{\mathrm{D},1}(t)$ are additive white Gaussian noise random processes with zero mean and PSD $N_0/2$. Let $h_{\mathrm{SR}_k}[m]=h_{\mathrm{SR}_k,m}\exp(-j2\pi f_0\tau_{\mathrm{SR}_k,m})$, $h_{\mathrm{SD}}[l]=h_{\mathrm{SD},l}\exp(-j2\pi f_0\tau_{\mathrm{SD},l})$, $\widetilde{h}_{\mathrm{SR}_k,m}=h_{\mathrm{SR}_k}[m]\exp(-j2\pi\tau_{\mathrm{SR}_k,m}n/T)$ and $\widetilde{h}_{\mathrm{SD},l}=h_{\mathrm{SD}}[l]\exp(-j2\pi\tau_{\mathrm{SD},l}n/T)$. The continuous time complex baseband received signals at k^{th} relay and destination nodes are, respectively, given by

$$y_{\mathrm{R}_k}(t)=\sum_{n=0}^{N-1}\sqrt{G_{\mathrm{SR}_k}(f)E_s}\,x[n]\sum_{m=1}^{N_{\mathrm{R}}^k}\widetilde{h}_{\mathrm{SR}_k,m}\,e^{j2\pi b_m^k f_0 t}e^{j2\pi(t+b_m^k t)n/T}$$
$$\times p(t+b_m^k t-\tau_{\mathrm{SR}_k,m})+z_{\mathrm{R}_k}(t), \tag{6.7}$$
$$y_{\mathrm{D},1}(t)=\sum_{n=0}^{N-1}\sqrt{G_{\mathrm{SD}}(f)E_s}x[n]\sum_{l=1}^{N_{\mathrm{S}}}\widetilde{h}_{\mathrm{SD},l}\,e^{j2\pi a_l f_0 t}e^{j2\pi(t+a_l t)n/T}$$
$$\times p(t+a_l t-\tau_{\mathrm{SD},l})+z_{\mathrm{D},1}(t) \tag{6.8}$$

where $z_{\mathrm{R}_k}(t)$ and $z_{\mathrm{D},1}(t)$ are complex additive white Gaussian noise random processes with zero mean and PSD N_0. The k^{th} relay node scales the received signal over each subcarrier by a fixed amplification gain of $\overline{\eta}_k = \sqrt{G_{\mathrm{SR}_k}(f)E_s + N_0}$. Continuous time baseband received signal in the relaying phase at the destination node after scaling by $\overline{\eta}_k$ at the k^{th} relay node is given by

$$\begin{aligned} y_{\mathrm{D},2}(t) = & \sum_{n=0}^{N-1} \sqrt{\frac{G_{\mathrm{SR}_k}(f)G_{\mathrm{R}_k\mathrm{D}}(f)E_s^2}{\overline{\eta}_k^2}} \sum_{m=1}^{N_{\mathrm{R}}^k} \sum_{p=1}^{N_{\mathrm{D}}^k} \underbrace{h_{\mathrm{SR}_k,m} \mathrm{e}^{-j2\pi f_0 \tau_{\mathrm{SR}_k,m}}}_{h_{\mathrm{SR}_k}[m]} \underbrace{h_{\mathrm{R}_k\mathrm{D},p} \mathrm{e}^{-j2\pi f_0 \left(1+b_m^k\right)\tau_{\mathrm{R}_k\mathrm{D},p}}}_{h_{\mathrm{R}_k\mathrm{D}}[p]} \\ & \times x[n]\, \mathrm{e}^{-j2\pi\tau_{\mathrm{SR}_k,m} n/T} \mathrm{e}^{-j2\pi\left(1+b_m^k\right)\tau_{\mathrm{R}_k\mathrm{D},p} n/T} e^{j2\pi\left\{b_m^k\left(1+c_p^k\right)+c_p^k\right\}f_0 t} e^{j2\pi\left(1+b_m^k\right)\left(1+c_p^k\right)nt/T} \\ & \times p\left(\left(1+b_m^k\right)\left(1+c_p^k\right)t - \left(\tau_{\mathrm{SR}_k,m} + \left(1+b_m^k\right)\tau_{\mathrm{R}_k\mathrm{D},p}\right)\right) \\ & + \sqrt{\frac{G_{\mathrm{R}_k\mathrm{D}}(f)E_s}{\overline{\eta}_k^2}} \sum_{p=1}^{N_{\mathrm{D}}^k} h_{\mathrm{R}_k\mathrm{D},p}\, \mathrm{e}^{-j2\pi f_0 \tau_{\mathrm{R}_k\mathrm{D},p}} \mathrm{e}^{-j2\pi\tau_{\mathrm{R}_k\mathrm{D},p} n/T} z_{\mathrm{R}_k}(t) + \widehat{z}_{\mathrm{D},2}(t) \end{aligned} \tag{6.9}$$

where $\widehat{z}_{\mathrm{D},2}(t)$ is a complex additive white Gaussian noise random processes with zero mean and PSD N_0.

6.2 Receiver Design in Doppler-Distorted Channels

6.2.1 Conventional Receiver

First, we consider a conventional OFDM receiver that ignores compensation for Doppler offset and/or time scaling caused by various Doppler scaling factors in the multiple paths. Let $\{\phi_m(t)\}_{m=0}^{N-1}$ denote the set of orthonormal basis functions defined as

$$\phi_m(t) = \begin{cases} \frac{1}{\sqrt{T}} \exp\left(j2\pi mt/T\right), & 0 \le t \le T,\ m = 0,\ \ldots, N-1 \\ 0 \quad , & \text{elsewhere} \end{cases} \tag{6.10}$$

The received signals after the broadcasting phase over the $(i+1)^{\text{th}}$ subcarrier at the k^{th} relay node and the destination node using conventional OFDM receiver are

$$y_{\mathrm{R}_k}[i] = \sqrt{G_{\mathrm{SR}_k}(f)E_s}\, \widetilde{\Phi}_{i,i}^{\mathrm{SR}_k}\ x[i] + \sqrt{G_{\mathrm{SR}_k}(f)E_s} \sum_{\substack{n=0 \\ n\neq i}}^{N-1} \widetilde{\Phi}_{i,n}^{\mathrm{SR}_k}\ x[n]\ + z_i^{\mathrm{R}_k}, \tag{6.11}$$

$$y_{\mathrm{D},1}[i] = \sqrt{G_{\mathrm{SD}}(f)E_s}\ \widetilde{\Phi}_{i,i}^{\mathrm{SD}}\, x[i] + \sqrt{G_{\mathrm{SD}}(f)E_s} \sum_{\substack{n=0 \\ n\neq i}}^{N-1} \widetilde{\Phi}_{i,n}^{\mathrm{SD}}\, x[n]\ + z_i^{\mathrm{D},1} \tag{6.12}$$

where the elements of $\widetilde{\Phi}_{i,n}^{\mathrm{SR}_k}$ and $\widetilde{\Phi}_{i,n}^{\mathrm{SD}}$ in (6.11) and (6.12) in closed-form expressions, respectively, are

$$\widetilde{\Phi}_{i,n}^{\mathrm{SR}_k} = \frac{1}{T}\sum_{m=1}^{N_{\mathrm{R}}^k} h_{\mathrm{SR}_k}[m] e^{-j2\pi\tau_{\mathrm{SR}_k,m} n/T} f_s\left(l_{2,k} - l_{1,k}, v_{\mathrm{SR}_k}, l_{1,k}\right), \tag{6.13}$$

$$\widetilde{\Phi}_{i,n}^{\mathrm{SD}} = \frac{1}{T}\sum_{l=1}^{N_{\mathrm{S}}} h_{\mathrm{SD}}[l]\, e^{-j2\pi\tau_{\mathrm{SD},l} n/T} f_s\left(t_2 - t_1, v_{\mathrm{D},0}, t_1\right) \tag{6.14}$$

where $l_{1,k} = \max\left(0\ ,\ (-T_g + \tau_{\mathrm{SR}_k,m})\ /\ (1+b_m^k)\right)$, $l_{2,k} = \min\left(T, (T+\tau_{\mathrm{SR}_k,m})/(1+b_m^k)\right)$, $v_{\mathrm{SR}_k} = i/T - (1+b_m^k)n/T - b_m^k f_0$, $t_1 = \max(\ 0\ ,\ (-T_g + \tau_{\mathrm{SD},l})\ /\ (1+a_l))$, $t_2 = \min\left(T, (T+\tau_{\mathrm{SD},l})/(1+a_l)\right)$, and $v_{\mathrm{D},0} = i/T - (1+a_l)n/T - a_l f_0$. The multivariate function $f_s\left(x,y,z\right)$ is defined as

$$f_s\left(x,y,z\right) = x\ \mathrm{sinc}\left(x\,y\right)\ e^{-j2\pi(x/2+z)y} \tag{6.15}$$

where sinc(.) is the normalized sinc function, i.e. sinc(x) =$\sin(\pi x)/\pi x$. For the hardware implementation at the receiver side, we have $l_{1,k}, t_1 \to 0$, $l_{2,k} \to T/(1+b_m^k)$ and $t_2 \to T/(1+a_l)$, then the elements of ICI matrices $\Phi_{i,n}^{\mathrm{SR}_k}$ and $\Phi_{i,n}^{\mathrm{SD}}$ are given by

$$\Phi_{i,n}^{\mathrm{SR}_k} = \sum_{m=1}^{N_{\mathrm{R}}^k} \frac{h_{\mathrm{SR}_k}[m] e^{-j2\pi\tau_{\mathrm{SR}_k,m} n/T}}{1+b_m^k}\,\mathrm{sinc}\left(\frac{i-(1+b_m^k)n - b_m^k f_0 T}{1+b_m^k}\right) e^{-j\pi\frac{i-(1+b_m^k)n-b_m^k f_0 T}{1+b_m^k}}, \tag{6.16}$$

$$\Phi_{i,n}^{\mathrm{SD}} = \sum_{l=1}^{N_{\mathrm{S}}} \frac{h_{\mathrm{SD}}[l] \mathrm{e}^{-j2\pi\tau_{\mathrm{SD},l} n/T}}{1+a_l}\mathrm{sinc}\left(\frac{i-(1+a_l)n - a_l f_0 T}{1+a_l}\right) e^{-j\pi\frac{i-(1+a_l)n-a_l f_0 T}{1+a_l}} \tag{6.17}$$

The baseband received signal over the $(i+1)^{\mathrm{th}}$ subcarrier after the relaying phase and normalization at the destination node is

$$y_{\mathrm{D},2}[i] = \widetilde{\Phi}_{i,i}^{\mathrm{R}_k}\ \sqrt{\frac{G_{\mathrm{SR}_k}(f) G_{\mathrm{R}_k\mathrm{D}}(f) E_s^2}{\widetilde{\eta}_k^2}} x[i] + \sum_{\substack{n=0 \\ n\neq i}}^{N-1} \widetilde{\Phi}_{i,n}^{\mathrm{R}_k}\ \sqrt{\frac{G_{\mathrm{SR}_k}(f) G_{\mathrm{R}_k\mathrm{D}}(f) E_s^2}{\widetilde{\eta}_k^2}} x[n]\ + z_i^{\mathrm{D},2} \tag{6.18}$$

where $z_i^{\mathrm{D},2}$ is the effective additive noise after normalization at the destination node and $\widetilde{\eta}_k^2$ is

$$\widetilde{\eta}_k^2 = G_{\mathrm{SR}_k}(f) E_s + \left|\sum_{p=1}^{N_{\mathrm{D}}^k} h_{\mathrm{R}_k\mathrm{D},p}\, \mathrm{e}^{-j2\pi f_0 \tau_{\mathrm{R}_k\mathrm{D},p}} \mathrm{e}^{-j2\pi\tau_{\mathrm{R}_k\mathrm{D},p} n/T}\right|^2 G_{\mathrm{R}_k\mathrm{D}}(f) E_s + N_0, \tag{6.19}$$

and the elements of $\widetilde{\Phi}_{i,n}^{\mathrm{R}_k}$ in closed-form expressions is

$$\widetilde{\Phi}_{i,n}^{\mathrm{R}_k} = \frac{1}{T}\sum_{m=1}^{N_{\mathrm{R}}^k}\sum_{p=1}^{N_{\mathrm{D}}^k} h_{\mathrm{SR}_k}[m]\mathrm{e}^{-j2\pi\tau_{\mathrm{SR}_k,m}n/T}\, h_{\mathrm{R}_k\mathrm{D}}[p]\,\mathrm{e}^{-j2\pi\left(1+b_m^k\right)\tau_{\mathrm{R}_k\mathrm{D},p}n/T}\; f_s\left(u_{2,k}-u_{1,k}, v_{\mathrm{R},k}, u_{1,k}\right) \tag{6.20}$$

where $u_{1,k} = \max\left(0, (-T_g + \tau_{\mathrm{SR}_k,m} + (1+b_m^k)\tau_{\mathrm{R}_k\mathrm{D},p})/((1+b_m^k)(1+c_p^k))\right)$, $u_{2,k} = \min\left(T,\right.$ $\left.(T+\tau_{\mathrm{SR}_k,m}+(1+b_m^k)\tau_{\mathrm{R}_k\mathrm{D},p})/((1+b_m^k)(1+c_p^k))\right)$, and $v_{\mathrm{R},k} = i/T - \left(1+b_m^k\right)\left(1+c_p^k\right)n/T - \left(b_m^k\left(1+c_p^k\right)+c_p^k\right)f_0$. To improve the hardware implementation at the receiver side for the signal received from the cascaded relay link, assume $u_{1,k}\to 0$, $u_{2,k}\to T/((1+b_m^k)(1+c_p^k))$, then the approximate elements of ICI matrix $\Phi_{i,n}^{\mathrm{R}_k}$ is given by

$$\begin{aligned}\Phi_{i,n}^{\mathrm{R}_k} =& \sum_{m=1}^{N_{\mathrm{R}}^k}\sum_{p=1}^{N_{\mathrm{D}}^k} \frac{h_{\mathrm{SR}_k}[m]\mathrm{e}^{-j2\pi\tau_{\mathrm{SR}_k,m}n/T} h_{\mathrm{R}_k\mathrm{D}}[p]\mathrm{e}^{-j2\pi\left(1+b_m^k\right)\tau_{\mathrm{R}_k\mathrm{D},p}n/T}}{\left(1+b_m^k\right)\left(1+c_p^k\right)} \\ &\times \mathrm{sinc}\left(\frac{i-(1+b_m^k)(1+c_p^k)n-(b_m^k(1+c_p^k)+c_p^k)f_0T}{(1+b_m^k)(1+c_p^k)}\right) \\ &\times e^{-j\pi\left(\frac{i-(1+b_m^k)(1+c_p^k)n-(b_m^k(1+c_p^k)+c_p^k)f_0T}{(1+b_m^k)(1+c_p^k)}\right)}.\end{aligned} \tag{6.21}$$

The received signals after broadcasting and relaying phase from k^{th} relay node over the $(i+1)^{\mathrm{th}}$ subcarrier at the destination node are

$$r_{\mathrm{D},1}[i] = \Phi_{i,i}^{\mathrm{SD}}\ \sqrt{G_{\mathrm{SD}}(f)E_s}x[i] + \sum_{\substack{n=0\\n\neq i}}^{N-1}\Phi_{i,n}^{\mathrm{SD}}\ \sqrt{G_{\mathrm{SD}}(f)E_s}x[n]\ + z_i^{\mathrm{D},1}, \tag{6.22}$$

$$r_{\mathrm{D},2}[i] = \Phi_{i,i}^{\mathrm{R}_k}\ \sqrt{\frac{G_{\mathrm{SR}_k}(f)G_{\mathrm{R}_k\mathrm{D}}(f)E_s^2}{\widetilde{\eta}_k^2}}x[i] + \sum_{\substack{n=0\\n\neq i}}^{N-1}\Phi_{i,n}^{\mathrm{R}_k}\ \sqrt{\frac{G_{\mathrm{SR}_k}(f)G_{\mathrm{R}_k\mathrm{D}}(f)E_s^2}{\widetilde{\eta}_k^2}}x[n]\ + z_i^{\mathrm{D},2} \tag{6.23}$$

Let us define

$\mathbf{r}_{\mathrm{D},1} = [\ r_{\mathrm{D},1}[0]\ \ \ldots\ \ r_{\mathrm{D},1}[i]\ \ \ldots\ \ r_{\mathrm{D},1}[N-1]\ ]^T$,

$\mathbf{r}_{\mathrm{D},2} = [r_{\mathrm{D},2}[0]\ \ldots\ r_{\mathrm{D},2}[i]\ \ldots\ r_{\mathrm{D},2}[N-1]]^T$,

$\mathbf{z}_{\mathrm{D},1} = [\ z_0^{\mathrm{D},1}\ \ \cdots\ \ z_i^{\mathrm{D},1}\ \ \cdots\ \ z_{N-1}^{\mathrm{D},1}\ ]^T$, and

$\mathbf{z}_{\mathrm{D},2} = [\ z_0^{\mathrm{D},2} \quad \cdots \quad z_i^{\mathrm{D},2} \quad \cdots \quad z_{N-1}^{\mathrm{D},2}\ ]^T$. Therefore, the received signals in matrix form is

$$\underbrace{\begin{bmatrix} \mathbf{r}_{\mathrm{D},1} \\ \mathbf{r}_{\mathrm{D},2} \end{bmatrix}}_{\mathbf{r}^{\mathrm{CR}}} = \underbrace{\begin{bmatrix} \sqrt{G_{\mathrm{SD}}(f)E_s}\,\mathbf{\Phi}_{\mathrm{SD}} \\ \sqrt{\frac{G_{\mathrm{SR}_k}(f)G_{\mathrm{R}_k\mathrm{D}}(f)E_s^2}{\widetilde{\eta}_k^2}}\mathbf{\Phi}_{\mathrm{R}_k} \end{bmatrix}}_{\mathbf{H}^{\mathrm{CR}}} \mathbf{x} + \underbrace{\begin{bmatrix} \mathbf{z}_{\mathrm{D},1} \\ \mathbf{z}_{\mathrm{D},2} \end{bmatrix}}_{\mathbf{z}^{\mathrm{CR}}} \tag{6.24}$$

where the $(m+1, n+1)^{\mathrm{th}}$ element of $\mathbf{\Phi}_{\mathrm{SD}}$ is $\Phi_{m,n}^{\mathrm{SD}}$ defined in (6.17),$(m+1, n+1)^{\mathrm{th}}$ element of $\mathbf{\Phi}_{\mathrm{R}_k}$ is $\Phi_{m,n}^{\mathrm{R}_k}$ defined in (6.21).

6.2.2 Receiver with Single Resampling

Single resampling receiver compensates for the Doppler offset of the path with the maximum Doppler scaling factor; further, it considers this path in resampling the resulting signal. There are residual Doppler effects in the signal remaining due to the various Doppler distorted paths in the channel link. The continuous time bandpass received signals at k^{th} relay and destination nodes are given in (6.5) and (6.6), respectively. The continuous time complex baseband received signals at k^{th} relay and destination nodes are, respectively, given by (6.7) and (6.8).

Let $\widehat{a} = \max_l (a_l)$ and $\widehat{b}_k = \max_{m,p} \left(b_m^k \left(1 + c_p^k\right) + c_p^k\right)$ be the maximum Doppler scaling factors for the direct link S $\rightarrow$ D and the k^{th} cascaded underwater path S $\rightarrow$ R$_k$ $\rightarrow$ D, respectively. Consider two sets of orthonormal basis functions, i.e. $\left\{\phi_m^d(t)\right\}_{m=0}^{N-1}$ and $\left\{\phi_m^k(t)\right\}_{m=0}^{N-1}$, defined as

$$\phi_m^d(t) = \begin{cases} \sqrt{\frac{1+\widehat{a}}{T}} \exp\left(j2\pi m(1+\widehat{a})t/T\right) & , \quad 0 \le t \le \frac{T}{1+\widehat{a}},\ m = 0,\ \ldots, N-1 \\ 0 & , \quad \text{elsewhere} \end{cases}, \tag{6.25}$$

$$\phi_m^k(t) = \begin{cases} \sqrt{\frac{1+\widehat{b}_k}{T}} \exp\left(j2\pi m(1+\widehat{b}_k)t/T\right), & 0 \le t \le \frac{T}{1+\widehat{b}_k},\ m = 0,\ \ldots, N-1 \\ 0 & , \quad \text{elsewhere} \end{cases}. \tag{6.26}$$

The received signal after the broadcasting and relaying phases are compensated by $\exp(-j2\pi f_0 \widehat{a} t)$ and $\exp(-j2\pi f_0 \widehat{b}_k t)$ for the Doppler offset in the direct path and k^{th} relay link, respectively. The received signal after the broadcasting over the $(i+1)^{\mathrm{th}}$ subcarrier at the destination node using single-resampling OFDM receiver is

$$\overline{y}_{\mathrm{D},1}[i] = \sqrt{G_{\mathrm{SD}}(f)E_s}\ \widetilde{\Psi}_{i,i}^{\mathrm{SD}}\, x[i] + \sqrt{G_{\mathrm{SD}}(f)E_s} \sum_{\substack{n=0 \\ n \neq i}}^{N-1} \widetilde{\Psi}_{i,n}^{\mathrm{SD}}\, x[n]\ + \overline{z}_i^{\mathrm{D},1} \tag{6.27}$$

where the $(i+1, n+1)^{\text{th}}$ element of ICI matrix, $\widetilde{\Psi}_{i,n}^{\text{SD}}$ in (6.27), in closed-form expression is

$$\widetilde{\Psi}_{i,n}^{\text{SD}} = \frac{\sqrt{1+\widehat{a}}}{T} \sum_{l=1}^{N_{\text{S}}} h_{\text{SD}}[l]\, e^{-j2\pi\tau_{\text{SD},l} n/T}\, f_s\left(\bar{t}_2 - \bar{t}_1, \overline{v}_{\text{D},0}, \bar{t}_1\right) \tag{6.28}$$

where $\bar{t}_1 = \max\left(0, (-T_g + \tau_{\text{SD},l})/(1+a_l)\right)$, $\bar{t}_2 = \min\left(T/(1+\widehat{a}), (T+\tau_{\text{SD},l})/(1+a_l)\right)$, and $\overline{v}_{\text{D},0} = (\widehat{a} - a_l) f_0 + (1+\widehat{a}) i/T - (1+a_l) n/T$. For improving the hardware implementation at the receiver side, assume $\bar{t}_1 \to 0$, and $\bar{t}_2 \to T/(1+\widehat{a})$, then the received signal at the destination node is given by

$$\overline{r}_{\text{D},1}[i] = \sqrt{G_{\text{SD}}(f) E_s}\ \Psi_{i,i}^{\text{SD}}\, x[i] + \sqrt{G_{\text{SD}}(f) E_s} \sum_{\substack{n=0 \\ n\neq i}}^{N-1} \Psi_{i,n}^{\text{SD}}\, x[n]\ + \overline{z}_i^{\text{D},1} \tag{6.29}$$

where the element $\Psi_{i,n}^{\text{SD}}$ in (6.29) is

$$\begin{aligned}\Psi_{i,n}^{\text{SD}} =& \sum_{l=1}^{N_{\text{S}}} \frac{h_{\text{SD}}[l] \mathrm{e}^{-j2\pi\tau_{\text{SD},l} n/T}}{\sqrt{1+\widehat{a}}} \text{sinc}\left(\frac{(1+\widehat{a}) i - (1+a_l) n - (a_l - \widehat{a}) f_0 T}{1+\widehat{a}}\right) \\ & \times e^{-j\pi \frac{(1+\widehat{a}) i - (1+a_l) n - (a_l-\widehat{a}) f_0 T}{(1+\widehat{a})}}. \end{aligned} \tag{6.30}$$

In the cascaded underwater channel $\text{S} \to \text{R}_k \to \text{D}$, the compensation for the compounded frequency offset by m^{th} path in $\text{S} \to \text{R}_k$ and p^{th} path in $\text{R}_k \to \text{D}$ is $\exp(-j2\pi(1+\widehat{b}_k) f_0 t)$ at the destination node. After frequency offset compensation, the received signal is correlated with the orthonormal basis set for the k^{th} relay. The baseband received signal over the $(i+1)^{\text{th}}$ subcarrier after the relaying phase and normalization, and applying orthonormal functions $\phi_m^k(t)$ in (6.26), at the destination node is

$$\overline{y}_{\text{D},2}[i] = \widetilde{\Psi}_{i,i}^{\text{R}_k} \sqrt{\frac{G_{\text{SR}_k}(f) G_{\text{R}_k\text{D}}(f) E_s^2}{\widetilde{\eta}_k^2}} x[i] + \sum_{\substack{n=0 \\ n\neq i}}^{N-1} \widetilde{\Psi}_{i,n}^{\text{R}_k} \sqrt{\frac{G_{\text{SR}_k}(f) G_{\text{R}_k\text{D}}(f) E_s^2}{\widetilde{\eta}_k^2}} x[n]\ + \overline{z}_i^{\text{D},2} \tag{6.31}$$

where $\overline{z}_i^{\text{D},2}$ is the effective additive noise after normalization at the destination node and the element $\widetilde{\Psi}_{i,n}^{\text{R}_k}$ in (6.31), considering the m^{th} and p^{th} branches, in closed-form expression is given by

$$\begin{aligned}\widetilde{\Psi}_{i,n}^{\text{R}_k} =& \frac{\sqrt{1+\widehat{b}_k}}{T} \sum_{m=1}^{N_{\text{R}}^k} \sum_{p=1}^{N_{\text{D}}^k} h_{\text{SR}_k}[m] \mathrm{e}^{-j2\pi\tau_{\text{SR}_k,m} n/T} h_{\text{R}_k\text{D}}[p] \\ & \times \mathrm{e}^{-j2\pi\left(1+b_m^k\right)\tau_{\text{R}_k\text{D},p} n/T} f_s\left(\overline{u}_{2,k} - \overline{u}_{1,k}, \overline{v}_{\text{R},k}, \overline{u}_{1,k}\right) \end{aligned} \tag{6.32}$$

where

$\overline{u}_{1,k} = \max\big(0,\ (-T_g + \tau_{\mathrm{SR}_k,m} + (1+b_m^k)\tau_{\mathrm{R}_k\mathrm{D},p})/((1+b_m^k)(1+c_p^k))\big)$,

$\overline{u}_{2,k} = \min(T/(1+\widehat{b}_k), (T + \tau_{\mathrm{SR}_k,m} + (1+b_m^k)\tau_{\mathrm{R}_k\mathrm{D},p})/(1+\widehat{b}_k))$, and

$\overline{v}_{\mathrm{R},k} = ((1+\widehat{b}_k) - (b_{m_2}^k(1+c_{p_2}^k) + c_{p_2}^k))f_0 + (1+\widehat{b}_k)i/T - ((1+b_m^k)(1+c_p^k))n/T$.

The derivations of $\widetilde{\Psi}_{i,n}^{\mathrm{SD}}$ and $\widetilde{\Psi}_{i,n}^{\mathrm{R}_k}$ in (6.28) and (6.32), respectively, are shown in Appendix D.1. For improving the hardware implementation at the receiver side, assume $\overline{u}_{1,k} \to 0$, and $\overline{u}_{2,k} \to T/(1+\widehat{b}_k)$, then the received signal at the destination node is

$$\overline{r}_{\mathrm{D},2}[i] = \Psi_{i,i}^{\mathrm{R}_k}\sqrt{\frac{G_{\mathrm{SR}_k}(f)G_{\mathrm{R}_k\mathrm{D}}(f)E_s^2}{\widetilde{\eta}_k^2}}x[i] + \sum_{\substack{n=0\\n\neq i}}^{N-1}\Psi_{i,n}^{\mathrm{R}_k}\sqrt{\frac{G_{\mathrm{SR}_k}(f)G_{\mathrm{R}_k\mathrm{D}}(f)E_s^2}{\widetilde{\eta}_k^2}}x[n] + \overline{z}_i^{\mathrm{D},2} \tag{6.33}$$

where the approximate elements of ICI matrix, $\Psi_{i,n}^{\mathrm{R}_k}$, in (6.33) in closed-form expressions is given by

$$\begin{aligned}\Psi_{i,n}^{\mathrm{R}_k} = &\sum_{m=1}^{N_{\mathrm{R}}^k}\sum_{p=1}^{N_{\mathrm{D}}^k}\frac{h_{\mathrm{SR}_k}[m]\mathrm{e}^{-j2\pi\tau_{\mathrm{SR}_k,m}n/T}h_{\mathrm{R}_k\mathrm{D}}[p]\mathrm{e}^{-j2\pi\left(1+b_m^k\right)\tau_{\mathrm{R}_k\mathrm{D},p}n/T}}{\sqrt{1+\widehat{b}_k}}\\ &\times\ \mathrm{sinc}\left(\frac{(1+\widehat{b}_k)i - (1+b_m^k)(1+c_p^k)n - ((b_m^k(1+c_p^k)+c_p^k) - \widehat{b}_k)f_0T}{1+\widehat{b}_k}\right)\\ &\times e^{\frac{(1+\widehat{b}_k)i-(1+b_m^k)(1+c_p^k)n-((b_m^k(1+c_p^k)+c_p^k)-\widehat{b}_k)f_0T}{1+\widehat{b}_k}}.\end{aligned} \tag{6.34}$$

Let us define

$\overline{\mathbf{r}}_{\mathrm{D},1} = [\ \overline{r}_{\mathrm{D},1}[0]\ \ \cdots\ \ \overline{r}_{\mathrm{D},1}[i]\ \ \cdots\ \ \overline{r}_{\mathrm{D},1}[N-1]\ ]^T$,

$\overline{\mathbf{r}}_{\mathrm{D},2} = [\overline{r}_{\mathrm{D},2}[0]\ \ldots\ \overline{r}_{\mathrm{D},2}[i]\ \ldots\ \overline{r}_{\mathrm{D},2}[N-1]]^T$,

$\overline{\mathbf{z}}_{\mathrm{D},1} = [\ \overline{z}_0^{\mathrm{D},1}\ \ \cdots\ \ \overline{z}_i^{\mathrm{D},1}\ \ \cdots\ \ \overline{z}_{N-1}^{\mathrm{D},1}\ ]^T$, and

$\overline{\mathbf{z}}_{\mathrm{D},2} = [\ \overline{z}_0^{\mathrm{D},2}\ \ \cdots\ \ \overline{z}_i^{\mathrm{D},2}\ \ \cdots\ \ \overline{z}_{N-1}^{\mathrm{D},2}\ ]^T$. Therefore, the received signals in matrix form is

$$\underbrace{\begin{bmatrix}\overline{\mathbf{r}}_{\mathrm{D},1}\\ \overline{\mathbf{r}}_{\mathrm{D},2}\end{bmatrix}}_{\mathbf{r}^{\mathrm{SR}}} = \underbrace{\begin{bmatrix}\sqrt{G_{\mathrm{SD}}(f)E_s}\,\mathbf{\Psi}_{\mathrm{SD}}\\ \sqrt{\frac{G_{\mathrm{SR}_k}(f)G_{\mathrm{R}_k\mathrm{D}}(f)E_s^2}{\widetilde{\eta}_k^2}}\,\mathbf{\Psi}_{\mathrm{R}_k}\end{bmatrix}}_{\mathbf{H}^{\mathrm{SR}}}\mathbf{x} + \underbrace{\begin{bmatrix}\overline{\mathbf{z}}_{\mathrm{D},1}\\ \overline{\mathbf{z}}_{\mathrm{D},2}\end{bmatrix}}_{\mathbf{z}^{\mathrm{SR}}} \tag{6.35}$$

where $(m+1, n+1)^{\mathrm{th}}$ element of $\mathbf{\Psi}_{\mathrm{SD}}$ is $\Psi_{m,n}^{\mathrm{SD}}$ defined in (6.30), and $(m+1, n+1)^{\mathrm{th}}$ element of $\mathbf{\Psi}_{\mathrm{R}_k}$ is $\Psi_{m,n}^{\mathrm{R}_k}$ defined in (6.34).

6.2.3 Receiver with Multiple Resampling

In multiple resampling receiver, it compensates for the frequency offset in the various paths affected by non-uniform Doppler scaling factors; further, it considers every path in resampling the resulting received signal. Consider two sets of orthonormal basis functions, $\left\{\phi^d_{m,l}(t)\right\}_{m=0}^{N-1}$ and $\left\{\phi^k_{m,i,j}(t)\right\}_{m=0}^{N-1}$, defined as

$$\phi^d_{m,l}(t) = \begin{cases} \sqrt{\frac{1+a_l}{T}} \exp\left(j2\pi m(1+a_l)t/T\right), 0 \le t \le \frac{T}{1+a_l}, m = 0, ..., N-1, l = 1, ..., N_{\mathrm{S}} \\ 0 \qquad\qquad , \qquad \text{elsewhere} \end{cases} \tag{6.36}$$

$$\phi^k_{m,i,j}(t) = \begin{cases} \sqrt{\frac{(1+b^k_i)(1+c^k_j)}{T}} e^{\frac{j2\pi m(1+b^k_i)(1+c^k_j)t}{T}}, \ 0 \le t \le \frac{T}{(1+b^k_i)(1+c^k_j)}, \ m = 0, \ \dots, N-1 \\ 0 \qquad\qquad , \text{elsewhere} \end{cases} \tag{6.37}$$

for all $i \in \left\{1, \dots, N^k_{\mathrm{R}}\right\}$, $j \in \left\{1, \dots, N^k_{\mathrm{D}}\right\}$. Note that in (6.36), $\left\{\phi^d_{m,l}(t)\right\}$ forms a set of orthonormal basis functions for each l. Similarly, $\left\{\phi^k_{m,i,j}(t)\right\}$ forms a set of orthonormal basis functions for each triple tuple (k, i, j). Received signals at the destination node are compensated for the frequency offset experienced along the multiple resolvable paths. For the direct link S $\to$ D, the compensation for frequency offset in l^{th} underwater path is $\exp(-j2\pi a_l f_0 t)$. The received signal after the broadcasting phase over the $(i+1)^{\text{th}}$ subcarrier at the destination node correlating with the orthonormal basis functions $\phi^d_{m,l}(t)$ in (6.36) is

$$y^l_{\mathrm{D},1}[i] = \sqrt{G_{\mathrm{SD}}(f)E_s}\ \widetilde{\Upsilon}^{\mathrm{SD}}_{i,i}\, x[i] + \sqrt{G_{\mathrm{SD}}(f)E_s} \sum_{\substack{n=0 \\ n\neq i}}^{N-1} \widetilde{\Upsilon}^{\mathrm{SD}}_{i,n}\, x[n] \ + \widetilde{z}^{\mathrm{D},1}_i \tag{6.38}$$

where the ICI matrix element, $\widetilde{\Upsilon}^{\mathrm{SD}}_{i,n}$ in (6.38), considering the l^{th} branch, in closed-form expression is given by

$$\widetilde{\Upsilon}^{\mathrm{SD}}_{i,n} = \frac{\sqrt{1+a_l}}{T} \sum_{l_2=0}^{N_{\mathrm{S}}} h_{\mathrm{SD}}[l_2] \mathrm{e}^{-j2\pi\tau_{\mathrm{SD},l_2} n/T} f_s\left(\widetilde{t}_2 - \widetilde{t}_1, \widetilde{v}_{\mathrm{D},0}, \widetilde{t}_1\right) \tag{6.39}$$

where $\widetilde{t}_1 = \max\left(0, (-T_g + \tau_{\mathrm{SD},l_2})/(1+a_{l_2})\right)$, $\widetilde{t}_2 = \min\left(T/(1+a_l), (T+\tau_{\mathrm{SD},l_2})/(1+a_{l_2})\right)$, and $\widetilde{v}_{\mathrm{D},0} = (a_l - a_{l_2})f_0 + (1+a_l)i/T - (1+a_{l_2})n/T$. The received signal after combining

all different branches is given by

$$\widetilde{y}_{\mathrm{D},1}[i] = \sum_{l=1}^{N_{\mathrm{S}}} \widetilde{h}^{*}_{\mathrm{SD},l}\, y^{l}_{\mathrm{D},1}[i]. \tag{6.40}$$

For improving the hardware implementation at the receiver side, assume $\widetilde{t}_1 \rightarrow 0$, and $\widetilde{t}_2 \rightarrow T/(1+a_l)$, then the approximate elements of ICI matrix in direct link considering the l^{th} branch is

$$\sum_{l_2=1}^{N_{\mathrm{S}}} \frac{h_{\mathrm{SD}}[l_2]\mathrm{e}^{-j2\pi f_0 \tau_{\mathrm{SD},l_2}}}{\sqrt{1+a_l}} \mathrm{sinc}\left(\frac{(1+a_l)i-(1+a_{l_2})n-(a_{l_2}-a_l)f_0T}{1+a_l}\right) \times e^{-j\pi\frac{(1+a_l)i-(1+a_{l_2})n-(a_{l_2}-a_l)f_0T}{(1+a_l)}},$$

and the received signal after combining all branches at the destination node is

$$\widetilde{r}_{\mathrm{D},1}[i] = \sqrt{G_{\mathrm{SD}}(f)E_s}\ \Upsilon^{\mathrm{SD}}_{i,i}\, x[i] + \sqrt{G_{\mathrm{SD}}(f)E_s} \sum_{\substack{n=0 \\ n\neq i}}^{N-1} \Upsilon^{\mathrm{SD}}_{i,n}\, x[n]\ + \widetilde{z}^{\mathrm{D},1}_i \tag{6.41}$$

where the element $\Upsilon^{\mathrm{SD}}_{i,n}$ in (6.41),

$$\Upsilon^{\mathrm{SD}}_{i,n} = \sum_{l=1}^{N_{\mathrm{S}}}\sum_{l_2=1}^{N_{\mathrm{S}}} \frac{\widetilde{h}^{*}_{\mathrm{SD},l}\, h_{\mathrm{SD}}[l_2]\mathrm{e}^{-j2\pi\tau_{\mathrm{SD},l_2}n/T}}{\sqrt{1+a_l}} \times \mathrm{sinc}\left(\frac{(1+a_l)i-(1+a_{l_2})n-(a_{l_2}-a_l)f_0T}{1+a_l}\right) e^{-j\pi\frac{(1+a_l)i-(1+a_{l_2})n-(a_{l_2}-a_l)f_0T}{(1+a_l)}}. \tag{6.42}$$

In the cascaded underwater channel $\mathrm{S} \rightarrow \mathrm{R}_k \rightarrow \mathrm{D}$, the compensation for the compounded frequency offset by m^{th} path in $\mathrm{S} \rightarrow \mathrm{R}_k$ and p^{th} path in $\mathrm{R}_k \rightarrow \mathrm{D}$ is $\exp(-j2\pi(c^k_p + b^k_m(1+c^k_p))f_0 t)$. After Doppler offset compensation, the received signal is correlated with the orthonormal basis set for the m^{th} path in $\mathrm{S} \rightarrow \mathrm{R}_k$ and p^{th} path in $\mathrm{R}_k \rightarrow \mathrm{D}$. The baseband received signal over the $(i+1)^{\mathrm{th}}$ subcarrier after the relaying phase and normalization, and applying orthonormal functions $\phi^k_{i,m,p}(t)$ in (6.37), at the destination node is

$$y^{(m,p)}_{\mathrm{D},2}[i] = \sqrt{\frac{G_{\mathrm{SR}_k}(f)G_{\mathrm{R}_k\mathrm{D}}(f)E_s^2}{\widetilde{\eta}^2_k}}\widetilde{\Upsilon}^{\mathrm{R}_k}_{i,i}\ x[i] + \sum_{\substack{n=0 \\ n\neq i}}^{N-1} \sqrt{\frac{G_{\mathrm{SR}_k}(f)G_{\mathrm{R}_k\mathrm{D}}(f)E_s^2}{\widetilde{\eta}^2_k}}\widetilde{\Upsilon}^{\mathrm{R}_k}_{i,n}\, x[n]\ + \widetilde{z}^{\mathrm{D},2}_i \tag{6.43}$$

where $\widetilde{z}^{\mathrm{D},2}_i$ is the effective additive noise after normalization at the destination node and the element $\widetilde{\Upsilon}^{\mathrm{R}_k}_{i,n}$ in (6.43), considering the m^{th} and p^{th} branches, in closed-form expression

is given by

$$\widetilde{\Upsilon}_{i,n}^{\mathrm{R}_k} = \frac{\sqrt{(1+b_m^k)(1+c_p^k)}}{T} \sum_{m_2=1}^{N_{\mathrm{R}}^k} \sum_{p_2=1}^{N_{\mathrm{D}}^k} h_{\mathrm{SR}_k}[m_2] \mathrm{e}^{-j2\pi\tau_{\mathrm{SR}_k,m_2} n/T} h_{\mathrm{R}_k\mathrm{D}}[p_2] \times \mathrm{e}^{-j2\pi\left(1+b_{m_2}^k\right)\tau_{\mathrm{R}_k\mathrm{D},p_2} n/T} f_s\left(\widetilde{u}_{2,k} - \widetilde{u}_{1,k}, \widetilde{v}_{\mathrm{R},k}, \widetilde{u}_{1,k}\right) \tag{6.44}$$

where $\widetilde{u}_{1,k} = \max\left(0, (-T_g + \tau_{\mathrm{SR}_k,m_2} + (1+b_{m_2}^k)\tau_{\mathrm{R}_k\mathrm{D},p_2})/((1+b_{m_2}^k)(1+c_{p_2}^k))\right)$,
$\widetilde{u}_{2,k} = \min\left(T/(1+b_m^k)(1+c_p^k), (T + \tau_{\mathrm{SR}_k,m_2} + (1+b_{m_2}^k)\tau_{\mathrm{R}_k\mathrm{D},p_2})/((1+b_m^k)(1+c_p^k))\right)$, and
$\widetilde{v}_{\mathrm{R},k} = (b_m^k(1+c_p^k) + c_p^k - b_{m_2}^k(1+c_{p_2}^k) - c_{p_2}^k) f_0 + ((1+b_m^k)(1+c_p^k))i/T - ((1+b_{m_2}^k)(1+c_{p_2}^k))n/T$.

The derivations of $\widetilde{\Upsilon}_{i,n}^{\mathrm{SD}}$ and $\widetilde{\Upsilon}_{i,n}^{\mathrm{R}_k}$ in (6.39) and (6.44), respectively, are shown in Appendix D.2. Then, the received signal after combining all different m^{th} and p^{th} branches is

$$\widetilde{y}_{\mathrm{D},2}[i] = \sum_{m=0}^{N_{\mathrm{R}}^k} \sum_{p=0}^{N_{\mathrm{D}}^k} \widetilde{h}_{\mathrm{SR}_k,m}^* \widetilde{h}_{\mathrm{R}_k\mathrm{D},p}^* \, y_{\mathrm{D},2}^{(m,p)}[i]. \tag{6.45}$$

For improving the hardware implementation at the receiver side, assume $\widetilde{u}_{1,k} \to 0$, and $\widetilde{u}_{2,k} \to T/(1+b_m^k)(1+c_p^k)$, then the approximate $(i+1, n+1)^{\mathrm{th}}$ element of ICI matrices $\Upsilon_{i,n}^{\mathrm{R}_k}$ after combining all different m^{th} and p^{th} branches is given by

$$\Upsilon_{i,n}^{\mathrm{R}_k} = \sum_{m=1}^{N_{\mathrm{R}}^k} \sum_{p=1}^{N_{\mathrm{D}}^k} \sum_{m_2=1}^{N_{\mathrm{R}}^k} \sum_{p_2=1}^{N_{\mathrm{D}}^k} \frac{\widetilde{h}_{\mathrm{SR}_k,m}^* \widetilde{h}_{\mathrm{R}_k\mathrm{D},p}^* h_{\mathrm{SR}_k}[m_2] \mathrm{e}^{-j2\pi\tau_{\mathrm{SR}_k,m_2} n/T} h_{\mathrm{R}_k\mathrm{D}}[p_2] \mathrm{e}^{-j2\pi\left(1+b_{m_2}^k\right)\tau_{\mathrm{R}_k\mathrm{D},p_2} n/T}}{\sqrt{(1+b_m^k)(1+c_p^k)}} \times \mathrm{sinc}\left(\frac{\widetilde{v}_{\mathrm{R},k} T}{(1+b_m^k)(1+c_p^k)}\right) \exp\left(\frac{\widetilde{v}_{\mathrm{R},k} T}{(1+b_m^k)(1+c_p^k)}\right). \tag{6.46}$$

The received signals after relaying phase from k^{th} relay node over the $(i+1)^{\mathrm{th}}$ subcarrier at the destination node using multiple resampling OFDM receiver is

$$\widetilde{r}_{\mathrm{D},2}[i] = \sqrt{\frac{G_{\mathrm{SR}_k}(f) G_{\mathrm{R}_k\mathrm{D}}(f) E_s^2}{\widetilde{\eta}_k^2}} \, \Upsilon_{i,i}^{\mathrm{R}_k} \, x[i] + \sum_{\substack{n=0 \\ n \neq i}}^{N-1} \sqrt{\frac{G_{\mathrm{SR}_k}(f) G_{\mathrm{R}_k\mathrm{D}}(f) E_s^2}{\widetilde{\eta}_k^2}} \, \Upsilon_{i,n}^{\mathrm{R}_k} \, x[n] \, + \widetilde{z}_i^{\mathrm{D},2}. \tag{6.47}$$

Let us define
$\mathbf{r}_{\mathrm{D},1}^{\mathrm{M}} = \mathbf{Q}_1^{-1/2}[\ \widetilde{r}_{\mathrm{D},1}[0] \quad ... \quad \widetilde{r}_{\mathrm{D},1}[i] \quad ... \quad \widetilde{r}_{\mathrm{D},1}[N-1]\ ]^T$,
$\mathbf{r}_{\mathrm{D},2}^{\mathrm{M}} = \mathbf{Q}_{2,k}^{-1/2}[\widetilde{r}_{\mathrm{D},2}[0] \ ... \ \widetilde{r}_{\mathrm{D},2}[i] \quad ... \ \widetilde{r}_{\mathrm{D},2}[N-1]]^T$,
$\mathbf{z}_{\mathrm{D},1}^{\mathrm{M}} = \mathbf{Q}_1^{-1/2}[\ \widetilde{z}_0^{\mathrm{D},1} \quad \cdots \quad \widetilde{z}_i^{\mathrm{D},1} \quad \cdots \quad \widetilde{z}_{N-1}^{\mathrm{D},1}\ ]^T$,
$\mathbf{z}_{\mathrm{D},2}^{\mathrm{M}} = \mathbf{Q}_{2,k}^{-1/2}[\widetilde{z}_0^{\mathrm{D},2} \quad ... \quad \widetilde{z}_i^{\mathrm{D},2} \quad ... \quad \widetilde{z}_{N-1}^{\mathrm{D},2}]^T$
where

$\mathbf{Q}_1^{-1/2} \approx N_0\,\mathbf{U}_{\mathrm{MR}}\mathbf{D}_{\mathrm{MR}}^{-1/2}\mathbf{U}_{\mathrm{MR}}^{H}$, and $\mathbf{Q}_{2,k}^{-1/2} \approx N_0\mathbf{V}_{\mathrm{M},k}\mathbf{D}_{\mathrm{M},k}^{-1/2}\mathbf{V}_{\mathrm{M},k}^{H}$. $\mathbf{D}_{\mathrm{MR}}$ and $\mathbf{D}_{\mathrm{M},k}$ are the diagonal eigenvalues matrices of the Hermitian matrices $\boldsymbol{\Upsilon}_{\mathrm{SD}}$ and $\boldsymbol{\Upsilon}_{\mathrm{R_k}}$, respectively. $\mathbf{U}_{\mathrm{MR}}$ and $\mathbf{V}_{2,k}$ are the eigenvectors matrices of $\boldsymbol{\Upsilon}_{\mathrm{SD}}$ and $\boldsymbol{\Upsilon}_{\mathrm{R_k}}$ respectively. Therefore, the received signals in (6.41) and (6.47) after whitening the resulting noise vectors from branches combination in matrix form are

$$\underbrace{\begin{bmatrix}\mathbf{r}_{\mathrm{D},1}^{\mathrm{M}}\\ \mathbf{r}_{\mathrm{D},2}^{\mathrm{M}}\end{bmatrix}}_{\mathbf{r}^{\mathrm{MR}}} = \underbrace{\begin{bmatrix}\sqrt{G_{\mathrm{SD}}(f)E_s}\,\mathbf{Q}_1^{-1/2}\boldsymbol{\Upsilon}_{\mathrm{SD}}\\ \sqrt{\frac{G_{\mathrm{SR}_k}(f)G_{\mathrm{R}_k\mathrm{D}}(f)E_s^2}{\widetilde{\eta}_k^2}}\mathbf{Q}_{2,k}^{-1/2}\boldsymbol{\Upsilon}_{\mathrm{R_k}}\end{bmatrix}}_{\mathbf{H}^{\mathrm{MR}}}\mathbf{x} + \underbrace{\begin{bmatrix}\mathbf{z}_{\mathrm{D},1}^{\mathrm{M}}\\ \mathbf{z}_{\mathrm{D},2}^{\mathrm{M}}\end{bmatrix}}_{\mathbf{z}^{\mathrm{MR}}} \tag{6.48}$$

where elements of $\boldsymbol{\Upsilon}_{\mathrm{SD}}$ are given by $\Upsilon_{i,n}^{\mathrm{SD}}$ defined in (6.42), and elements of $\boldsymbol{\Upsilon}_{\mathrm{R_k}}$ are $\Upsilon_{i,n}^{\mathrm{R}_k}$ defined in (6.46).

Maximum-likelihood decision metric for multiple resampling demodulation assuming perfect channel state information and Doppler scaling factors at the receiver side is given by

$$\begin{aligned}\widehat{\mathbf{x}} = \arg\min_{\mathbf{x}}\Bigg\{&\left\|\mathbf{r}_{\mathrm{D},1}^{\mathrm{M}} - \sqrt{G_{\mathrm{SD}}(f)E_s}\mathbf{Q}_1^{-1/2}\boldsymbol{\Upsilon}_{\mathrm{SD}}\mathbf{x}\right\|^2\\ &+\left\|\mathbf{r}_{\mathrm{D},2}^{\mathrm{M}} - \sqrt{G_{\mathrm{SR}_k}(f)G_{\mathrm{R}_k\mathrm{D}}(f)E_s^2/\widetilde{\eta}_k^2}\mathbf{Q}_{2,k}^{-1/2}\boldsymbol{\Upsilon}_{\mathrm{R_k}}\mathbf{x}\right\|^2\Bigg\}.\end{aligned} \tag{6.49}$$

Due to complexity in applying ML detection for systems with large number of subcarriers as in UWA communication systems, we have resorted to linear detection techniques. Let the optimal linear receiver $\mathbf{F}_{\mathrm{M}} \in \mathbb{C}^{N\times 2N}$ be applied on a received vector at the destination node as a linear minimum mean square error (LMMSE) receiver. The optimal linear receiver $\mathbf{F}_{\mathrm{M}}$ is based on minimizing MSE, i.e. $J\left(\overline{\mathbf{F}}\right) = E\left[\mathrm{Tr}\left\{\left(\overline{\mathbf{F}}\mathbf{r}-\mathbf{x}\right)\left(\overline{\mathbf{F}}\mathbf{r}-\mathbf{x}\right)^{H}\right\}\right]$, which is given by

$$\mathbf{F}_{\mathrm{M}} = \underset{\overline{\mathbf{F}}\in\mathbb{C}^{N\times 2N}}{\arg\min}\; E\left[||\overline{\mathbf{F}}\mathbf{r}-\mathbf{x}||^2\right]. \tag{6.50}$$

The linear MMSE receiver for the AF cooperative OFDM system effected by an approximate noise covariance matrix, $\mathbf{K}_n = \mathrm{diag}(N_0\boldsymbol{\Upsilon}_{\mathrm{SD}}, N_0\boldsymbol{\Upsilon}_{\mathrm{R,k}})$, is

$$\mathbf{F}_{\mathrm{M}} = \left(\left(\mathbf{H}^{\mathrm{MR}}\right)^{H}\mathbf{H}^{\mathrm{MR}} + N_0\mathbf{I}_N\right)^{-1}\left(\mathbf{H}^{\mathrm{MR}}\right)^{H} \tag{6.51}$$

where $\mathbf{H}^{\mathrm{MR}}$ in (6.48) denote the whitened channel. The decoded symbols by LMMSE receiver are $\widehat{\mathbf{x}} = \mathrm{dec}\{\mathbf{F}_{\mathrm{M}}\mathbf{r}^{\mathrm{MR}}\}$, by applying the linear receiver of (6.51) to received signals in (6.48) where dec{.} denotes decoding based on the modulation constellation considered.

As another alternative, we consider Zero Forcing (ZF) linear receiver at the destination node, ZF receiver minimizes the MSE, $J\left(\overline{\mathbf{F}}\right)$ under the constraint that $\overline{\mathbf{F}}\mathbf{H}^{\mathrm{MR}}\mathbf{x} = \mathbf{x}$. The decoded symbols after applying the linear ZF receiver for the AF cooperative OFDM system are given by

$$\widehat{\mathbf{x}} = \mathrm{dec}\{\Big(\left(\mathbf{H}^{\mathrm{MR}}\right)^{H}\mathbf{H}^{\mathrm{MR}}\Big)^{-1}\left(\mathbf{H}^{\mathrm{MR}}\right)^{H}\mathbf{r}^{\mathrm{MR}}\}. \tag{6.52}$$

A simplified detection technique at the destination node without inversion in (6.51) and (6.52) is referred to as Matched Filter (MF) detection. In MF receiver, the filter is matched to the channel and maximizes the SNR at filter output while ignoring the ICI. The decoded symbols are obtained by $\widehat{\mathbf{x}} = \mathrm{dec}\{\left(\mathbf{H}^{\mathrm{MR}}\right)^{H}\mathbf{r}^{\mathrm{MR}}\}$ where there is no inversion process as in (6.51) and (6.52). Similarly, these linear detectors can also be applied for the conventional and single resampling receivers in Sections 6.2.1 and 6.2.2, respectively.

6.3 SNR-based Relay Selection Rules

In this section, we consider relay selection based on SNR maximization. For multi-carrier communication systems, we can select the best relay for each subcarrier, where each relay transmits selected subcarrier(s) and nulls the unselected subcarriers. This approach is known as per-subcarrier (PS) relay selection [108]. The indirect SNR for the cooperative UWA system using multiple resampling receiver over the n^{th} subcarrier is

$$\gamma_{\mathrm{R}_k}^{n} = \frac{|\Upsilon_{n,n}^{\mathrm{R}_k}|^2 G_{\mathrm{SR}_k}(f) G_{\mathrm{R}_k\mathrm{D}}(f)\gamma^2}{G_{\mathrm{SR}_k}(f)\gamma + \left|\sum_{p=1}^{N_{\mathrm{D}}^{k}} \overline{h}_{\mathrm{R}_k\mathrm{D}}[p]\mathrm{e}^{-j2\pi\tau_{\mathrm{R}_k\mathrm{D},p}n/T}\right|^2 G_{\mathrm{R}_k\mathrm{D}}(f)\gamma + 1} \tag{6.53}$$

where $\overline{h}_{\mathrm{R}_k\mathrm{D}}[p] = h_{\mathrm{R}_k\mathrm{D},p}\,\mathrm{e}^{-j2\pi f_0\tau_{\mathrm{R}_k\mathrm{D},p}}$. For each subcarrier n, we select the relay that results in the maximum indirect SNR expressed in (6.53). Therefore, selection rule can be expressed as

$$\arg\max_{k}\left\{\gamma_{\mathrm{R}_k}^{n}\right\}. \tag{6.54}$$

Another approach in relay selection for multicarrier systems is to select a single relay for all the subcarriers, also known as all-subcarriers (AS) relay selection. In this approach, the sum of indirect SNR in (6.53) for all subcarriers is maximized. Therefore the selection

rule can be expressed as

$$\arg\max_{k} \left\{ \sum_{n=0}^{N-1} \gamma_{\mathrm{R}_k}^{n} \right\}. \tag{6.55}$$

These relay selection techniques can be extended to single resampling and conventional receivers discussed earlier by replacing $\Upsilon_{n,n}^{\mathrm{R}_k}$ in (6.53) with $\Psi_{n,n}^{\mathrm{R}_k}$, defined in (6.34), and $\Phi_{n,n}^{\mathrm{R}_k}$ defined in (6.21), respectively.

6.4 ICI-based Relay Selection Rules

In this section, we consider relay selection based on minimizing the resulting ICI. We consider two approaches, namely PS and AS in relay selection. The power of interfering subcarriers for the n^{th} subcarrier for the indirect cooperative link of the k^{th} relay using multiple resampling receiver is

$$I(n,k) = \frac{\left| \sum\limits_{i=0, i\neq n}^{N-1} \Upsilon_{n,i}^{\mathrm{R}_k} \right|^2 G_{\mathrm{SR}_k}(f) G_{\mathrm{R}_k\mathrm{D}}(f) \gamma^2}{G_{\mathrm{SR}_k}(f)\gamma + \left| \sum\limits_{p=1}^{N_{\mathrm{D}}^k} \overline{h}_{\mathrm{R}_k\mathrm{D}}[p] \mathrm{e}^{-j2\pi\tau_{\mathrm{R}_k\mathrm{D},p} n/T} \right|^2 G_{\mathrm{R}_k\mathrm{D}}(f)\gamma + 1}. \tag{6.56}$$

We select the relay for each subcarrier n that results in the minimum power of interfering subcarriers for the n^{th} subcarrier, $I(n,k)$, for the indirect k^{th} cooperative link. ICI-based relay selection rule of multiple relay AF cooperative UWA system with PS approach is given by

$$\arg\min_{k} \left\{ I(n,k) \right\}. \tag{6.57}$$

On the other hand, in AS approach, the ICI-based relay selection rule is given by

$$\arg\min_{k} \left\{ \sum_{n=0}^{N-1} I(n,k) \right\}. \tag{6.58}$$

Similarly, these relay selection techniques can be extended to single resampling and conventional receivers discussed earlier by replacing $\Upsilon_{n,i}^{\mathrm{R}_k}$ in (6.56) with $\Psi_{n,i}^{\mathrm{R}_k}$, defined in (6.34), and $\Phi_{n,i}^{\mathrm{R}_k}$ defined in (6.21), respectively.

6.5 Numerical Results and Discussions

In this section, we present numerical results on the BER performance of multi-relay cooperative OFDM systems for various linear receivers with appropriate resampling techniques. We further consider the dual-hop transmission in the case of direct link's absence. We consider a setting of four relays ($K = 4$), a carrier frequency of 16 kHz, $N = 256$ subcarriers, system bandwidth of 2.5 kHz which corresponds, nominally, to symbol duration, T, of 0.4 ms, and a transmission distance of $d_{\mathrm{SD}} = 3$ km. We assume that $\beta_i = 0$ dB $\forall i \in \{1, \ldots, 4\}$, and all channels experience two dominant paths. For benchmarking purposes, we include the BER performance of direct transmission with single resampling receiver.

We consider S $\rightarrow$ D channel link with path-dependent Doppler scaling factors of $[a_1 \;\; a_2] = [0.001 \;\; 0.0025]$, path delays (in ms) of $[\tau_{\mathrm{SD},1} \;\; \tau_{\mathrm{SD},2}] = [0 \;\; 5]$. For cascaded S $\rightarrow$ R$_i$ $\rightarrow$ D channels, $i = 1, \ldots, 4$, path-dependent Doppler scaling factors and delays are given in Table 6.1. For environmental parameters, we assume temperature of 25 °C, depth of 50 m, acidity of 8 pH, salinity of 35‰, and spreading factor of 1.5. In our system of four relays, we consider Rician fading model for the small-scale effects in all UWA channels with uniform PDP and Rician factor of 2.

Table 6.1: Doppler scaling factors and path delays for $K = 4$.

Channel links	**Path-dependent Doppler scaling factors**		**Path delays [ms]**	
S $\rightarrow$ R$_k$ $\rightarrow$ D	$[\; b_1^k \;\; b_2^k \;]$	$[\; c_1^k \;\; c_2^k \;]$	$[\; \tau_{\mathrm{SR}_k,1} \;\; \tau_{\mathrm{SR}_k,2} \;]$	$[\; \tau_{\mathrm{R}_k\mathrm{D},1} \;\; \tau_{\mathrm{R}_k\mathrm{D},2} \;]$
S $\rightarrow$ R$_1$ $\rightarrow$ D	[0.002 0.005]	[0.001 0.004]	[3 7]	[2 10]
S $\rightarrow$ R$_2$ $\rightarrow$ D	[0.001 0.003]	[0.002 0.003]	[1 3]	[0 4]
S $\rightarrow$ R$_3$ $\rightarrow$ D	[0.001 0.004]	[0.002 0.005]	[0 5]	[1 3]
S $\rightarrow$ R$_4$ $\rightarrow$ D	[0.002 0.003]	[0.001 0.004]	[0 3]	[2 7]

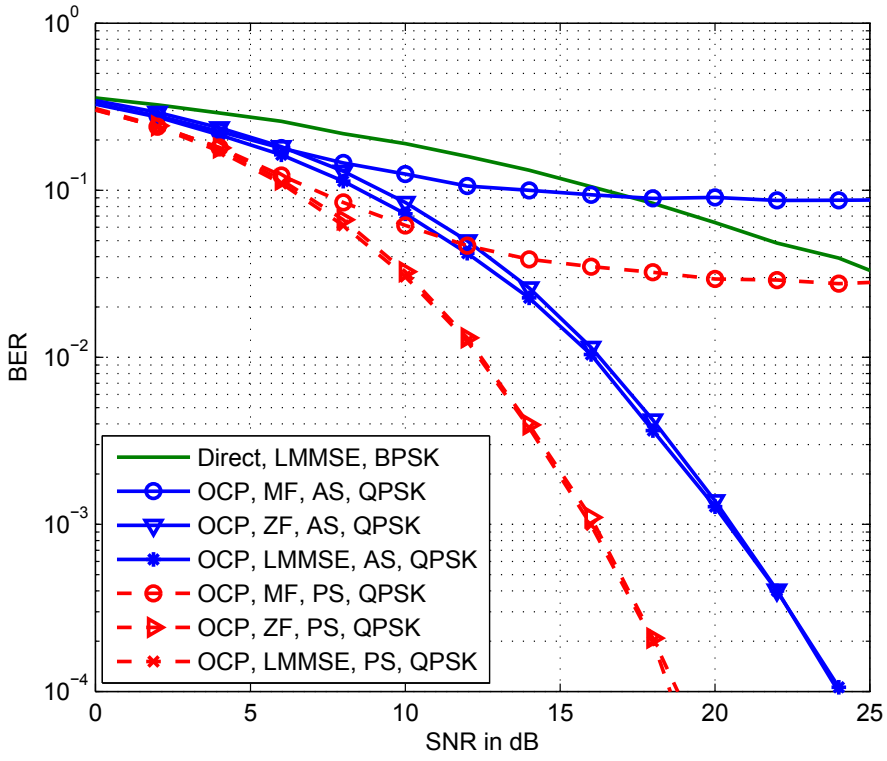

Figure 6.2: BER performance of SNR-based relay selection for cooperative OFDM UWA system with AF relaying. (OCP: Orthogonal cooperation protocol)

In Figure 6.2, we present the BER performance of cooperative OFDM UWA system with SNR-based relay selection. We assume both AS and PS approaches and consider multiple resampling techniques, and various linear detectors, i.e. LMMSE, ZF, and MF receivers. It is observed that cooperative OFDM UWA communication outperforms the direct transmission using LMMSE and ZF detection. Particularly, we observe that PS approach with SNR-based relay selection outperforms AS approach; however, the complexity at the receiver side increases with the number of subcarriers. Specifically, we observe that at BER of 10^{-3}, the SNR requirement in cooperative system with PS approach is smaller by 4.4 dB compared to AS approach. The performance exhibits error floor at high SNR values for MF receivers, where the filter is matched to the channel and maximizes the output SNR but ignores ICI.

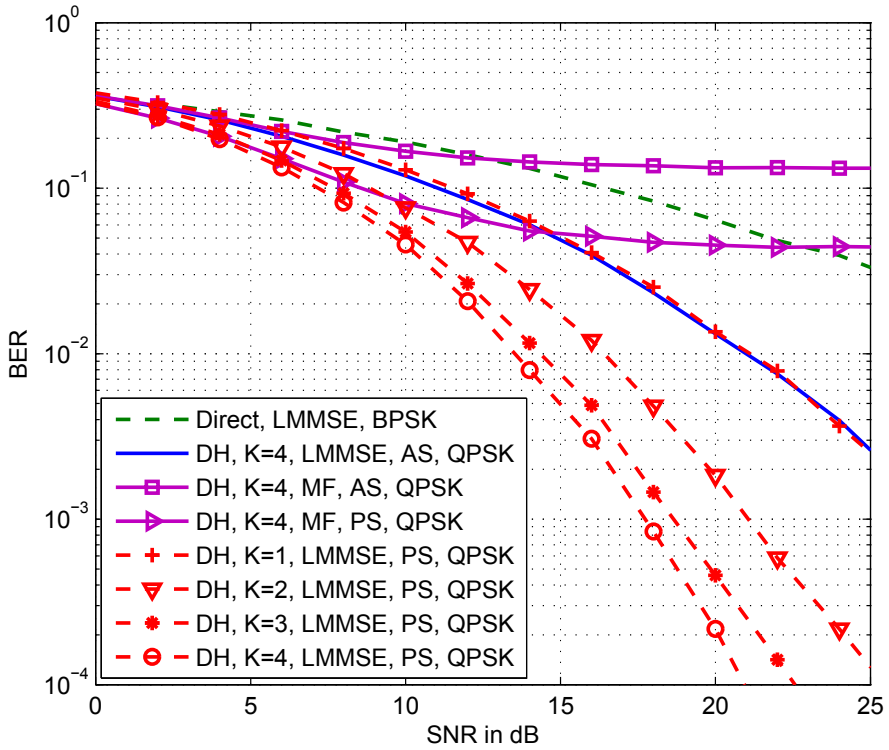

Figure 6.3: BER performance of SNR-based relay selection for cooperative OFDM UWA system with AF relaying. (DH: Dual-hop)

In Figure 6.3, we present the BER performance for dual-hop cooperative OFDM UWA system with various number of relays. We consider SNR-based relay selection and multiple resampling technique at the receiver side. We observe the decrease in BER performance as we increase the number of relays participating in selection. Specifically, at BER= 10^{-3} and $K = 4$, we observe an SNR improvement around 0.92 and 2.4 dB compared to systems with $K = 3$ and 2 respectively. Similarly, we observe that performance of dual-hop systems with MF receiver depicts error floor at high SNR.

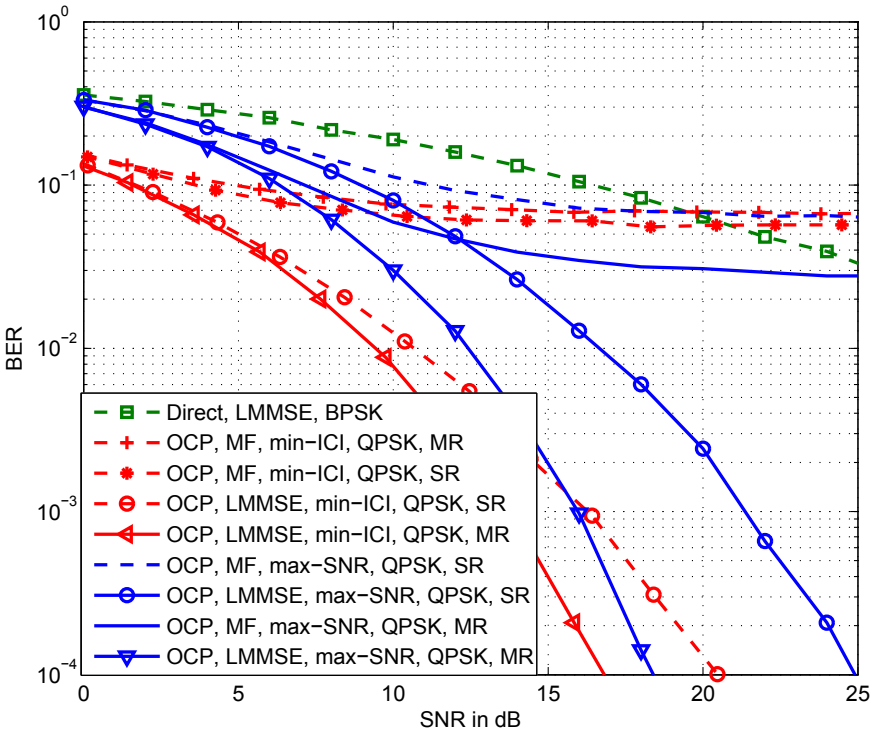

Figure 6.4: BER performance of multi-relay cooperative OFDM UWA system with SNR and ICI based selection rules. (OCP: Orthogonal cooperation protocol, MR: Multiple resampling, SR: Single resampling)

In Figure 6.4, we compare the BER performance of SNR-based and ICI-based relay selection techniques. We assume orthogonal cooperation protocol and consider $K = 4$ relays and LMMSE receivers. We observe that ICI-based multiple-relay selection systems outperform SNR-based in both resampling techniques. Specifically, at BER of 10^{-3} under multiple resampling assumption, we observe an SNR improvement of 2.18 dB in ICI-based selection compared to SNR-based one. Comparing the single and multiple resampling techniques under the assumption of SNR-based relay selection, we observe multiple resampling results in an improvement of around 5.4 dB at BER= 10^{-3} at the expense of complexity in implementation.

Chapter 7

Conclusions and Future Research

Building on the promising combination of multi-carrier and cooperative communication techniques, this dissertation has investigated the fundamental performance bounds of cooperative OFDM UWA communication systems taking into account the inherent unique characteristics of the UWA channel. We have derived outage probability and capacity expressions for cooperative UWA systems with AF and DF relaying. Through the derived expressions, we have demonstrated the effect of several system and channel parameters on the performance. We have also investigated the performance of cooperative UWA systems in the presence of non-uniform Doppler distortion and proposed receiver designs to mitigate the degrading Doppler effects.

In Chapter 2, we propose an approximate statistical model for the non-stationary ambient noise. The proposed model allows mathematical tractability and is a good fit for most operating frequencies in practical UWA communication systems.

In Chapter 3, we have investigated the outage performance for AF cooperative OFDM system over UWA channels based on the availability of ambient noise statistics. We have derived closed-form expressions for the outage probability and outage capacity for the precoded OFDM cooperative UWA system over sparse Rician fading channel. The outage performance of multi-hop UWA system is also studied. Our results demonstrated a close match between derived expressions and the exact outage performance. The performance improvement of AF cooperative UWA system over direct transmission at high SNR values is observed. Moreover, we have studied the effect of relay location, operating frequency,

availability of ambient noise statistics, and underwater temperature on the outage performance.

In Chapter 4, we have investigated the information-theoretic outage performance of DF cooperation over UWA channels. We have derived closed-form expressions for the outage probability in DF cooperative OFDM UWA system under the assumption of unknown ambient noise covariance. Simplified expressions under the high SNR assumption are provided. Based on these expressions, we studied the optimal relay location that minimizes the overall outage probability of the UWA communication system. The effects of Rician k-factor and operating carrier frequency on the optimal relay location are observed.

In Chapter 5, we consider three cooperation protocols that vary in degrees of broadcasting and collision, and derive the maximum achievable sum-rate expressions and common/individual outage capacity regions. The effects of several system and environmental parameters such as underwater temperature, carrier frequency, and noise correlation on the outage capacity regions are analyzed.

In Chapter 6, we have studied the performance of multiple relay selection over non-uniform Doppler distorted UWA channels. We proposed receiver structures for multi-relay cooperative systems over UWA channels with motion-induced Doppler spreading. Relay selection in multicarrier systems based on SNR maximization and ICI minimization with AS and PS approaches are investigated. We observe improvements under multiple resampling technique which provides higher ICI suppression at the expense of higher complexity. Furthermore, we demonstrated that PS approach in relay selection outperforms AS under various Doppler distorted UWA channels.

The current research can be extended in several directions. For example, we have investigated the outage performance assuming equal power allocation between the source and relay nodes and among the subcarriers as well. The optimum power allocation among the nodes and/or the subcarriers can be pursued to minimize the overall outage probability of the system under total power constraint and at a fixed transmission rate exploiting the derived expressions.

Another assumption in our outage performance derivations is the availability of known channel state information at the relay and destination nodes. However, in practice, the fading coefficients are unknown at the receiver and need to be estimated. The derivations

can be further extended to include the effects of imperfect channel estimation. In such a derivation, the sparse characteristics of the UWA channel should be particularly considered.

In Chapter 5, we have investigated the receiver design for multi-relay cooperative OFDM system with different relay selection techniques. This scheme deals with a relay-assisted point-to-point UWA communication and can be extended to the multi-user case where more than one node communicate to a single destination node. This occurs when different underwater sensors (or AUVs) communicate with a single underwater gateway (analogous to base station in RF wireless communication). Multi-user OFDM is another open research problem to pursue in underwater.

APPENDICES

Appendix A

Approximation of Ambient Noise PSD

In this appendix, we present the approximation for the underwater ambient noise PSD. First, we consider the waves noise PSD, i.e.

$$N(f) \approx \frac{\widetilde{\alpha}_3 f^2}{(f+0.4)^4} \tag{A.1}$$

where $\widetilde{\alpha}_3 = 10^{5+0.75\sqrt{w}}$, and w is wind speed in m/s. This is based on the fact that waves noise PSD is the major contributing noise in the range 100 Hz -100 kHz which is the operating region for most acoustical communication systems [109].

We further approximate $N(f)$ for the frequency range 10-100 kHz by

$$N(f) \approx \frac{\widetilde{\alpha}_3}{f^2}, \tag{A.2}$$

This results in an $1/f$ fractal (statistically self-similar) random process [93] for ambient noise. For this spectrum, spectral parameter is two; and it results in non-stationary random process.

We approximate the non-stationary $1/f$ fractal random process by a stationary process. For short observation of time, it is observed that ambient noise appears stationary. We further introduce $\widetilde{\beta}$ to smooth the power spectral density function approximating ambient noise for UWA channel such that at low frequency it will not diverge,

$$N(f) \approx \frac{\widetilde{\alpha}_3}{f^2 + \widetilde{\beta}}. \tag{A.3}$$

Let

$$P_0 = \lim_{f \to 0} N(f) = \lim_{f \to 0} \frac{\widetilde{\alpha}_3}{f^2 + \widetilde{\beta}} = \frac{\widetilde{\alpha}_3}{\widetilde{\beta}}. \tag{A.4}$$

Define $\overline{f}_0$ in kHz such that $N\left(\overline{f}_0\right) = P_0/2$. Hence, $\widetilde{\beta} = \overline{f}_0^2$ and

$$N(f) \approx \frac{\widetilde{\alpha}_3}{f^2 + \overline{f}_0^2} = N_a(f). \tag{A.5}$$

This approximation is in a similar approach given by Keshner in [95]. Finally, rewriting approximate PSD $N_a(f)$ in terms of variance of complex-valued baseband ambient noise $n(t)$, σ_n^2, where $\sigma_n^2 = E[n(t)n^*(t)]$. Let $\sigma_n^2 = \pi\widetilde{\alpha}_3/\overline{f}_0$, then we have

$$N(f) \approx N_a(f) = \frac{\overline{f}_0 \sigma_n^2}{\pi\left(f^2 + \overline{f}_0^2\right)}. \tag{A.6}$$

Appendix B

Calculation of μ_{T_l} and $\sigma^2_{T_l}$

In this appendix, we derive μ_{T_l} and $\sigma^2_{T_l}$ in (3.18). Let $\gamma_{\rm SD}$ and $\gamma_{\rm R}$ be, respectively, defined as $\gamma_{\rm SD} = (1/N)\sum_{k=0}^{N-1}\gamma G_{\rm SD}(f)\mathbf{\Gamma}_{\rm SD}(k)$, and $\gamma_{\rm R} = (1/N)\sum_{k=0}^{N-1}(\gamma^2 G_{\rm SR}(f)G_{\rm RD}(f)\mathbf{\Gamma}_{\rm SR}(k)$ $\mathbf{\Gamma}_{\rm RD}(k))/(\gamma\, G_{\rm RD}\,(f)\mathbf{\Gamma}_{\rm RD}(k) + \gamma\; G_{\rm SR}(f) + 1)$. For the convenience of the presentation, we will drop f of $G_{\rm SD}(f)$, $G_{\rm SR}(f)$, and $G_{\rm RD}(f)$ in the following. μ_{T_l} is given by

$$\mu_{T_l} = \gamma G_{\rm SD} + \frac{\gamma^2 G_{\rm SR} G_{\rm RD}}{N}\sum_{i=0}^{N-1} M_{1,i}M_{2,i} \tag{B.1}$$

where $M_{1,i}$ and $M_{2,i}$ are expressed as

$$M_{1,i} = 1 + 2\sum_{k=0}^{L_{\rm SR}}\sum_{\substack{l=0\\k<l}}^{L_{\rm SR}} \mu_{{\rm SR},k}\mu_{{\rm SR},l}\Re\left\{\exp\left(j2\pi(v^l_{\rm SR} - v^k_{\rm SR})i/N\right)\right\}, \tag{B.2}$$

$$M_{2,i} = \frac{1}{\widetilde{\beta}_1} - \frac{\widetilde{\beta}_2}{\widetilde{\beta}_1^2\Psi}\exp\left(-\frac{1}{2}\left(s_i^2 - \frac{\widetilde{\beta}_2}{\widetilde{\beta}_1\Psi}\right)\right)\sum_{k=0}^{\infty}\frac{s_i^{2k}\Psi^{(1-k)/2}}{k!2^k}\widetilde{\beta}_1^{(1-k)/2}\widetilde{\beta}_2^{(k-1)/2}\; W_{-\frac{k+1}{2},\frac{k}{2}}\left(\frac{\widetilde{\beta}_2}{\widetilde{\beta}_1\Psi}\right). \tag{B.3}$$

Here, $L_{\rm SD}$, $L_{\rm SR}$, and $L_{\rm RD}$ are significant number of ISI taps, $\widetilde{\beta}_1 = \gamma G_{\rm RD}$, $\widetilde{\beta}_2 = \gamma G_{\rm SR} + 1$, $\Psi = 2\sum_{l=0}^{L_{\rm RD}}\sigma^2_{{\rm RD},l}$, and $W_{\lambda,\mu}(.)$ is the Whittaker function [100] defined as

$$W_{\lambda,\mu}(z) = \frac{z^{\mu+0.5}e^{-z/2}}{\Gamma(\mu-\lambda+0.5)}\int_0^{\infty} e^{-zt}t^{\mu-\lambda-0.5}(1+t)^{\mu+\lambda-0.5}dt. \tag{B.4}$$

The non-centrality parameter for the non-central chi-square distributed random variable

$\mathbf{\Gamma}_{\mathrm{RD}}(i)$ for $(i+1)^{\mathrm{th}}$ subcarrier is given by

$$s_i^2 = \left(\sum_{l=0}^{L_{\mathrm{RD}}} \sigma_{\mathrm{RD},l}^2\right)^{-1} \left\{ \left(\sum_{k=0}^{L_{\mathrm{RD}}} \mu_{\mathrm{RD},k} \left[\Re\left(\exp(-j2\pi\, v_{\mathrm{RD}}^k i/N)\right) - \Im\left(\exp(-j2\pi v_{\mathrm{RD}}^k\, i/N)\right)\right] \right)^2 + \left(\sum_{m=0}^{L_{\mathrm{RD}}} \mu_{\mathrm{RD},m} \left[\Re\left(\exp(-j2\pi\, v_{\mathrm{RD}}^m i/N)\right) + \Im\left(\exp(-j2\pi\, v_{\mathrm{RD}}^m i/N)\right)\right] \right)^2 \right\}. \tag{B.5}$$

For deriving $\sigma_{T_l}^2$ in (3.18), first we need to calculate the second moment of T_l given by

$$E\left[{T_l}^2\right] = E\left[\gamma_{\mathrm{SD}}^2\right] + 2E\left[\gamma_{\mathrm{SD}}\right] E\left[\gamma_{\mathrm{R}}\right] + E\left[\gamma_{\mathrm{R}}^2\right] \tag{B.6}$$

where $E\left[\gamma_{\mathrm{SD}}\right] = \gamma G_{\mathrm{SD}}$ and $E\left[\gamma_{\mathrm{R}}\right] = (\gamma^2 G_{\mathrm{SR}} G_{\mathrm{RD}}/N) \sum_{i=0}^{N-1} M_{1,i} M_{2,i}$. Taking expectation with the respect to the direct link S $\rightarrow$ D, we have

$$E\left[\gamma_{\mathrm{SD}}^2\right] = \gamma^2 G_{\mathrm{SD}}^2 \times \underbrace{\left\{ \sum_{l=0}^{L_{\mathrm{SD}}} \left(\mu_{\mathrm{SD},l}^4 + 8\mu_{\mathrm{SD},l}^2 \sigma_{\mathrm{SD},l}^2 + 8\sigma_{\mathrm{SD},l}^2\right) + \sum_{k=0}^{L_{\mathrm{SD}}} \sum_{\substack{l=0 \\ k\neq l}}^{L_{\mathrm{SD}}} \left(2\sigma_{\mathrm{SD},k}^2 + \mu_{\mathrm{SD},k}^2\right)\left(2\sigma_{\mathrm{SD},l}^2 + \mu_{\mathrm{SD},l}^2\right) \right\}}_{Z}. \tag{B.7}$$

On the other hand, taking expectation with respect to S $\rightarrow$ R and R $\rightarrow$ D links, we obtain the approximation given by

$$E\left[\gamma_{\mathrm{R}}^2\right] \approx \frac{\gamma^4 G_{\mathrm{SR}}^2 G_{\mathrm{RD}}^2}{N^2} \times \left[\sum_{i=0}^{N-1} D_i \left(\widetilde{A}_{1,i} + \widetilde{A}_{2,i} + \widetilde{A}_{3,i} \right) + \sum_{n_1=0}^{N-1} \sum_{\substack{n_2=0 \\ n_1\neq n_2}}^{N-1} \widetilde{D}(n_1, n_2) \left(\widetilde{B}_1 + \widetilde{B}_2 + \widetilde{B}_3 + \widetilde{B}_4 \right) \right] \tag{B.8}$$

where $\widetilde{A}_{1,i}$ and $\widetilde{B}_1$ takes the form of Z in (B.7) and obtained by replacing $\mu_{\mathrm{SD},i}$ and $\sigma_{\mathrm{SD},i}$ in Z by $\mu_{\mathrm{SR},i}$ and $\sigma_{\mathrm{SR},i}$, respectively, and $\sigma_{T_l}^2 = E\left[{T_l}^2\right] - \mu_{T_l}^2$. D_i, $\widetilde{D}(n_1, n_2)$, $\widetilde{A}_{2,i}$, $\widetilde{A}_{3,i}$ are defined respectively as

$$D_i = \frac{1}{\widetilde{\beta}_1^2} \exp\left(-\frac{1}{2}\left(s_i^2 - \frac{\widetilde{\beta}_2}{\widetilde{\beta}_1 \Psi} \right) \right) \sum_{k=0}^{\infty} \frac{s_i^{2k} \widetilde{\beta}_2^{k/2} \Gamma(k+3)}{k! 2^k \Gamma(k+1) \left(\widetilde{\beta}_1 \Psi\right)^{k/2}} W_{-\frac{k+4}{2}, \frac{k+1}{2}}\left(\frac{\widetilde{\beta}_2}{\widetilde{\beta}_1 \Psi} \right), \tag{B.9}$$

$\widetilde{D}(n_1, n_2) \approx D_{n^*}$ with $n^* = \underset{n\in\{n_1,n_2\}}{\arg\min}\{D_n\}$

$$\widetilde{A}_{2,i} = 4\left[\Psi_{1,i} + \Psi_{2,i} + \Psi_{3,i}\right], \tag{B.10}$$

$$\widetilde{A}_{3,i} = 4\left[\widetilde{\Phi}_{1,i} + \widetilde{\Phi}_{2,i}\right] \tag{B.11}$$

where $\Psi_{1,i}$, $\Psi_{2,i}$, $\Psi_{3,i}$, $\widetilde{\Phi}_{1,i}$, and $\widetilde{\Phi}_{2,i}$ are defined as

$$\Psi_{1,i} = \sum_{l=0}^{L_{\mathrm{SR}}} \sum_{\substack{k=0 \\ l<k}}^{L_{\mathrm{SR}}} \left(\mu_{\mathrm{SR},l}^3 \mu_{\mathrm{SR},k} + 4\mu_{\mathrm{SR},l}\mu_{\mathrm{SR},k}\sigma_{\mathrm{SR},l}^2\right) \Re\left\{\exp\left(j2\pi(v_{\mathrm{SR}}^k - v_{\mathrm{SR}}^l)i/N\right)\right\}, \tag{B.12}$$

$$\Psi_{2,i} = \sum_{m=0}^{L_{\mathrm{SR}}} \sum_{\substack{k=0 \\ m<k}}^{L_{\mathrm{SR}}} \left(\mu_{\mathrm{SR},k}^3 \mu_{\mathrm{SR},m} + 4\mu_{\mathrm{SR},k}\mu_{\mathrm{SR},m}\sigma_{\mathrm{SR},k}^2\right) \Re\left\{\exp\left(j2\pi(v_{\mathrm{SR}}^k - v_{\mathrm{SR}}^m)i/N\right)\right\}, \tag{B.13}$$

$$\Psi_{3,i} = \sum_{l=0}^{L_{\mathrm{SR}}} \sum_{m=0}^{L_{\mathrm{SR}}} \sum_{\substack{k=0 \\ m<k}}^{L_{\mathrm{SR}}} \left(\mu_{\mathrm{SR},l}^2 \mu_{\mathrm{SR},m}\mu_{\mathrm{SR},k} + 2\mu_{\mathrm{SR},m}\mu_{\mathrm{SR},k}\sigma_{\mathrm{SR},l}^2\right) \Re\left\{\exp\left(j2\pi(v_{\mathrm{SR}}^k - v_{\mathrm{SR}}^m)i/N\right)\right\}, \tag{B.14}$$

$$\widetilde{\Phi}_{1,i} = \sum_{k=0}^{L_{\mathrm{SR}}} \sum_{\substack{l=0 \\ k<l}}^{L_{\mathrm{SR}}} \left(\alpha_{k,l}\left(\Re\left\{\exp(j2\pi(v_{\mathrm{SR}}^l - v_{\mathrm{SR}}^k)i/N)\right\}\right)^2 + \beta_{k,l}\left(\Im\left\{\exp\left(j2\pi(v_{\mathrm{SR}}^l - v_{\mathrm{SR}}^k)i/N\right)\right\}\right)^2\right), \tag{B.15}$$

$$\widetilde{\Phi}_{2,i} = \sum_{k_1=0}^{L_{\mathrm{SR}}} \sum_{\substack{l_1=0 \\ k_1<l_1}}^{L_{\mathrm{SR}}} \sum_{k_2=0}^{L_{\mathrm{SR}}} \sum_{\substack{l_2=0 \\ k_2<l_2}}^{L_{\mathrm{SR}}} \mu_{\mathrm{SR},k_1}\mu_{\mathrm{SR},l_1}\mu_{\mathrm{SR},k_2}\mu_{\mathrm{SR},l_2} \Re\left\{\exp\left(j2\pi(v_{\mathrm{SR}}^{l_1} - v_{\mathrm{SR}}^{k_1})i/N\right)\right\}$$
$$\times \Re\left\{\exp\left(j2\pi(v_{\mathrm{SR}}^{l_2} - v_{\mathrm{SR}}^{k_2})i/N\right)\right\} \tag{B.16}$$

In the above, $\alpha_{k,l}$ and $\beta_{k,l}$ in $\widetilde{\Phi}_{1,i}$ are defined as

$$\alpha_{k,l} = 2\sigma_{\mathrm{SR},k}^2\sigma_{\mathrm{SR},l}^2 + \mu_{\mathrm{SR},k}^2\sigma_{\mathrm{SR},l}^2 + \mu_{\mathrm{SR},l}\sigma_{\mathrm{SR},k}^2 + \mu_{\mathrm{SR},k}^2\mu_{\mathrm{SR},l}^2, \tag{B.17}$$

$$\beta_{k,l} = 2\sigma_{\mathrm{SR},k}^2\sigma_{\mathrm{SR},l}^2 + \mu_{\mathrm{SR},k}^2\sigma_{\mathrm{SR},l}^2 + \mu_{\mathrm{SR},l}^2\sigma_{\mathrm{SR},k}^2. \tag{B.18}$$

On the other hand, $\widetilde{B}_2$, $\widetilde{B}_3$, and $\widetilde{B}_4$ in (B.8) are given by

$$\widetilde{B}_2 = 2\left[\Psi_{1,n_1} + \Psi_{2,n_1} + \Psi_{3,n_1}\right], \tag{B.19}$$

$$\widetilde{B}_3 = 2\left[\Psi_{1,n_2} + \Psi_{2,n_2} + \Psi_{3,n_2}\right], \tag{B.20}$$

$$\widetilde{B}_4 = 4\left[T_1 + T_2\right] \tag{B.21}$$

where T_1 and T_2 are defined as

$$T_1 = \sum_{k=0}^{L_{\mathrm{SR}}} \sum_{\substack{l=0 \\ k<l}}^{L_{\mathrm{SR}}} \Re\left\{\exp\left(j2\pi(v_{\mathrm{SR}}^{l} - v_{\mathrm{SR}}^{k})n_1/N\right)\right\} \Re\left\{\exp\left(j2\pi(v_{\mathrm{SR}}^{l} - v_{\mathrm{SR}}^{k})n_2/N\right)\right\} \left(\mu_{\mathrm{SR},k}^2 \mu_{\mathrm{SR},l}^2\right)$$
$$+ \left(\Re\left\{\exp\left(j2\pi(v_{\mathrm{SR}}^{l} - v_{\mathrm{SR}}^{k})n_1/N\right)\right\} \Re\left\{\exp\left(j2\pi(v_{\mathrm{SR}}^{l} - v_{\mathrm{SR}}^{k})n_2/N\right)\right\}\right.$$
$$\left. + \Im\left\{\exp\left(j2\pi(v_{\mathrm{SR}}^{l} - v_{\mathrm{SR}}^{k})n_1/N\right)\right\} \Im\left\{\exp\left(j2\pi(v_{\mathrm{SR}}^{l} - v_{\mathrm{SR}}^{k})n_2/N\right)\right\}\right)$$
$$\times \left(\mu_{\mathrm{SR},k}^2 \sigma_{\mathrm{SR},l}^2 + \sigma_{\mathrm{SR},k}^2 \mu_{\mathrm{SR},l}^2 + 2\sigma_{\mathrm{SR},k}^2 \sigma_{\mathrm{SR},l}^2\right), \tag{B.22}$$

$$T_2 = \sum_{k_1=0}^{L_{\mathrm{SR}}} \sum_{\substack{l_1=0 \\ k_1<l_1}}^{L_{\mathrm{SR}}} \sum_{k_2=0}^{L_{\mathrm{SR}}} \sum_{\substack{l_2=0 \\ k_2<l_2}}^{L_{\mathrm{SR}}} \mu_{\mathrm{SR},k_1} \mu_{\mathrm{SR},l_1} \mu_{\mathrm{SR},k_2} \mu_{\mathrm{SR},l_2} \Re\left\{\exp\left(j2\pi(v_{\mathrm{SR}}^{l_1} - v_{\mathrm{SR}}^{k_1})n_1/N\right)\right\}$$
$$\times \Re\left\{\exp\left(j2\pi(v_{\mathrm{SR}}^{l_2} - v_{\mathrm{SR}}^{k_2})n_2/N\right)\right\}. \tag{B.23}$$

Appendix C

Proofs and Derivations of CDF and MGF in Chapter 4

C.1 Proof of Lower Bound in Eq. (4.13)

In this appendix, we show that the bound in (4.13) is a lower bound to the exact outage probability $P_{\text{out,u}}^{\text{DF}}$ defined in (4.3). For simplicity of notation, let $P_1 = \Pr[I_{\text{C}} \leq R]$, $\overline{P_1} = \Pr[I_{\text{C,U}} \leq R]$, $P_2 = \Pr[I_{\text{R}} \leq R]$, $\overline{P_2} = \Pr[I_{\text{R,U}} \leq R]$, $P_3 = \Pr[I_{\text{D}} \leq R]$, and $\overline{P_3} = \Pr[I_{\text{D,U}} \leq R]$. This implies $P_{\text{out,u}}^{\text{DF}} = P_1(1 - P_2) + P_3 P_2$. Due to Jensen's inequality, $P_1 \geq \overline{P_1}$, $P_2 \geq \overline{P_2}$, and $P_3 \geq \overline{P_3}$. Further, $0 < 1 - P_2 < 1$, and we can lower bound $P_{\text{out,u}}^{\text{DF}}$ as

$$P_{\text{out,u}}^{\text{DF}} \geq \overline{P_1} + \left(\overline{P_3} - \overline{P_1}\right) P_2. \tag{C.1}$$

It can be shown that $\overline{P_3} - \overline{P_1} \geq 0$ by substituting corresponding derived CDFs in Appendices C.2 and C.3; hence,

$$\begin{aligned} P_{\text{out,u}}^{\text{DF}} &\geq \overline{P_1} + \left(\overline{P_3} - \overline{P_1}\right) \overline{P_2} \\ &= \Pr[I_{\text{C,U}} \leq R](1 - \Pr[I_{\text{R,U}} \leq R]) + \Pr[I_{\text{D,U}} \leq R] \Pr[I_{\text{R,U}} \leq R]. \end{aligned} \tag{C.2}$$

C.2 CDF Derivations of $I_{\mathrm{D,U}}$ and $I_{\mathrm{R,U}}$

As seen from (4.10) and (4.11), $I_{\mathrm{D,U}}$ and $I_{\mathrm{R,U}}$ have a form of

$$I_{\mathrm{XY}} = \frac{N}{2\left(N+L_c\right)}\log_2\left(1+\frac{1}{N}\sum_{n=0}^{N-1} G_{\mathrm{XY}}(f)\gamma\mathbf{\Gamma}_{\mathrm{XY}}(n)\right). \tag{C.3}$$

The detailed derivations of moment generating function (MGF) for $(1/N)\sum_{n=0}^{N-1}\mathbf{\Gamma}_{\mathrm{XY}}(n)$ in (C.3) is shown in Appendix C.4. The CDF of I_{XY} is given by

$$F_{I_{\mathrm{XY}}}(x) = \Pr\left\{\sum_{l=0}^{L_{\mathrm{XY}}} \underbrace{\frac{\Omega_{\mathrm{XY},l}}{2(k_{\mathrm{XY},l}+1)}}_{\alpha_l}\left\{\left(\frac{\Re\left(h_{\mathrm{XY}}(v_{\mathrm{XY}}^l)\right)}{\sigma_{\mathrm{XY},l}}\right)^2+\left(\frac{\Im\left(h_{\mathrm{XY}}(v_{\mathrm{XY}}^l)\right)}{\sigma_{\mathrm{XY},l}}\right)^2\right\} \leq \frac{2^{\frac{2(N+L_c)}{N}x}-1}{G_{\mathrm{XY}}(f)\gamma}\right\} \tag{C.4}$$

where $v_{\mathrm{XY}}^l \in \mathbf{v}_{\mathrm{XY}}, \forall l \in \{0,...,L_{\mathrm{XY}}\}$. Denote $Y_l^r = \left(\Re\left(h_{\mathrm{XY}}(v_{\mathrm{XY}}^l)\right)/\sigma_{\mathrm{XY},l}\right)^2$ and $Y_l^i = \left(\Im\left(h_{\mathrm{XY}}(v_{\mathrm{XY}}^l)\right)/\sigma_{\mathrm{XY},l}\right)^2$ then $Y_l = Y_l^r + Y_l^i$ is a noncentral chi-square random variable with two degrees of freedom and the noncentrality parameter $\rho_l = \mu_{\mathrm{XY},l}^2/\sigma_{\mathrm{XY},l}^2$. Denote $\eta = \sum_{l=0}^{L_{\mathrm{XY}}}\alpha_l Y_l$. Using the truncated CDF of η [111] and after simplifications, it is given by

$$F_\eta(x) = \frac{e^{-\frac{x}{2\mu_1}}x^{L_{\mathrm{XY}}+1}}{(2\mu_1)^{L_{\mathrm{XY}}+2}\Gamma\left(L_{\mathrm{XY}}+2\right)}\sum_{k=0}^{K_t-1}\frac{k!m_k}{\left(L_{\mathrm{XY}}+2\right)_k}L_k^{(L_{\mathrm{XY}}+1)}\left(\frac{(L_{\mathrm{XY}}+2)x}{2\mu_0\mu_1}\right), \quad \mu_0,\mu_1>0 \tag{C.5}$$

where $(.)_k$ is the rising factorial power (Pochhammer symbol), $\Gamma(.)$ is the complete Gamma function, $L_k^{(\alpha)}(.)$ is the k^{th} generalized Leguerre polynomial, and the coefficients m_k can be obtained from the recurrence relations

$$\begin{aligned} m_0 =& 2(L_{\mathrm{XY}}+2)^{L_{\mathrm{XY}}+2}\exp\left\{-\frac{1}{2}\sum_{i=1}^{L_{\mathrm{XY}}+1}\frac{\mu_{\mathrm{XY},i}^2\Omega_{\mathrm{XY},i}\left(L_{\mathrm{XY}}+2-\mu_0\right)}{2\sigma_{\mathrm{XY},i}^2\left(k_{\mathrm{XY},i}+1\right)\mu_0\mu_1+\sigma_{\mathrm{XY},i}^2\Omega_{\mathrm{XY},i}\left(L_{\mathrm{XY}}+2-\mu_0\right)}\right\} \\ &\times\frac{\mu_1^{L_{\mathrm{XY}}+2}}{L_{\mathrm{XY}}+2-\mu_0}\prod_{i=1}^{L_{\mathrm{XY}}+1}\left(\mu_0\mu_1+\frac{\Omega_{\mathrm{XY},i}}{2(k_{\mathrm{XY},i}+1)}\left(L_{\mathrm{XY}}+2-\mu_0\right)\right)^{-1}, \end{aligned} \tag{C.6}$$

$$m_k = \frac{1}{k}\sum_{j=0}^{k-1} m_j d_{k-j}, \quad k\geq 1 \tag{C.7}$$

where d_j is given by

$$d_j = -\frac{j\mu_1(L_{\mathrm{XY}}+2)}{2\mu_0}\sum_{i=1}^{L_{\mathrm{XY}}+1}\frac{\mu_{\mathrm{XY},i}^2\Omega_{\mathrm{XY},i}}{2\sigma_{\mathrm{XY},i}^2\left(k_{\mathrm{XY},i}+1\right)}\left(\mu_1-\frac{\Omega_{\mathrm{XY},i}}{2\left(k_{\mathrm{XY},i}+1\right)}\right)^{j-1}$$
$$\times\left(\frac{2\mu_0\left(k_{\mathrm{XY},i}+1\right)}{2\mu_0\mu_1\left(k_{\mathrm{XY},i}+1\right)+\Omega_{\mathrm{XY},i}\left(L_{\mathrm{XY}}+2-\mu_0\right)}\right)^{j+1}+\left(\frac{-\mu_0}{L_{\mathrm{XY}}+2-\mu_0}\right)^{j}$$
$$+\sum_{i=1}^{L_{\mathrm{XY}}+1}\left(\frac{2\left(k_{\mathrm{XY},i}+1\right)\mu_0\mu_1-\Omega_{\mathrm{XY},i}}{2\left(k_{\mathrm{XY},i}+1\right)\mu_0\mu_1+\Omega_{\mathrm{XY},i}\left(L_{\mathrm{XY}}+2-\mu_0\right)}\right)^{j},\qquad j\geq 1. \tag{C.8}$$

The k^{th} generalized Leguerre polynomial is given by [110]

$$L_k^{(\alpha)}(x)=\frac{\Gamma(k+\alpha+1)}{\Gamma(k+1)\Gamma(\alpha+1)}{}_1F_1\left(-k;\alpha+1;x\right) \tag{C.9}$$

where ${}_1F_1\left(a;b;c\right)$ is the confluent hypergeometric function of the first kind in [100], the complete Gamma function $\Gamma(x)=\int_0^\infty t^{x-1}e^{-t}dt$ and Pochhammer symbol $(x)_k=\Gamma(x+k)/\Gamma(x)$, $k\geq 0$. By substituting $x=\left(2^{2(N+L_c)y/N}-1\right)/(G_{\mathrm{XY}}(f)\gamma)$ in (C.5), the CDF of I_{XY}, i.e. $F_{I_{\mathrm{XY}}}(y)$, can be expressed as

$$F_{I_{\mathrm{XY}}}(y)=F_\eta\left((2^{2(N+L_c)y/N}-1)/(G_{\mathrm{XY}}(f)\gamma)\right). \tag{C.10}$$

C.3 CDF Derivation of $I_{\mathrm{C,U}}$

$I_{\mathrm{C,U}}$ is given by (4.12). Its CDF is therefore given by

$$F_{I_{\mathrm{C,U}}}(x)=\Pr\left\{\sum_{l=0}^{L_{\mathrm{SD}}}\frac{G_{\mathrm{SD}}(f)\gamma\,\Omega_{\mathrm{SD},l}}{2(k_{\mathrm{SD},l}+1)}\left\{\left(\frac{\Re\left(h_{\mathrm{SD}}(v_{\mathrm{SD}}^l)\right)}{\sigma_{\mathrm{SD},l}}\right)^2+\left(\frac{\Im\left(h_{\mathrm{SD}}(v_{\mathrm{SD}}^l)\right)}{\sigma_{\mathrm{SD},l}}\right)^2\right\}\right.$$
$$\left.+\sum_{p=0}^{L_{\mathrm{RD}}}\frac{G_{\mathrm{RD}}(f)\gamma\,\Omega_{\mathrm{RD},p}}{2(k_{\mathrm{RD},p}+1)}\left\{\left(\frac{\Re\left(h_{\mathrm{RD}}(v_{\mathrm{RD}}^p)\right)}{\sigma_{\mathrm{RD},p}}\right)^2+\left(\frac{\Im\left(h_{\mathrm{RD}}(v_{\mathrm{RD}}^p)\right)}{\sigma_{\mathrm{RD},p}}\right)^2\right\}\leq 2^{2(N+L_c)x/N}-1\right\} \tag{C.11}$$

where $v_{\mathrm{SD}}^l\in\mathbf{v}_{\mathrm{SD}},\forall l\in\{0,...,L_{\mathrm{SD}}\}$ and $v_{\mathrm{RD}}^p\in\mathbf{v}_{\mathrm{RD}},\forall p\in\{0,...,L_{\mathrm{RD}}\}$. Let $\widetilde{\mathbf{v}}=[\ \mathbf{v}_{\mathrm{SD}}\quad\mathbf{v}_{\mathrm{RD}}\ ]$, $X_{1,i}=\left(\Re\left(h_{\mathrm{SD}}(v_{\mathrm{SD}}^i)\right)/\sigma_{\mathrm{SD},i}\right)^2$, and $X_{2,i}=\left(\Im\left(h_{\mathrm{SD}}(v_{\mathrm{SD}}^i)\right)/\sigma_{\mathrm{SD},i}\right)^2$, $\forall i\in\{0,...,L_{\mathrm{SD}}\}$, $X_{1,j}=\left(\Re\left(h_{\mathrm{RD}}(v_{\mathrm{RD}}^j)\right)\right)/\sigma_{\mathrm{RD},j}\right)^2$, $X_{2,j}=\left(\Im\left(h_{\mathrm{RD}}(v_{\mathrm{RD}}^j)\right)\right)/\sigma_{\mathrm{RD},j}\right)^2$, $\forall j\in\{L_{\mathrm{SD}}+1,...,L_{\mathrm{SD}}+L_{\mathrm{RD}}+1\}$ then $X_i=X_{1,i}+X_{2,i}$ for any $i\in\{0,...,L_{\mathrm{SD}}+L_{\mathrm{RD}}+1\}$ is a noncentral chi-square random

variable with two degrees of freedom and the noncentrality parameter $\widetilde{\rho}_i$ is given by

$$\widetilde{\rho}_i = \begin{cases} \frac{\mu_{\mathrm{SD},i}^2}{\sigma_{\mathrm{SD,i}}^2}, \ i \in \{0, 1, \ldots, L_{\mathrm{SD}}\} \\ \\ \frac{\mu_{\mathrm{SD},i-(L_{\mathrm{SD}}+1)}^2}{\sigma_{\mathrm{SD,i}-(L_{\mathrm{SD}}+1)}^2}, \ i \in \{L_{\mathrm{SD}}+1, \ldots, L_{\mathrm{SD}}+L_{\mathrm{RD}}+1\} \end{cases}. \tag{C.12}$$

The scaling vector for noncentral chi-square random variables X_i's, $\boldsymbol{\Xi}$, is expressed as

$$\boldsymbol{\Xi} = \left[\ \frac{G_{\mathrm{SD}}(f)\gamma\,\Omega_{\mathrm{SD},0}}{2(k_{\mathrm{SD},0}+1)} \cdots \frac{G_{\mathrm{SD}}(f)\gamma\,\Omega_{\mathrm{SD},L_{\mathrm{SD}}}}{2(k_{\mathrm{SD},L_{\mathrm{SD}}}+1)} \frac{G_{\mathrm{RD}}(f)\gamma\,\Omega_{\mathrm{RD},0}}{2(k_{\mathrm{RD},0}+1)} \cdots \frac{G_{\mathrm{RD}}(f)\gamma\,\Omega_{\mathrm{RD},L_{\mathrm{RD}}}}{2(k_{\mathrm{RD},L_{\mathrm{RD}}}+1)} \ \right]. \tag{C.13}$$

Denote $\widetilde{\eta} = \sum_{i=0}^{L_{\mathrm{SD}}+L_{\mathrm{RD}}+1} \phi_i \, X_i$, where ϕ_i is the $(i+1)^{\mathrm{th}}$ element of $\boldsymbol{\Xi}$. Then, using the truncated CDF of $\widetilde{\eta}$ [105] and after simplifications, it is given by

$$\begin{aligned} F_{\widetilde{\eta}}(x) =& \frac{e^{-\frac{x}{2\mu_1}} x^{L_{\mathrm{SD}}+L_{\mathrm{RD}}+2}}{(2\mu_1)^{L_{\mathrm{SD}}+L_{\mathrm{RD}}+3}\Gamma\left(L_{\mathrm{SD}}+L_{\mathrm{RD}}+3\right)} \sum_{k=0}^{K_t-1} \frac{k!\widetilde{m}_k}{\left(L_{\mathrm{SD}}+L_{\mathrm{RD}}+3\right)_k} \\ & \times L_k^{(L_{\mathrm{SD}}+L_{\mathrm{RD}}+2)}\left(\frac{(L_{\mathrm{SD}}+L_{\mathrm{RD}}+3)x}{2\mu_0\mu_1}\right) \end{aligned} \tag{C.14}$$

where $\mu_0, \mu_1 > 0$ and the coefficients $\widetilde{m}_k$ can be obtained from the recurrence relations

$$\begin{aligned} \widetilde{m}_0 =& 2(L_{\mathrm{SD}}+L_{\mathrm{RD}}+3)^{L_{\mathrm{SD}}+L_{\mathrm{RD}}+3} \exp\left\{-\frac{1}{2}\sum_{i=1}^{L_{\mathrm{SD}}+L_{\mathrm{RD}}+2} \frac{\widetilde{\rho}_i\,\phi_i\,(L_{\mathrm{SD}}+L_{\mathrm{RD}}+3-\mu_0)}{\mu_0\mu_1+\phi_i\,(L_{\mathrm{SD}}+L_{\mathrm{RD}}+3-\mu_0)}\right\} \\ & \times \frac{\mu_1^{L_{\mathrm{SD}}+L_{\mathrm{RD}}+3}}{L_{\mathrm{SD}}+L_{\mathrm{RD}}+3-\mu_0} \prod_{i=1}^{L_{\mathrm{SD}}+L_{\mathrm{RD}}+2} \left(\mu_0\mu_1+\phi_i\ \ (L_{\mathrm{SD}}+L_{\mathrm{RD}}+3-\mu_0)\right)^{-1}, \end{aligned} \tag{C.15}$$

$$\widetilde{m}_k = \frac{1}{k}\sum_{j=0}^{k-1} \widetilde{m}_j \widetilde{d}_{k-j}, \quad k \geq 1 \tag{C.16}$$

where $\widetilde{d}_j$ is given by

$$\begin{aligned} \widetilde{d}_j =& \frac{-j\mu_1(L_{\mathrm{SD}}+L_{\mathrm{RD}}+3)}{2\mu_0} \sum_{i=1}^{L_{\mathrm{SD}}+L_{\mathrm{RD}}+2} \phi_i(\mu_1-\phi_i)^{j-1}\left(\frac{\widetilde{\rho}_i^{1/(j+1)}\mu_0}{\mu_0\mu_1+\phi_i\,(L_{\mathrm{SD}}+L_{\mathrm{RD}}+3-\mu_0)}\right)^{j+1} \\ & + \left(\frac{-\mu_0}{L_{\mathrm{SD}}+L_{\mathrm{RD}}+3-\mu_0}\right)^j + \sum_{i=1}^{L_{\mathrm{SD}}+L_{\mathrm{RD}}+2}\left(\frac{\mu_0\,(\mu_1-\phi_i)}{\mu_0\mu_1+\phi_i\,(L_{\mathrm{SD}}+L_{\mathrm{RD}}+3-\mu_0)}\right)^j, \quad j \geq 1. \end{aligned} \tag{C.17}$$

By substituting $x = 2^{2(N+L_c)y/N} - 1$ in (C.14), the CDF for $I_{\mathrm{C,U}}$ in (4.12), i.e. $F_{I_{\mathrm{C,U}}}(y)$, is given by

$$F_{I_{\mathrm{C,U}}}(y) = F_{\widetilde{\eta}}\left(2^{2(N+L_c)y/N}-1\right). \tag{C.18}$$

C.4 MGF Derivations in Sparse Rician Channel

In this appendix, we derive the moment generating function for $(1/N)\sum_{n=0}^{N-1}\mathbf{\Gamma}_{\mathrm{XY}}(n)$ and $(1/N)\sum_{n=0}^{N-1}\left(G_{\mathrm{SD}}(f)\gamma\mathbf{\Gamma}_{\mathrm{SD}}(n)+G_{\mathrm{RD}}(f)\gamma\mathbf{\Gamma}_{\mathrm{RD}}(n)\right)$ random variables in sparse Rician fading channel.

For sparse Rician fading in X $\rightarrow$ Y channel with arbitrary PDP, the MGF of the random variable $\lambda_{\mathrm{XY}}=(1/N)\sum_{n=0}^{N-1}\mathbf{\Gamma}_{\mathrm{XY}}(n)$ is given by

$$M_{\lambda_{\mathrm{XY}}}(s)=E\left[\exp\left(\sum_{l=0}^{L_{\mathrm{XY}}}\sum_{p=0}^{L_{\mathrm{XY}}}h_{\mathrm{XY}}(v_l)h_{\mathrm{XY}}^{*}(v_p)\frac{s}{N}\sum_{n=0}^{N-1}\exp\left(-j\frac{2\pi(v_l-v_p)n}{N}\right)\right)\right]. \quad \text{(C.19)}$$

Here,

$$\frac{1}{N}\sum_{n=0}^{N-1}\exp\left(-j\frac{2\pi(v_l-v_p)n}{N}\right)=\begin{cases}0, & \forall\ v_l\neq v_p\\ 1, & \text{otherwise}\end{cases}. \quad \text{(C.20)}$$

Hence,

$$M_{\lambda_{\mathrm{XY}}}(s)=\prod_{l=0}^{L_{\mathrm{XY}}}E\left[\exp\left(s|h_{\mathrm{XY}}(v_l)|^2\right)\right] \quad \text{(C.21)}$$

where $h_{\mathrm{XY}}(v_l)$ is defined in Section 3.1. Let $Z_l=|h_{\mathrm{XY}}(v_l)|^2$, $l\in\{0,1,...,L_{\mathrm{XY}}\}$, from the MGF in (C.21), the random variable λ_{XY} is a sum of independent Z_l $\forall l\in\{0,1,...,L_{\mathrm{XY}}\}$. If we denote the real and imaginary parts of $h_{\mathrm{XY}}(v_l)$ by $Z_{1,l}$ and $Z_{2,l}$ respectively, then $|Y_l|^2=\left(Z_{1,l}/\sigma_{\mathrm{XY},l}\right)^2+\left(Z_{2,l}/\sigma_{\mathrm{XY},l}\right)^2$ is noncentral chi-square distributed with two degrees of freedom and noncentrality parameter given by

$$\widehat{s}_l^2=\left(E\left[\Re\left(Y_l\right)\right]\right)^2+\left(E\left[\Im\left(Y_l\right)\right]\right)^2=\frac{\mu_{\mathrm{XY},l}^2}{\sigma_{\mathrm{XY},l}^2}. \quad \text{(C.22)}$$

The probability density function for $|Y_l|^2$ is

$$f_{|Y_l|^2}(x)=\frac{1}{2}\exp\left(-\frac{x+\widehat{s}_l^2}{2}\right)I_0\left(\widehat{s}_l\sqrt{x}\right),\quad x\geq 0 \quad \text{(C.23)}$$

where $I_0(.)$ is the zero-order modified Bessel function of the first kind. Using proper random variable transformation, the probability density function of Z_l is

$$f_{Z_l}(x)=\frac{1}{2\sigma_{\mathrm{XY},l}^2}\exp\left(-\frac{x+\widehat{s}_l^2\sigma_{\mathrm{XY},l}^2}{2\sigma_{\mathrm{XY},l}^2}\right)I_0\left(\widehat{s}_l\sqrt{\frac{x}{\sigma_{\mathrm{XY},l}^2}}\right),\quad x\geq 0. \quad \text{(C.24)}$$

The explicit MGF for the random variable Z_l, after some mathematical manipulation

is given by

$$M_{Z_l}(s) = \frac{1}{1-2\sigma^2_{\mathrm{XY},l}s}\exp\left(\frac{\mu^2_{\mathrm{XY},l}s}{1-2\sigma^2_{\mathrm{XY},l}s}\right). \tag{C.25}$$

Substituting (C.25) in (C.21), we obtain the MGF for λ_{XY}.

Similarly, for sparse Rician fading underwater channels S $\rightarrow$ D and R $\rightarrow$ D with arbitrary PDP, the MGF of the random variable $\lambda_C = (1/N)\sum_{n=0}^{N-1}(G_{\mathrm{SD}}(f)\gamma\mathbf{\Gamma}_{\mathrm{SD}}(n)$ $+ G_{\mathrm{RD}}(f)\gamma\mathbf{\Gamma}_{\mathrm{RD}}(n))$ is given by

$$\begin{aligned} M_{\lambda_C}(s) =& E\left[\exp\left(\sum_{l=0}^{L_{\mathrm{SD}}}\sum_{p=0}^{L_{\mathrm{SD}}} G_{\mathrm{SD}}(f)\gamma h_{\mathrm{SD}}(v_l)h^*_{\mathrm{SD}}(v_p)\frac{s}{N}\sum_{n=0}^{N-1}\exp\left(-j\frac{2\pi(v_l-v_p)n}{N}\right)\right)\right] \\ &\times E\left[\exp\left(\sum_{m=0}^{L_{\mathrm{RD}}}\sum_{k=0}^{L_{\mathrm{RD}}} G_{\mathrm{RD}}(f)\gamma h_{\mathrm{RD}}(v_m)h^*_{\mathrm{RD}}(v_k)\frac{s}{N}\sum_{n=0}^{N-1}\exp\left(-j\frac{2\pi(v_m-v_k)n}{N}\right)\right)\right]. \end{aligned} \tag{C.26}$$

Using (C.20), MGF in (C.26) can be expressed as

$$M_{\lambda_C}(s) = \prod_{l=0}^{L_{\mathrm{SD}}} E\left[\exp\left(sG_{\mathrm{SD}}(f)\gamma|h_{\mathrm{SD}}(v_l)|^2\right)\right] \prod_{m=0}^{L_{\mathrm{RD}}} E\left[\exp\left(sG_{\mathrm{RD}}(f)\gamma|h_{\mathrm{RD}}(v_m)|^2\right)\right]. \tag{C.27}$$

Let $\widehat{X}_l = G_{\mathrm{SD}}(f)\gamma|h_{\mathrm{SD}}(v_l)|^2$ and $\widehat{Y}_p = G_{\mathrm{RD}}(f)\gamma|h_{\mathrm{RD}}(v_p)|^2$, $l \in \{0,...,L_{\mathrm{SD}}\}, p \in \{0,...,L_{\mathrm{RD}}\}$, from the MGF in (C.27), the random variable λ_C is a sum of independent $\widehat{X}_l$ and $\widehat{Y}_p$ $\forall l \in \{0,1,...,L_{\mathrm{SD}}\},\ p \in \{0,1,...,L_{\mathrm{RD}}\}$. If $\widehat{X}_l = G_{\mathrm{SD}}(f)\gamma\sigma^2_{\mathrm{SD},l}|\widetilde{X}_l|^2$ and $\widehat{Y}_p = G_{\mathrm{RD}}(f)\gamma\sigma^2_{\mathrm{RD},l}|\widetilde{Y}_p|^2$, then $|\widetilde{X}_l|^2$ and $|\widetilde{Y}_p|^2$ are noncentral chi-square distributed with two degrees of freedom and noncentrality parameters $\rho_{1,l} = \mu^2_{\mathrm{SD},l}/\sigma^2_{\mathrm{SD},l}$ and $\rho_{2,p} = \mu^2_{\mathrm{RD},p}/\sigma^2_{\mathrm{RD},p}$ respectively. The probability density function for $|\widetilde{X}_l|^2$ and $|\widetilde{Y}_p|^2$, respectively, are

$$f_{|\widetilde{X}_l|^2}(x) = \frac{1}{2}\exp\left(-\frac{x+\rho_{1,l}}{2}\right) I_0\left(\sqrt{\rho_{1,l}x}\right), \quad x \geq 0, \tag{C.28}$$

$$f_{|\widetilde{Y}_p|^2}(x) = \frac{1}{2}\exp\left(-\frac{x+\rho_{2,p}}{2}\right) I_0\left(\sqrt{\rho_{2,p}x}\right), \quad x \geq 0. \tag{C.29}$$

Using proper random variable transformation, the probability density function of $\widehat{X}_l$

and $\widehat{Y}_p$, respectively, are

$$f_{\widehat{X}_l}(x) = \frac{1}{2G_{\mathrm{SD}}(f)\gamma\sigma^2_{\mathrm{SD},l}} \exp\left(-\frac{x+\rho_{1,l}G_{\mathrm{SD}}(f)\gamma\sigma^2_{\mathrm{SD},l}}{2G_{\mathrm{SD}}(f)\gamma\sigma^2_{\mathrm{SD},l}}\right) I_0\left(\sqrt{\frac{\rho_{1,l}x}{G_{\mathrm{SD}}(f)\gamma\sigma^2_{\mathrm{SD},l}}}\right), x \geq 0, \tag{C.30}$$

$$f_{\widehat{Y}_p}(x) = \frac{1}{2G_{\mathrm{RD}}(f)\gamma\sigma^2_{\mathrm{RD},p}} \exp\left(-\frac{x+\rho_{2,p}G_{\mathrm{RD}}(f)\gamma\sigma^2_{\mathrm{RD},p}}{2G_{\mathrm{RD}}(f)\gamma\sigma^2_{\mathrm{RD},p}}\right) I_0\left(\sqrt{\frac{\rho_{2,p}x}{G_{\mathrm{RD}}(f)\gamma\sigma^2_{\mathrm{RD},p}}}\right), x \geq 0. \tag{C.31}$$

The explicit MGF for the random variables $\widehat{X}_l$ and $\widehat{Y}_p$ is obtained as follows. First, the MGF for $\Delta_{1,l} = \sigma^2_{\mathrm{SD},l}|\widetilde{X}_l|^2$ and $\Delta_{2,p} = \sigma^2_{\mathrm{RD},p}|\widetilde{Y}_p|^2$ after some mathematical manipulation, respectively, are

$$M_{\Delta_{1,l}}(s) = \frac{1}{1-2\sigma^2_{\mathrm{SD},l}s} \exp\left(\frac{\mu^2_{\mathrm{SD},l}s}{1-2\sigma^2_{\mathrm{SD},l}s}\right), \tag{C.32}$$

$$M_{\Delta_{2,p}}(s) = \frac{1}{1-2\sigma^2_{\mathrm{RD},p}s} \exp\left(\frac{\mu^2_{\mathrm{RD},p}s}{1-2\sigma^2_{\mathrm{RD},p}s}\right). \tag{C.33}$$

Then, MGF for $\widehat{X}_l$ and $\widehat{Y}_p$, respectively, are

$$M_{\widehat{X}_l}(s) = \frac{1}{1-2\sigma^2_{\mathrm{SD},l}G_{\mathrm{SD}}(f)\gamma s} \exp\left(\frac{\mu^2_{\mathrm{SD},l}G_{\mathrm{SD}}(f)\gamma s}{1-2\sigma^2_{\mathrm{SD},l}G_{\mathrm{SD}}(f)\gamma s}\right), \tag{C.34}$$

$$M_{\widehat{Y}_p}(s) = \frac{1}{1-2\sigma^2_{\mathrm{RD},p}G_{\mathrm{RD}}(f)\gamma s} \exp\left(\frac{\mu^2_{\mathrm{RD,p}}G_{\mathrm{RD}}(f)\gamma s}{1-2\sigma^2_{\mathrm{RD},p}G_{\mathrm{RD}}(f)\gamma s}\right). \tag{C.35}$$

Substituting (C.34) and (C.35) in (C.27), we obtain the MGF for λ_C.

C.5 Derivations of High SNR Approximation

In this appendix, we show the derivation of the lower bound on $P^{\mathrm{DF}}_{\mathrm{out,u}}$ under high SNR assumption. We consider the limit for the CDFs of $I_{\mathrm{D,U}}$ and $I_{\mathrm{R,U}}$ as $\gamma \to \infty$. Let

$$F_{I_{\mathrm{R,U}}}(y) = \Pr\left\{\sum_{l=0}^{L_{\mathrm{SR}}} \underbrace{\frac{\Omega_{\mathrm{SR},l}}{2(k_{\mathrm{SR},l}+1)}}_{\alpha_l} \left\{\left(\frac{\Re\left(h_{\mathrm{SR}}(v_l)\right)}{\sigma_{\mathrm{SR},l}}\right)^2 + \left(\frac{\Im\left(h_{\mathrm{SR}}(v_l)\right)}{\sigma_{\mathrm{SR},l}}\right)^2\right\} \leq \frac{2^{y/\overline{a}}-1}{G_{\mathrm{SR}}(f)\gamma}\right\} \tag{C.36}$$

where $\overline{a} = N/(2(N+L_c))$. Further let $\eta = \sum_{l=0}^{L_{\rm SR}} \alpha_l Y_l$ with $Y_l = \left(\Re\left(h_{\rm SR}(v_l)\right)/\sigma_{{\rm SR},l}\right)^2 + \left(\Im\left(h_{\rm SR}(v_l)\right)/\sigma_{{\rm SR},l}\right)^2$, then as $\gamma \to \infty$, we will have

$$\lim_{\gamma\to\infty} F_{I_{\rm R,U}}(y) = \lim_{x\to 0} F_\eta(x) \tag{C.37}$$

where $x = (2^{y/\overline{a}} - 1)/G_{\rm SR}(f)\gamma$. Now, the limit of $F_\eta(x)/x^{L_{\rm SR}+1}$ as $x \to 0$ is given by

$$\lim_{x\to 0} x^{-(L_{\rm SR}+1)} F_\eta(x) = \frac{1}{(2\mu_1)^{L_{\rm SR}+2}\Gamma(L_{\rm SR}+2)} \sum_{k=0}^{K_t-1} \frac{k! m_k}{(L_{\rm SR}+2)_k} \begin{pmatrix} L_{\rm SR}+1+k \\ k \end{pmatrix}, \mu_0, \mu_1 > 0 \tag{C.38}$$

Hence, the limit of $F_{I_{\rm R,U}}(y)$ as $\gamma \to \infty$ is

$$\begin{aligned}\lim_{\gamma\to\infty} F_{I_{\rm R,U}}(R) =& \frac{\left(\left(2^{2(N+L_c)R/N} - 1\right)/G_{\rm SR}(f)\right)^{L_{\rm SR}+1}}{(2\mu_1)^{L_{\rm SR}+2}\Gamma(L_{\rm SR}+2)} \\ &\times \left\{ \sum_{k=0}^{K_t-1} \frac{k! m_k}{(L_{\rm SR}+2)_k} \begin{pmatrix} L_{\rm SR}+1+k \\ k \end{pmatrix} \right\} \gamma^{-(L_{\rm SR}+1)},\ \mu_0, \mu_1 > 0 \end{aligned} \tag{C.39}$$

Similarly, we have derived the high SNR approximation for $F_{I_{\rm D,U}}(y)$ as $\gamma \to \infty$, and obtained

$$\begin{aligned}\lim_{\gamma\to\infty} F_{I_{\rm D,U}}(R) =& \frac{\left(\left(2^{2(N+L_c)R/N} - 1\right)/G_{\rm SD}(f)\right)^{L_{\rm SD}+1}}{(2\mu_1)^{L_{\rm SD}+2}\Gamma(L_{\rm SD}+2)} \\ &\times \left\{ \sum_{k=0}^{K_t-1} \frac{k! m_k}{(L_{\rm SD}+2)_k} \begin{pmatrix} L_{\rm SD}+1+k \\ k \end{pmatrix} \right\} \gamma^{-(L_{\rm SD}+1)},\ \mu_0, \mu_1 > 0 \end{aligned} \tag{C.40}$$

In the case of combined received signals from the source and relay, the high SNR approximation in similar approach for the CDF of $I_{\rm C,U}$ at spectral efficiency R is

$$\begin{aligned}\lim_{\gamma\to\infty} F_{I_{\rm C,U}}(R) =& \frac{\left(2^{2(N+L_c)R/N} - 1\right)^{L_{\rm SD}+L_{\rm RD}+2}}{(2\mu_1)^{L_{\rm SD}+L_{\rm RD}+3}\Gamma(L_{\rm SD}+L_{\rm RD}+3)} \\ &\times \left\{ \sum_{k=0}^{K_t-1} \frac{k! \widetilde{m}_k}{(L_{\rm SD}+L_{\rm RD}+3)_k} \begin{pmatrix} L_{\rm SD}+L_{\rm RD}+2+k \\ k \end{pmatrix} \right\} \\ &\times \gamma^{-(L_{\rm SD}+L_{\rm RD}+2)},\ \mu_0, \mu_1 > 0 \end{aligned} \tag{C.41}$$

The lower bound in (4.14) can be approximated for high SNR, i.e. as $\gamma \to \infty$, and we obtain (4.15).

C.6 Proof of Maximum Diversity Order in DF Cooperation

We use the derived high SNR approximation expressions to show that the maximum achievable diversity order for our cooperative DF system is $L_{\mathrm{SD}}+1+\min\left(L_{\mathrm{SR}}+1, L_{\mathrm{RD}}+1\right)$. For simplicity of notation, let $L_0 = F_{\eta_0}(x)\left(1-F_{\eta_1}(x)\right)+F_{\eta_1}(x)F_{\eta_2}(x)$ where the random variables η_0, η_1, and η_2 are , respectively, given by

$$\begin{aligned}\eta_0 =& \sum_{l=0}^{L_{\mathrm{SD}}} \frac{G_{\mathrm{SD}}(f)\,\Omega_{\mathrm{SD},l}}{2(k_{\mathrm{SD},l}+1)}\left\{\left(\frac{\Re\left(h_{\mathrm{SD}}(v_l)\right)}{\sigma_{\mathrm{SD},l}}\right)^2+\left(\frac{\Im\left(h_{\mathrm{SD}}(v_l)\right)}{\sigma_{\mathrm{SD},l}}\right)^2\right\}\\ &+\sum_{p=0}^{L_{\mathrm{RD}}} \frac{G_{\mathrm{RD}}(f)\,\Omega_{\mathrm{RD},p}}{2(k_{\mathrm{RD},p}+1)}\left\{\left(\frac{\Re\left(h_{\mathrm{RD}}(v_p)\right)}{\sigma_{\mathrm{RD},p}}\right)^2+\left(\frac{\Im\left(h_{\mathrm{RD}}(v_p)\right)}{\sigma_{\mathrm{RD},p}}\right)^2\right\}, \qquad \text{(C.42)}\\ \eta_1 =& \sum_{l=0}^{L_{\mathrm{SR}}} \frac{G_{\mathrm{SR}}(f)\Omega_{\mathrm{SR},l}}{2(k_{\mathrm{SR},l}+1)}\left\{\left(\frac{\Re\left(h_{\mathrm{SR}}(v_l)\right)}{\sigma_{\mathrm{SR},l}}\right)^2+\left(\frac{\Im\left(h_{\mathrm{SR}}(v_l)\right)}{\sigma_{\mathrm{SR},l}}\right)^2\right\}, \qquad \text{(C.43)}\\ \eta_2 =& \sum_{l=0}^{L_{\mathrm{SD}}} \frac{G_{\mathrm{SD}}(f)\Omega_{\mathrm{SD},l}}{2(k_{\mathrm{SD},l}+1)}\left\{\left(\frac{\Re\left(h_{\mathrm{SD}}(v_l)\right)}{\sigma_{\mathrm{SD},l}}\right)^2+\left(\frac{\Im\left(h_{\mathrm{SD}}(v_l)\right)}{\sigma_{\mathrm{SD},l}}\right)^2\right\}, \qquad \text{(C.44)}\end{aligned}$$

and their corresponding CDFs are derived in Appendices C.2 and C.3. Assume that $L_{\mathrm{SR}} < L_{\mathrm{RD}}$, then

$$\begin{aligned}\lim_{x\to 0} x^{-(L_{\mathrm{SD}}+L_{\mathrm{SR}}+2)} L_0 =& \lim_{x\to 0} x^{-(L_{\mathrm{SD}}+L_{\mathrm{SR}}+2)} F_{\eta_0}(x)\left(1-F_{\eta_1}(x)\right)+x^{-(L_{\mathrm{SD}}+L_{\mathrm{SR}}+2)}F_{\eta_1}(x)F_{\eta_2}(x)\\ =& \lim_{x\to 0} x^{-(L_{\mathrm{SD}}+L_{\mathrm{SR}}+2)} F_{\eta_0}(x) - \lim_{x\to 0} x^{-(L_{\mathrm{SD}}+L_{\mathrm{SR}}+2)} F_{\eta_0}(x)F_{\eta_1}(x)\\ &+\lim_{x\to 0} x^{-(L_{\mathrm{SD}}+L_{\mathrm{SR}}+2)} F_{\eta_1}(x)F_{\eta_2}(x) \qquad \text{(C.45)}\end{aligned}$$

Let $\Psi_0 = \lim\limits_{x\to 0} x^{-(L_{\mathrm{SD}}+L_{\mathrm{SR}}+2)} F_{\eta_0}(x)$, $\Psi_1 = \lim\limits_{x\to 0} x^{-(L_{\mathrm{SD}}+L_{\mathrm{SR}}+2)} F_{\eta_0}(x)F_{\eta_1}(x)$, and $\Psi_2 = \lim\limits_{x\to 0} x^{-(L_{\mathrm{SD}}+L_{\mathrm{SR}}+2)} F_{\eta_1}(x)F_{\eta_2}(x)$. Here,

$$\Psi_0 = \lim_{x\to 0} \frac{\sum\limits_{k=0}^{K_t-1} \frac{k!\widetilde{m}_k}{(L_{\mathrm{SD}}+L_{\mathrm{RD}}+3)_k}\begin{pmatrix} L_{\mathrm{SD}}+L_{\mathrm{RD}}+2+k \\ k\end{pmatrix}}{(2\mu_1)^{L_{\mathrm{SD}}+L_{\mathrm{RD}}+3}\Gamma\left(L_{\mathrm{SD}}+L_{\mathrm{RD}}+3\right)}\; x^{L_{\mathrm{RD}}-L_{\mathrm{SR}}} \qquad \text{(C.46)}$$

$\Psi_0 \to 0$ as $x \to 0$ because $L_{\mathrm{RD}} - L_{\mathrm{SR}} > 0$; we also have

$$\Psi_1 = \lim_{x\to 0} \frac{\sum_{k_1=0}^{K_t-1}\sum_{k_2=0}^{K_t-1} \frac{k_1!k_2!\widetilde{m}_{k_1}c_{1,k_2}}{(L_{\mathrm{SD}}+L_{\mathrm{RD}}+3)_{k_1}(L_{\mathrm{SR}}+2)_{k_2}} \begin{pmatrix} L_{\mathrm{SD}}+L_{\mathrm{RD}}+2+k_1 \\ k_1 \end{pmatrix} \begin{pmatrix} L_{\mathrm{SR}}+1+k_2 \\ k_2 \end{pmatrix}}{(2\mu_1)^{L_{\mathrm{SR}}+L_{\mathrm{SD}}+L_{\mathrm{RD}}+5}\Gamma(L_{\mathrm{SR}}+2)\Gamma(L_{\mathrm{SD}}+L_{\mathrm{RD}}+3)x^{-(L_{\mathrm{RD}}+1)}} \tag{C.47}$$

$\Psi_1 \to 0$ as $x \to 0$ because $L_{\mathrm{RD}} \geq 0$. Further,

$$\Psi_2 = \frac{\sum_{k_1=0}^{K_t-1}\sum_{k_2=0}^{K_t-1} \frac{k_1!k_2!c_{1,k_1}c_{2,k_2}}{(L_{\mathrm{SR}}+2)_{k_1}(L_{\mathrm{SD}}+2)_{k_2}} \begin{pmatrix} L_{\mathrm{SR}}+1+k_1 \\ k_1 \end{pmatrix} \begin{pmatrix} L_{\mathrm{SD}}+1+k_2 \\ k_2 \end{pmatrix}}{(2\mu_1)^{L_{\mathrm{SR}}+L_{\mathrm{SD}}+4}\Gamma(L_{\mathrm{SD}}+2)\Gamma(L_{\mathrm{SR}}+2)} \tag{C.48}$$

From (C.46), (C.47), and (C.48), we have

$$\lim_{x\to 0} L_0 = \frac{\sum_{k_1=0}^{K_t-1}\sum_{k_2=0}^{K_t-1} \frac{k_1!k_2!c_{1,k_1}c_{2,k_2}}{(L_{\mathrm{SR}}+2)_{k_1}(L_{\mathrm{SD}}+2)_{k_2}} \begin{pmatrix} L_{\mathrm{SR}}+1+k_1 \\ k_1 \end{pmatrix} \begin{pmatrix} L_{\mathrm{SD}}+1+k_2 \\ k_2 \end{pmatrix}}{(2\mu_1)^{L_{\mathrm{SR}}+L_{\mathrm{SD}}+4}\Gamma(L_{\mathrm{SD}}+2)\Gamma(L_{\mathrm{SR}}+2)} \; x^{(L_{\mathrm{SD}}+L_{\mathrm{SR}}+2)} \tag{C.49}$$

Let the constant gain, G, which is not function of SNR be denoted by

$$G = \frac{\sum_{k_1=0}^{K_t-1}\sum_{k_2=0}^{K_t-1} \frac{k_1!k_2!c_{1,k_1}c_{2,k_2}}{(L_{\mathrm{SR}}+2)_{k_1}(L_{\mathrm{SD}}+2)_{k_2}} \begin{pmatrix} L_{\mathrm{SR}}+1+k_1 \\ k_1 \end{pmatrix} \begin{pmatrix} L_{\mathrm{SD}}+1+k_2 \\ k_2 \end{pmatrix}}{(2\mu_1)^{L_{\mathrm{SR}}+L_{\mathrm{SD}}+4}\Gamma(L_{\mathrm{SD}}+2)\Gamma(L_{\mathrm{SR}}+2)} \tag{C.50}$$

and substituting $x = \left(2^{R/\overline{a}} - 1\right)/\gamma$ in L_0 expression and taking the limit of $\gamma \to \infty$ with $\overline{a} = N/2(N + L_c)$ yields

$$\lim_{\gamma\to\infty} L_0 = G\big(2^{R/\overline{a}} - 1\big)^{L_{\mathrm{SD}}+L_{\mathrm{SR}}+2}\gamma^{-(L_{\mathrm{SD}}+1+L_{\mathrm{SR}}+1)} \tag{C.51}$$

Clearly, from (C.51), the maximum achievable diversity order is $L_{\mathrm{SD}} + 1 + L_{\mathrm{SR}} + 1$. Now, if we assume that $L_{\mathrm{RD}} < L_{\mathrm{SR}}$, then

$$\lim_{x\to 0} x^{-(L_{\mathrm{SD}}+L_{\mathrm{RD}}+2)}L = \lim_{x\to 0} x^{-(L_{\mathrm{SD}}+L_{\mathrm{RD}}+2)}F_{\eta_0}(x)\left(1 - F_{\eta_1}(x)\right) + x^{-(L_{\mathrm{SD}}+L_{\mathrm{RD}}+2)}F_{\eta_1}(x)F_{\eta_2}(x) \tag{C.52}$$

Let $\widetilde{\Psi}_0 = \lim_{x\to 0} x^{-(L_{\mathrm{SD}}+L_{\mathrm{RD}}+2)}F_{\eta_0}(x)$, $\widetilde{\Psi}_1 = \lim_{x\to 0} x^{-(L_{\mathrm{SD}}+L_{\mathrm{RD}}+2)}F_{\eta_0}(x)F_{\eta_1}(x)$, and $\widetilde{\Psi}_2 = \lim_{x\to 0} x^{-(L_{\mathrm{SD}}+L_{\mathrm{RD}}+2)}F_{\eta_1}(x)F_{\eta_2}(x)$. Following similar steps, we obtain $\widetilde{\Psi}_1 \to 0$ as $x \to 0$

because $L_{\mathrm{SR}} \geq 0$ and $\widetilde{\Psi}_2 \to 0$ as $x \to 0$ because $L_{\mathrm{SR}} - L_{\mathrm{RD}} > 0$. Furthermore,

$$\widetilde{\Psi}_0 = \frac{\sum_{k=0}^{K_t-1} \frac{k!\widetilde{m}_k}{(L_{\mathrm{SD}}+L_{\mathrm{RD}}+3)_k} \begin{pmatrix} L_{\mathrm{SD}}+L_{\mathrm{RD}}+2+k \\ k \end{pmatrix}}{(2\mu_1)^{L_{\mathrm{SD}}+L_{\mathrm{RD}}+3}\Gamma\left(L_{\mathrm{SD}}+L_{\mathrm{RD}}+3\right)} \tag{C.53}$$

Let the constant gain, $\widetilde{G}$, which is not function of x or SNR be given as

$$\widetilde{G} = \frac{\sum_{k=0}^{K_t-1} \frac{k!\widetilde{m}_k}{(L_{\mathrm{SD}}+L_{\mathrm{RD}}+3)_k} \begin{pmatrix} L_{\mathrm{SD}}+L_{\mathrm{RD}}+2+k \\ k \end{pmatrix}}{(2\mu_1)^{L_{\mathrm{SD}}+L_{\mathrm{RD}}+3}\Gamma\left(L_{\mathrm{SD}}+L_{\mathrm{RD}}+3\right)} \tag{C.54}$$

and substituting $x = \left(2^{R/\overline{a}} - 1\right)/\gamma$ in L expression and taking the limit of $\gamma \to \infty$ with $\overline{a} = N/2(N + L_c)$ yields

$$\lim_{\gamma\to\infty} L_0 = \widetilde{G}\left(2^{R/\overline{a}} - 1\right)^{L_{\mathrm{SD}}+L_{\mathrm{RD}}+2} \gamma^{-(L_{\mathrm{SD}}+1+L_{\mathrm{RD}}+1)} \tag{C.55}$$

Hence, the maximum achievable diversity order is $L_{\mathrm{SD}} + 1 + L_{\mathrm{RD}} + 1$. From (C.51) and (C.55), the maximum achievable diversity order is $L_{\mathrm{SD}} + 1 + \min\left(L_{\mathrm{SR}} + 1, L_{\mathrm{RD}} + 1\right)$.

Appendix D

Derivations of ICI Coefficients in Chapter 6

D.1 Derivations of ICI Coefficients in Single Resampling

In this appendix, we derive the $(i+1, n+1)^{\text{th}}$ elements of the ICI matrices, $\widetilde{\Psi}_{i,n}^{\text{SD}}$ and $\widetilde{\Psi}_{i,n}^{\text{R}_k}$, in (6.28) and (6.32), respectively. First, we consider the direct channel S $\rightarrow$ D where the received baseband signal at destination is given in (6.8). At the receiver, the Doppler offset compensated signal is $y_{\text{D},1}(t)e^{-j2\pi\widehat{a}f_0 t}$. We correlate the signal with the orthonormal basis function, $\big(\phi_i^d(t)\big)^*$, (or equivalently applying a matched filter with an impulse response $\big(\phi_i^d(T-t)\big)^*$ followed by a sampler at $t=T$), and we have

$$\begin{aligned}
\overline{y}_{\text{D},1}[i] &= \int_{-\infty}^{\infty} y_{\text{D},1}(t)e^{-j2\pi\widehat{a}f_0 t}\big(\phi_i^d(t)\big)^* dt \\
&= \sum_{n=0}^{N-1} \sqrt{G_{\text{SD}}(f)E_s}x[n] \sum_{l=1}^{N_{\text{S}}} h_{\text{SD}}[l]\, e^{-j2\pi\tau_{\text{SD},l}n/T} \\
&\quad \times \int_{-\infty}^{\infty} e^{-j2\pi[(a_l-\widehat{a})f_0-(1+a_l)n/T]t} p(t+a_l t-\tau_{\text{SD},l})\big(\phi_i^d(t)\big)^* dt + \int_{-\infty}^{\infty} z_{\text{D},1}(t)\big(\phi_i^d(t)\big)^* dt
\end{aligned} \tag{D.1}$$

where $p(t + a_l t - \tau_{\mathrm{SD},l})$ is given by

$$p(t + a_l t - \tau_{\mathrm{SD},l}) = \begin{cases} \frac{1}{\sqrt{T}}, & \frac{-T_g + \tau_{\mathrm{SD},l}}{1+a_l} \leq t \leq \frac{T + \tau_{\mathrm{SD},l}}{1+a_l} \\ 0 \ , & \text{elsewhere} \end{cases} \tag{D.2}$$

From (D.2) and (6.25), the lower and upper limits of integration in first term of (D.1) are $\bar{t}_1 = \max\left(0, (-T_g + \tau_{\mathrm{SD},l})/(1 + a_l)\right)$ and $\bar{t}_2 = \min\left(T/(1+\widehat{a}), (T + \tau_{\mathrm{SD},l})/(1 + a_l)\right)$, respectively. The second integration in (D.1) is denoted by $\overline{z}_i^{\mathrm{D},1}$. Substituting (D.2) and (6.25) in (D.1), the received signal $\overline{y}_{\mathrm{D},1}[i]$ is

$$\begin{aligned} \overline{y}_{\mathrm{D},1}[i] =& \sum_{n=0}^{N-1} \sqrt{G_{\mathrm{SD}}(f) E_s} x[n] \frac{\sqrt{1+\widehat{a}}}{T} \\ & \times \sum_{l=1}^{N_{\mathrm{S}}} h_{\mathrm{SD}}[l]\, e^{-j2\pi\tau_{\mathrm{SD},l} n/T} \int_{\bar{t}_1}^{\bar{t}_2} e^{-j2\pi[(a_l - \widehat{a})f_0 - (1+a_l)n/T + (1+\widehat{a})i/T]t}\, dt + \overline{z}_i^{\mathrm{D},1} \\ =& \sqrt{G_{\mathrm{SD}}(f) E_s}\ \widetilde{\Psi}_{i,i}^{\mathrm{SD}}\, x[i] + \sqrt{G_{\mathrm{SD}}(f) E_s} \sum_{\substack{n=0 \\ n \neq i}}^{N-1} \widetilde{\Psi}_{i,n}^{\mathrm{SD}}\, x[n] \ + \overline{z}_i^{\mathrm{D},1} \end{aligned} \tag{D.3}$$

with

$$\widetilde{\Psi}_{i,n}^{\mathrm{SD}} = \frac{\sqrt{1+\widehat{a}}}{T} \sum_{l=1}^{N_{\mathrm{S}}} h_{\mathrm{SD}}[l]\, e^{-j2\pi\tau_{\mathrm{SD},l} n/T} \left\{ (\bar{t}_2 - \bar{t}_1) \mathrm{sinc}\left((\bar{t}_2 - \bar{t}_1)\overline{v}_{\mathrm{D},0}\right) e^{-j2\pi\left((\bar{t}_1 + \bar{t}_2)/2\right)\overline{v}_{\mathrm{D},0}} \right\} \tag{D.4}$$

where $\overline{v}_{\mathrm{D},0} = (\widehat{a} - a_l) f_0 + (1 + \widehat{a}) i/T - (1 + a_l) n/T$. This requires N correlator blocks (or matched filters). For simplicity in hardware implementation, we assume $\bar{t}_1 \to 0$, $\bar{t}_2 \to T/(1+\widehat{a})$, and $\widehat{y}(t) = y_{\mathrm{D},1}(t) e^{-j2\pi\widehat{a} f_0 t}$. The received approximate signal $\overline{r}_{\mathrm{D},1}[i]$ in (6.29) is

$$\overline{r}_{\mathrm{D},1}[i] = \sqrt{\frac{1+\widehat{a}}{T}} \int_0^{\frac{T}{1+\widehat{a}}} \widehat{y}(t) e^{-j2\pi i (1+\widehat{a}) t/T} dt$$

Using change of variable, i.e. $u = (1 + \widehat{a})t$, then

$$\overline{r}_{\mathrm{D},1}[i] = \frac{1}{\sqrt{1+\widehat{a}}} \frac{1}{\sqrt{T}} \int_0^T \widehat{y}\left(\frac{u}{1+\widehat{a}}\right) e^{-j2\pi i\, u/T} du \tag{D.5}$$

which represents a single resampling of the offset compensated signal $\widehat{y}(t)$ by the Doppler rate $\widehat{a}$, followed by FFT block as a discrete-time domain representation of the integral in (D.5). After some mathematical manipulation, we obtain approximate $\Psi_{i,n}^{\mathrm{SD}}$ in (6.30).

In the cascaded channel $\mathrm{S} \to \mathrm{R}_k \to \mathrm{D}$, the received baseband signal

$$
\begin{aligned}
y_{\mathrm{D},2}(t) = & \sum_{n=0}^{N-1} \sqrt{\frac{G_{\mathrm{SR}_k}(f) G_{\mathrm{R}_k\mathrm{D}}(f) E_s^2}{\eta_k^2}} \sum_{m=1}^{N_{\mathrm{R}}^k} \sum_{p=1}^{N_{\mathrm{D}}^k} \underbrace{h_{\mathrm{SR}_k,m} \mathrm{e}^{-j2\pi f_0 \tau_{\mathrm{SR}_k,m}}}_{h_{\mathrm{SR}_k}[m]} \underbrace{h_{\mathrm{R}_k\mathrm{D},p} \mathrm{e}^{-j2\pi f_0 \left(1+b_m^k\right)\tau_{\mathrm{R}_k\mathrm{D},p}}}_{h_{\mathrm{R}_k\mathrm{D}}[p]} \\
& \times x[n]\, \mathrm{e}^{-j2\pi\tau_{\mathrm{SR}_k,m} n/T} \mathrm{e}^{-j2\pi\left(1+b_m^k\right)\tau_{\mathrm{R}_k\mathrm{D},p} n/T} e^{j2\pi\left\{b_m^k\left(1+c_p^k\right)+c_p^k\right\} f_0 t} e^{j2\pi\left(1+b_m^k\right)\left(1+c_p^k\right) nt/T} \\
& \times p\left(\left(1+b_m^k\right)\left(1+c_p^k\right) t - \left(\tau_{\mathrm{SR}_k,m} + \left(1+b_m^k\right)\tau_{\mathrm{R}_k\mathrm{D},p}\right)\right) \\
& + \sqrt{\frac{G_{\mathrm{R}_k\mathrm{D}}(f) E_s}{\eta_k^2}} \sum_{p=1}^{N_{\mathrm{D}}^k} h_{\mathrm{R}_k\mathrm{D},p}\, \mathrm{e}^{-j2\pi f_0 \tau_{\mathrm{R}_k\mathrm{D},p}} \mathrm{e}^{-j2\pi\tau_{\mathrm{R}_k\mathrm{D},p} n/T} z_{\mathrm{R}_k}(t + c_p t - \tau_{\mathrm{RD},p}) + \widehat{z}_{\mathrm{D},2}(t)
\end{aligned}
\tag{D.6}
$$

Here, the additive Gaussian noise random process at the relay $z_{\mathrm{R}_k}(t)$ in the p^{th} path of $\mathrm{R} \to \mathrm{D}$ underwater link is time shifted by $\tau'_{\mathrm{RD},p} = \tau_{\mathrm{RD},p}/\left(1+c_p\right)$, and time-scaled by $1+c_p$.

Due to wide sense stationary assumption of additive white Gaussian noise random process $z_{\mathrm{R}_k}(t)$, $z_{\mathrm{R}_k}((1+c_p)(t-\tau'_{\mathrm{RD},p})) \overset{d}{=} z_{\mathrm{R}_k}((1+c_p)t)$, where $\overset{d}{=}$ denotes equality of the finite-dimensional probability distributions. Further, we assume the additive noise random process $n_{\mathrm{R}}(t)$ is scale-invariant, i.e $z_{\mathrm{R}_k}((1+c_p)t) \overset{d}{\sim} z_{\mathrm{R}_k}(t)$ for $|c_p| \ll 1$, $\forall p = 1, ..., N_{\mathrm{D}}^k$, which is given in (6.9).

After Doppler offset compensation, the received signal is $y_{\mathrm{D},2}(t) e^{-j2\pi f_0 \widehat{b}_k t}$, and we correlate the signal $y_{\mathrm{D},2}(t) e^{-j2\pi f_0 \widehat{b}_k t}$ with the orthonormal basis function of the k^{th} relay, $\left(\phi_i^k(t)\right)^*$, to obtain $\overline{y}_{\mathrm{D},2}[i]$ in (6.32) with

$$
\begin{aligned}
\widetilde{\Psi}_{i,n}^{\mathrm{R}_k} = & \frac{\sqrt{1+\widehat{b}_k}}{T} \sum_{m=1}^{N_{\mathrm{R}}^k} \sum_{p=1}^{N_{\mathrm{D}}^k} h_{\mathrm{SR}_k}[m] \mathrm{e}^{-j2\pi\tau_{\mathrm{SR}_k,m} n/T} h_{\mathrm{R}_k\mathrm{D}}[p] \mathrm{e}^{-j2\pi\left(1+b_m^k\right)\tau_{\mathrm{R}_k\mathrm{D},p} n/T} (\overline{u}_{2,k} - \overline{u}_{1,k}) \\
& \times \mathrm{sinc}\left((\overline{u}_{2,k} - \overline{u}_{1,k})\overline{v}_{\mathrm{R},k}\right) e^{-j2\pi\left((\overline{u}_{1,k}+\overline{u}_{2,k})/2\right)\overline{v}_{\mathrm{R},k}}
\end{aligned}
\tag{D.7}
$$

where $\overline{u}_{1,k} = \max\left(0\,,\ \left(-T_g + \tau_{\mathrm{SR}_k,m} + (1+b_m^k)\tau_{\mathrm{R}_k\mathrm{D},p}\right) / \left((1+b_m^k)(1+c_p^k)\right)\right)$, $\overline{u}_{2,k} = \min\left(T/(1+\widehat{b}_k), (T + \tau_{\mathrm{SR}_k,m} + (1+b_m^k)\tau_{\mathrm{R}_k\mathrm{D},p})/(1+\widehat{b}_k)\right)$, and $\overline{v}_{\mathrm{R},k} = ((1+\widehat{b}_k) - (b_{m_2}^k(1+c_{p_2}^k)+c_{p_2}^k))f_0 + (1+\widehat{b}_k)i/T - ((1+b_m^k)(1+c_p^k))n/T$. Similarly, we can obtain the approximated $\Psi_{i,n}^{\mathrm{R}_k}$ in (6.34).

D.2 Derivations of ICI Coefficients in Multiple Resampling

In this appendix, we derive the $(i+1, n+1)^{\text{th}}$ elements of the ICI matrices, $\widetilde{\Upsilon}_{i,n}^{\text{SD}}$ and $\widetilde{\Upsilon}_{i,n}^{\text{R}_k}$, in (6.39) and (6.44), respectively. In direct channel, the received signal in the l^{th} branch after Doppler offset compensation is $y_{\text{D},1}(t)e^{-j2\pi f_0 a_l t}$. After correlating the compensated signal with the orthonormal basis function, $\left(\phi_{i,l}^{d}(t)\right)^*$ in (6.36), to obtain in (6.38) with

$$\widetilde{\Upsilon}_{i,n}^{\text{SD}} = \frac{\sqrt{1+a_l}}{T} \sum_{l_2=1}^{N_{\text{S}}} h_{\text{SD}}[l_2]\, e^{-j2\pi\tau_{\text{SD},l_2} n/T}\, (\widetilde{t}_2 - \widetilde{t}_1)\text{sinc}\left((\widetilde{t}_2 - \widetilde{t}_1)\widetilde{v}_{\text{D},0}\right) e^{-j2\pi\left((\widetilde{t}_1+\widetilde{t}_2)/2\right)\widetilde{v}_{\text{D},0}} \tag{D.8}$$

where $\widetilde{t}_1 = \max\left(0, (-T_g + \tau_{\text{SD},l_2})/(1+a_{l_2})\right)$, $\widetilde{t}_2 = \min\left(T/(1+a_l), (T+\tau_{\text{SD},l_2})/(1+a_{l_2})\right)$, and $\widetilde{v}_{\text{D},0} = (a_l - a_{l_2})f_0 + (1+a_l)i/T - (1+a_{l_2})n/T$.

In a similar manner, the received signal in the $(m,p)^{\text{th}}$ branch after Doppler offset compensation is $y_{\text{D},2}(t)e^{-j2\pi(c_p^k + b_m^k(1+c_p^k))f_0 t}$. After correlating the compensated signal with the orthonormal basis function, $\left(\phi_{i,m,p}^{k}(t)\right)^*$ in (6.37), to obtain $y_{\text{D},2}^{(m,p)}[i]$ in (6.43) with

$$\begin{aligned}\widetilde{\Upsilon}_{i,n}^{\text{R}_k} =& \frac{\sqrt{(1+b_m^k)(1+c_p^k)}}{T} \sum_{m_2=1}^{N_{\text{R}}^k} \sum_{p_2=1}^{N_{\text{D}}^k} h_{\text{SR}_k}[m_2]\text{e}^{-j2\pi\tau_{\text{SR}_k,m_2} n/T} h_{\text{R}_k\text{D}}[p_2]\text{e}^{-j2\pi\left(1+b_{m_2}^k\right)\tau_{\text{R}_k\text{D},p_2} n/T} \\ & \times (\widetilde{u}_{2,k} - \widetilde{u}_{1,k})\text{sinc}\left((\widetilde{u}_{2,k} - \widetilde{u}_{1,k})\widetilde{v}_{\text{R},k}\right) e^{-j2\pi\left((\widetilde{u}_{1,k}+\widetilde{u}_{2,k})/2\right)\widetilde{v}_{\text{R},k}}\end{aligned} \tag{D.9}$$

where $\widetilde{u}_{1,k} = \max\Big(\, 0\,,\ (-T_g + \tau_{\text{SR}_k,m_2} + (1+b_{m_2}^k)\tau_{\text{R}_k\text{D},p_2}) \,/\, ((1+b_{m_2}^k)(1+c_{p_2}^k))\Big)$, $\widetilde{u}_{2,k} = \min\left(T/(1+b_m^k)(1+c_p^k), (T+\tau_{\text{SR}_k,m_2} + (1+b_{m_2}^k)\tau_{\text{R}_k\text{D},p_2})/((1+b_m^k)(1+c_p^k))\right)$, and $\widetilde{v}_{\text{R},k} = (b_m^k(1+c_p^k) + c_p^k - b_{m_2}^k(1+c_{p_2}^k) - c_{p_2}^k)f_0 + ((1+b_m^k)(1+c_p^k))i/T - ((1+b_{m_2}^k)(1+c_{p_2}^k))n/T$.

Copyright Permissions

Parts of Chapters 3 are 5 are reprinted from the following papers.

- S. Al-Dharrab and M. Uysal, "Information theoretic performance of cooperative underwater acoustic communications," in *Proc. IEEE International Symposium on Personal, Indoor and Mobile Radio Communications*, Toronto, Canada, Sep. 2011, pp. 1562-1566. DOI: 10.1109/PIMRC.2011.6139766.

- S. Al-Dharrab and M. Uysal, "Outage capacity regions of multicarrier DF relaying in underwater acoustic channels," in *Proc. IEEE 26th Biennial Symposium on Communications*, Kingston, Canada, May 2012, pp. 30-33.DOI:10.1109/QBSC.2012.6221345.

References

[1] M. Siegel and R. King, "Electromagnetic propagation between antennas submerged in the ocean," *IEEE Trans. Antennas Propag.*, vol. 21, no. 4, pp. 507-513, Jul. 1973.

[2] Wireless Fibre Systems Ltd (WFS) Technologies, West Lothian, UK. website: http://www.wfs-tech.com.

[3] S. Jaruwatanadilok, "Underwater wireless optical communication channel modeling and performance evaluation using vector radiative transfer theory," *IEEE J. Sel. Areas Commun.*, vol. 26, no. 9, pp. 1620-1627, Dec. 2008.

[4] S. Arnon, "Underwater optical wireless communication network," *Opt. Eng.*, vol. 49, no. 1, Jan. 2010.

[5] L. Lanbo, Z. Shengli, and C. Jun-Hong, "Prospects and problems of wireless communication for underwater sensor networks," *Wireless Communications and Mobile Computing*, vol. 8, no. 8, pp. 977-994, Oct. 2008.

[6] S. Arnon and D. Kedar, "Non-line-of-sight underwater optical wireless communication network," *J. Opt. Soc. Am.*, vol. 26, no. 3, pp. 530-539, Mar. 2009.

[7] G. Baiden, Y. Bissiri, and A. Masoti, "Paving the way for a future underwater omnidirectional wireless optical communication systems," *Ocean Eng.*, vol. 36, no. 9-10, pp. 633-640, 7, Jul. 2009.

[8] M. Doniec, I. Vasilescu, M. Chitre, C. Detweiler, M. Hoffmann-Kuhnt, and D. Rus, "AquaOptical: A lightweight device for high-rate long-range underwater point-to-point communication," in *Proc. MTS/IEEE Oceans'09 Conf.*, Biloxi, MS, USA, Oct. 2009, pp. 1-6.

[9] M. Stojanovic, "Underwater acoustic communications: Design considerations on the physical layer," in *5th Annu. Conf. Wireless on Demand Network Systems and Services*, Garmisch-Partenkirchen, Germany, Jan. 2008, pp. 1-10.

[10] A. Quazi and W. Konrad, "Underwater acoustic communications," *IEEE Commun. Mag.*, vol. 20, no. 2, pp. 24-30, Mar. 1982.

[11] M. Stojanovic, J. A. Catipovic, and J. G. Proakis, "Phase-coherent digital communications for underwater acoustic channels," *IEEE J. Ocean. Eng.*, vol. 19, no. 1, pp. 100-111, Jan. 1994.

[12] W. Li and J. C. Preisig, "Estimation of rapidly time-varying sparse channels," *IEEE J. Ocean. Eng.*, vol. 32, no. 4, pp. 927-939, Oct. 2007.

[13] A. Goldsmith, *Wireless Communications*. Cambridge University Press, 2005.

[14] G. J. Foschini, "Layered space-time architecture for wireless communication in a fading environment when using multiple antennas," *Bell Labs Tech. J.*, vol. 1, no. 2, pp. 41-59, Autumn 1996.

[15] H. El Gamal and A. R. Hammons Jr., "A new approach to layered space-time coding and signal processing," *IEEE Trans. Inf. Theory*, vol. 47, no. 6, pp. 2321-2334, Sep. 2001.

[16] B. Hassibi and B. M. Hochwald, "High-rate codes that are linear in space and time," *IEEE Trans. Inf. Theory*, vol. 48, no. 7, pp. 1804-1824, Jul. 2002.

[17] R. W. Heath Jr. and A. J. Paulraj, "Linear dispersion codes for MIMO systems based on frame theory," *IEEE Trans. Signal Process.*, vol. 50, no. 10, pp. 2429-2441, Oct. 2002.

[18] S. M. Alamouti, "A simple transmit diversity technique for wireless communications," *IEEE J. Sel. Areas Commun.*, vol. 16, no. 8, pp. 1451-1458, Oct. 1998.

[19] V. Tarokh, H. Jafarkhani, and A. R. Calderbank, "Space-time block codes from orthogonal designs," *IEEE Trans. Inf. Theory*, vol. 45, no. 5, pp. 1456-1467, Jul. 1999.

[20] J. Radon, "Lineare scharen orthogonaler matrizen," *Abh. Math. Sem. Univ. Hamburg*, vol. 1, no. 1, pp. 114, 1922.

[21] V. Tarokh, N. Seshadri, and A. R. Calderbank, "Space-time codes for high data rate wireless communication: performance criterion and code construction," *IEEE Trans. Inf. Theory*, vol. 44, no. 2, pp. 744-765, Mar. 1998.

[22] E. Biglieri, G. Taricco, and A. Tulino, "Performance of space-time codes for a large number of antennas," *IEEE Trans. Inf. Theory*, vol. 48, no. 7, pp. 1794-1803, Jul. 2002.

[23] Z. Chen, J. Yuan, and B. Vucetic, "An improved space-time trellis coded modulation scheme on slow Rayleigh fading channels," in *Proc. IEEE Int. Conf. Communications*, Helsinki, Finland, Jun. 2001, pp. 1110.

[24] D. M. Ionescu, "On space-time code design," *IEEE Trans. Wireless Commun.*, vol. 2, no. 1, pp. 20-28, Jan. 2003.

[25] M. Tao and R. S. Cheng, "Improved design criteria and new trellis codes for space-time coded modulation in slow flat fading channels," *IEEE Commun. Lett.*, vol. 5, no. 7, pp. 313-315, Jul. 2001.

[26] M. Di Renzo, H. Haas, and P. M. Grant, "Spatial modulation for multiple-antenna wireless systems: A survey," *IEEE Commun. Mag.*, vol. 49, no. 12, pp. 182-191, Dec. 2011.

[27] B.-G. Song and J. A. Ritcey, "Spatial diversity equalization for MIMO ocean acoustic communication channels," *IEEE J. Ocean. Eng.*, vol. 21, no. 4, pp. 505-512, Oct. 1996.

[28] D. B. Kilfoyle, J. C. Preisig, and A. B. Baggeroer, "Spatial modulation experiments in the underwater acoustic channel," *IEEE J. Ocean. Eng.*, vol. 30, no. 2, pp. 406-415, Apr. 2005.

[29] H. C. Song, P. Roux, W. S. Hodgkiss, W. A. Kuperman, T. Akal, and M. Stevenson, "Multiple-input-multiple-output coherent time reversal communications in a shallow-water acoustic channel," *IEEE J. Ocean. Eng.*, vol. 31, no. 1, pp. 170-178, Jan. 2006.

[30] S. Roy, T. M. Duman, V. McDonald, and J. G. Proakis, "High-rate communication for underwater acoustic channels using multiple transmitters and spacetime coding: Receiver structures and experimental results," *IEEE J. Ocean. Eng.*, vol. 32, no. 3, pp. 663-688, Jul. 2007.

[31] S. Roy, T. M. Duman, and V. K. McDonald, "Error rate improvement in underwater MIMO communications using sparse partial response equalization," *IEEE J. Ocean. Eng.*, vol. 34, no. 2, pp. 181-201, Apr. 2009.

[32] J. Tao, Y. R. Zheng, C. Xiao, and T. C. Yang, "Robust MIMO underwater acoustic communications using turbo block decision-feedback equalization," *IEEE J. Ocean. Eng.*, vol. 35, no. 4, pp. 948-960, Oct. 2010.

[33] E. C. Van der Meulen, "Three-terminal communication channels," *Adv. Appl. Prob.*, vol. 3, no. 1, pp. 120-154, 1971.

[34] J. N. Laneman and G. W. Wornell, "Energy-efficient antenna sharing and relaying for wireless networks," in *Proc. IEEE Wireless Communications and Networking Conf.*, Chicago, IL, USA, Sep. 2000, pp. 7-12.

[35] J. N. Laneman and G. W. Wornell, "Distributed space-time-coded protocols for exploiting cooperative diversity in wireless networks," *IEEE Trans. Inf. Theory*, vol. 49, no. 10, pp. 2415-2425, Oct. 2003.

[36] J. N. Laneman, D. N. C. Tse, and G. W. Wornell, "Cooperative diversity in wireless networks: Efficient protocols and outage behavior," *IEEE Trans. Inf. Theory*, vol. 50, no. 12, pp. 3062-3080, Dec. 2004.

[37] A. Sendonaris, E. Erkip, and B. Aazhang, "User cooperation diversity. Part I: System description," *IEEE Trans. Commun.*, vol. 51, no. 11, pp. 1927-1938, Nov. 2003.

[38] A. Sendonaris, E. Erkip, and B. Aazhang, "User cooperation diversity. Part II: Implementation aspects and performance analysis," *IEEE Trans. Commun.*, vol. 51, no. 11, pp. 1939-1948, Nov. 2003.

[39] A. Sendonaris, E. Erkip, and B. Aazhang, "Increasing uplink capacity via user cooperation diversity," in *Proc. IEEE Int. Symp. on Information Theory*, Cambridge, MA , USA, Aug. 1998.

[40] F. H. Fitzek and M. D. Katz (Eds.), *Cooperation in Wireless Networks: Principles and Applications*. Netherlands: Springer, 2006.

[41] M. Uysal (Ed.), *Cooperative Communications for Improved Wireless Network Transmission: Frameworks for Virtual Antenna Array Applications*. IGI Global, 2008.

[42] M. Vajapeyam, S. Vedantam, U. Mitra, J. C. Preisig, and M. Stojanovic, "Distributed space-time cooperative schemes for underwater acoustic communications," *IEEE J. Ocean. Eng.*, vol. 33, no. 4, pp. 489-501, Oct. 2008.

[43] C. Carbonelli and U. Mitra, "Cooperative multihop communication for underwater acoustic networks," in *Proc. 1st ACM Int. Workshop Underwater Networks*, Los Angeles, CA, USA, Sep. 2006, pp. 97-100.

[44] S. Yerramalli and U. Mitra, "Optimal power allocation and Doppler compensation in cooperative underwater networks using OFDM," in *Proc. MTS/IEEE Oceans'09 Conf.*, Biloxi, MS, USA, Oct. 2009, pp. 1-6.

[45] W. Zhang, M. Stojanovic, and U. Mitra, "Analysis of a linear multihop underwater acoustic network," *IEEE J. Ocean. Eng.*, vol. 35, no. 4, pp. 961-970, Oct. 2010.

[46] R. Cao, L. Yang, and F. Qu, "On the capacity and system design of relay-aided underwater acoustic communications," in *Proc. IEEE Wireless Communications and Networking Conf.*, Sydney, Australia, Apr. 2010, pp. 1-6.

[47] S. Mason, C. Berger, S. Zhou, and P. Willett, "Detection, synchronization, and Doppler scale estimation with multicarrier waveforms in underwater acoustic communication," *IEEE J. Sel. Areas Commun.*, vol. 26, no. 9, pp. 1638-1649, Dec. 2008.

[48] J. Huang, S. Zhou, and P. Willett, "Nonbinary LDPC coding for multicarrier underwater acoustic communication," *IEEE J. Sel. Areas Commun.*, vol. 26, no. 9, pp. 1684-1696, Dec. 2008.

[49] T. Kang and R. A. Iltis, "Iterative carrier frequency offset and channel estimation for underwater acoustic OFDM systems," *IEEE J. Sel. Areas Commun.*, vol. 26, no. 9, pp. 1650-1661, Dec. 2008.

[50] G. Leus and P. van Walree, "Multiband OFDM for covert acoustic communications," *IEEE J. Sel. Areas Commun.*, vol. 26, no. 9, pp. 1662-1673, Dec. 2008.

[51] B. Li, S. Zhou, M. Stojanovic, L. Freitag, and P. Willett, "Multicarrier communication over underwater acoustic channels with nonuniform Doppler shifts," *IEEE J. Ocean. Eng.*, vol. 33, no. 2, pp. 198-209, Apr. 2008.

[52] B. S. Sharif, J. Neasham, O. R. Hinton, and A. E. Adams, "A computationally efficient Doppler compensation system for underwater acoustic communications," *IEEE J. Ocean. Eng.*, vol. 25, no. 1, pp. 52-61, Jan. 2000.

[53] M. Stojanovic, "Low complexity OFDM detector for underwater acoustic channels," in *Proc. MTS/IEEE Oceans'06 Conf.*, Boston, MA, USA, Sep. 2006, pp. 1-6.

[54] J. Huang, S. Zhou, J. Huang, C. Berger, and P. Willett, "Progressive inter-carrier interference equalization for OFDM transmission over time-varying underwater acoustic channels," *IEEE J. Sel. Topics Signal Process.*, vol. 5, no. 8, pp. 1524-1536, Dec. 2011.

[55] S. Yerramalli and U. Mitra, "Optimal resampling of OFDM signals for multiscale-multilag underwater acoustic channels," *IEEE J. Ocean. Eng.*, vol. 36, no. 1, pp. 126-138, Jan. 2011.

[56] Z. Wang, S. Zhou, G. B. Giannakis, C. R. Berger, and J. Huang, "Frequency-domain oversampling for zero-padded OFDM in underwater acoustic communications," *IEEE J. Ocean. Eng.*, vol. 37, no. 1, pp. 14-24, Jan. 2012.

[57] P. C. Carrascosa and M. Stojanovic, "Adaptive channel estimation and data detection for underwater acoustic MIMOOFDM systems," *IEEE J. Ocean. Eng.*, vol. 35, no. 3, pp. 635-646, Jul. 2010.

[58] K. Tu, T. M. Duman, J. G. Proakis, and M. Stojanovic, "Cooperative MIMO-OFDM communications: Receiver design for Doppler-distorted underwater acoustic channels," in *Proc. IEEE Asilomar Conf. on Signals, Sys., and Comp.*, Pacific Grove, CA, USA, Nov. 2010, pp. 1335-1339.

[59] Z. Wang, J. Huang, S. Zhou, and Z. Wang, "Iterative receiver processing for OFDM modulated physical-layer network coding in underwater acoustic channels," *IEEE Trans. Commun.*, vol. 61, no. 2, pp. 541-553, Feb. 2013.

[60] M. Stojanovic, "Retrofocusing techniques for high rate acoustic communications," *J. Acoust. Soc. Am.*, vol. 117, no. 3, pp. 1173-1185, Mar. 2005.

[61] A. Zielinski, Y.-H. Yoon, and L. Wu, "Performance analysis of digital acoustic communication in a shallow water channel," *IEEE J. Ocean. Eng.*, vol. 20, no. 4, pp. 293-299, Oct. 1995.

[62] S. Al-Dharrab, M. Uysal, and T. M. Duman, "Cooperative underwater acoustic communications," *IEEE Commun. Mag.*, accepted for publication.

[63] S. Al-Dharrab and M. Uysal, "Outage performance of multicarrier cooperative underwater acoustic communications," under preparation.

[64] S. Al-Dharrab and M. Uysal, "Information theoretic performance of cooperative underwater acoustic communications," in *Proc. IEEE International Symposium on Personal, Indoor and Mobile Radio Communications*, Toronto, Canada, Sep. 2011, pp. 1562-1566.

[65] S. Al-Dharrab and M. Uysal, "Outage capacity regions of multicarrier DF relaying in underwater acoustic channels," in *Proc. IEEE 26th Biennial Symposium on Communications*, Kingston, Canada, May 2012, pp. 30-33.

[66] S. Al-Dharrab and M. Uysal, "Relay selection for cooperative multicarrier underwater acoustic communication in the presence of non-uniform Doppler-distortion," under preparation.

[67] M. Schulkin and H. W. Marsh, "Sound absorption in sea water," *J. Acoust. Soc. Am.*, vol. 34, no. 6, pp. 864-865, Jun. 1962.

[68] W. H. Thorp, "Deep ocean sound attenuation in the sub- and low-kilocycle-per-second region," *J. Acoust. Soc. Am.*, vol. 38, pp. 648-654, Oct. 1965.

[69] R. H. Mellen and D. G. Browning, "Low-frequency attenuation in the pacific ocean," *J. Acoust. Soc. Am.*, vol. 59, no. 3, pp. 700-702, Mar. 1976.

[70] F. H. Fisher and V. P. Simmons, "Sound absorption in sea water," *J. Acoust. Soc. Am.*, vol. 62, no. 3, pp. 558-564, Sep. 1977.

[71] R. E. Francois and G. R. Garrison, "Sound absorption based on ocean measurements. Part I: Pure water and magnesium sulfate contributions," *J. Acoust. Soc. Am.*, vol. 72, no. 3, pp. 896-907, Sep. 1982.

[72] R. E. Francois and G. R. Garrison, "Sound absorption based on ocean measurements. Part II: Boric acid contribution and equation for total absorption," *J. Acoust. Soc. Am.*, vol. 72, no. 6, pp. 1879-1890, Dec. 1982.

[73] M. Chitre, "A high-frequency warm shallow water acoustic communications channel model and measurements," *J. Acoust. Soc. Am.*, vol. 122, no. 5, pp. 2580-2586, Nov. 2007.

[74] J. Catipovic, A. Baggeroer, K. Von Der Heydt, and D. Koelsch, "Design and performance analysis of a digital acoustic telemetry system for the short range underwater channel," *IEEE J. Ocean. Eng.*, vol. 9, no. 4, pp. 242-252, Oct. 1984.

[75] A. Radosevic, J. G. Proakis, and M. Stojanovic, "Statistical characterization and capacity of shallow water acoustic channels," in *Proc. IEEE Oceans'09 Conf.*, Bremen, Germany, May 2009, pp. 1-8.

[76] X. Geng and A. Zielinski, "An eigenpath underwater acoustic communication channel model," in *Proc. MTS/IEEE Oceans'95 Conf.*, San Diego, CA, USA, Oct. 1995, pp. 1189-1196.

[77] D. Jourdain, "High frequency signal fluctuations in shallow water propagation," in *Proc. IEEE Oceans'94 Conf.*, Brest, France, Sep. 1994, pp. 278-283.

[78] W. B. Yang and T. C. Yang, "Characterization and modeling of underwater acoustic communications channels for frequency-shift-keying signals," in *Proc. IEEE Oceans'06 Conf.*, Boston, MA, USA, Sep. 2006, pp. 1-6.

[79] X. Lurton, *Introduction to Underwater Acoustics: Principles and Applications*. New York: Springer, 2002.

[80] M. Chitre, J. Potter, and O. S. Heng, "Underwater acoustic channel characterisation for medium-range shallow water communications," in *Proc. MTS/IEEE Oceans'04 Conf.*, Kobe, Japan, Nov. 2004, pp. 40 - 45.

[81] J. Catipovic, "Performance limitations in underwater acoustic telemetry," *IEEE J. Ocean. Eng.*, vol. 15, no. 3, pp. 205-216, 1990.

[82] R. Galvin and R. F. W. Coates, "Analysis of the performance of an underwater acoustic communications system and comparison with a stochastic model," in *Proc. IEEE Oceans'94 Conf.*, Brest , France, Sep. 1994, pp. 478-482.

[83] R. J. Urick, "Models for the amplitude fluctuations of narrow-band signals and noise in the sea," *J. Acoust. Soc. Am.*, vol. 62, no. 4, pp. 878-887, Oct. 1977.

[84] C. Bjerrum-Niese and R. Lutzen, "Stochastic simulation of acoustic communication in turbulent shallow water," *IEEE J. Ocean. Eng.*, vol. 25, no. 4, pp. 523-532, Oct. 2000.

[85] R. Galvin and R. E. W. Coats, "A stochastic underwater acoustic channel model," in *Proc. MTS/IEEE Oceans'96 Conf.*, Fort Lauderdale, FL, USA, Sep. 1996, pp. 203-210.

[86] M. A. Munoz Gutierrez, P. L. Prospero Sanchez, and J. V. do Vale Neto, "An eigenpath underwater acoustic communication channel simulation," in *Proc. MTS/IEEE Oceans'05 Conf.*, Washington D.C., USA, Sep. 2005, pp. 355-362.

[87] T. B. Aik, Q. S. Sen, and Z. Nan, "Characterization of multipath acoustic channels in very shallow waters for communications," in *Proc. IEEE Oceans'06 Conf.*, Singapore, pp. 1-8.

[88] P. Qarabaqi and M. Stojanovic, "Statistical modeling of a shallow water acoustic communication channel," in *Proc. of IACM UAM*, Nafplion, Greece, Jun. 2009.

[89] B. Borowski, "Characterization of a very shallow water acoustic communication channel," in *Proc. MTS/IEEE Oceans'09 Conf.*, Biloxi, MS, USA, Oct. 2009, pp. 1-10.

[90] S.-M. Kim, S.-H. Byun, S.-G. Kim, and Y.-K. Lim, "Experimental analysis of statistical properties of underwater channel in a very shallow water using narrow and broadband signals," in *Proc. MTS/IEEE Oceans'09 Conf.*, Biloxi, MS, USA, Oct. 2009, pp. 1-4.

[91] S. M. Flattè, R. Dashen, W. H. Munk, K. M. Watson and F. Zachariasen, *Sound transmission through a fluctuating ocean*. Cambridge University Press, 1979.

[92] R. F. W. Coates, *Underwater Acoustic Systems*. Hong Kong: Macmillan, 1990.

[93] G. W. Wornell, "Wavelet-based representations for the 1/f family of fractal processes," *Proc. IEEE*, vol. 81, no. 10, pp. 1428-1450, Oct. 1993.

[94] G. W. Wornell, "Synthesis, analysis, and processing of fractal signals," Ph.D. dissertation, Dept. Elect. Eng. Comp. Sci., Massachusetts Institute of Technology, Cambridge, MA, 1991.

[95] M. S. Keshner, "1/f noise," *Proc. IEEE*, vol. 70, no. 3, pp. 212-218, Mar. 1982.

[96] B. Kaulakys, J. Ruseckas, V. Gontis, and M. Alaburda, "Nonlinear stochastic models of 1/f noise and power-law distributions," *Phys. A Statistical Mechanics and its Applications*, vol. 365, no. 1, pp. 217-221, Jun. 2006.

[97] B. Kaulakys, "Autoregressive model of 1/f noise," *Physics Letters A*, vol. 257, no. 1-2, pp. 37-42, Jun. 1999.

[98] B. Mandelbrot, "Some noises with spectrum 1/f, a bridge between direct current and white noise," *IEEE Trans. Inf. Theory*, vol. 13, no. 2, pp. 289-298, Apr. 1967.

[99] R. J. Urick, *Ambient Noise in the Sea*. Undersea Warfare Technology Office, Dept. of the Navy, Washington D.C., USA, 1984.

[100] R. U. Nabar, H. Bölcskei, and F. W. Kneubühler, "Fading relay channels: Performance limits and space-time signal design," *IEEE J. Sel. Areas Commun.*, vol. 22, no. 6, pp. 1099-1109, Aug. 2004.

[101] S. Shamai and S. Verdu, "Worst-case power-constrained noise for binary-input channels," *IEEE Trans. Inf. Theory*, vol. 38, no. 5, pp. 1494-1511, Sep. 1992.

[102] H. Bölcskei, D. Gesbert, and A. J. Paulraj, "On the capacity of OFDM-based spatial multiplexing systems," *IEEE Trans. Commun.*, vol. 50, no. 2, pp. 225-234, Feb. 2002.

[103] E. Bejjani and J.-C. Belfiore, "Multicarrier coherent communications for the underwater acoustic channel," in *Proc. MTS/IEEE Oceans'96 Conf.*, Fort Lauderdale, FL, USA, Sep. 1996, pp. 1125-1130.

[104] H. Alves and R. D. Souza, "Selective decode-and-forward using fixed relays and packet accumulation," *IEEE Commun. Lett.*, vol. 15, no. 7, pp. 707-709, Jul. 2011.

[105] R. P. Brent, "An algorithm with guaranteed convergence for finding a zero of a function," *The Computer Journal*, vol. 14, no. 4, pp. 422-425, 1971.

[106] D. Tse and P. Viswanath, *Fundamentals of Wireless Communication*. Cambridge University Press, 2005.

[107] L. Li, N. Jindal, and A. Goldsmith, "Outage capacities and optimal power allocation for fading multiple-access channels," *IEEE Trans. Inf. Theory*, vol. 51, no. 4, pp. 1326-1347, Apr. 2005.

[108] B. Karakaya, M. O. Hasna, M. Uysal, T. M. Duman, and A. Ghrayeb, "Relay selection for cooperative underwater acoustic communication systems," in *Proc. IEEE Int. Conf. on Telecommunications*, Jounieh, Lebanon, Apr. 2012, pp. 1-6.

[109] M. Stojanovic, "On the relationship between capacity and distance in an underwater acoustic communication channel," in *Proc. 1st ACM Int. Workshop Underwater Networks*, Los Angeles, CA, USA, 2006, pp. 41-47.

[110] M. Abramowitz and I. A. Stegun, *Handbook of Mathematical Functions, with Formulas, Graphs, and Mathematical Tables*. Washington, D.C.: U.S. Dept. of Commerce, 1964.

[111] A. Castaño-Martínez and F. López-Blázquez, "Distribution of a sum of weighted noncentral chi-square variables," *Sociedad De Estadística e Investigación Operativa Test*, vol. 14, no. 2, pp. 397-415, Dec. 2005.